Supporting Information

Cytotoxic alkaloids from the twigs and leaves of *Cephalotaxus sinensis*

Fuxin Zhang, Tao Yang, Kailing Yang, Ruixi Zhou, Yu Zhang, Wenwen Chen, Zhetong Liu, Guanqun Zhan,* and Zengjun Guo*

School of Pharmacy, Health Science Center, Xi'an Jiaotong University, Xi'an 710061, P. R. China

List of Supporting Information

General experimental procedures 5
Plant material 5
Extraction and isolation 5
Spectroscopic data 7
Single-crystal X-ray diffraction analysis 9
Cytotoxicity evaluation 11
SARS-CoV-2 $3CL^{pro}$ enzyme inhibition assay 11
Table S1. SARS-CoV-2 $3CL^{pro}$ inhibitory activities of alkaloids **1-21** 12
Figure S1. ^{1}H–^{1}H COSY, key HMBC, and NOESY correlations of **1**–**4**, **5**, **7**, and **10**–**12**. 12
Figure S2. Concentration–response curves of cytotoxic compounds and positive control against five human cancer cell lines. 13
Figure S3. HPLC analysis for racemization of compound **2** using a chiral column (Daicel Chiralpak IC, MeOH/H_2O/$NH_3 \cdot H_2O$, 78:22:0.03, 0.8 mL/min). 13
Figure S4. ORTEP drawing of **1** 14
Figure S5. (+)-HR-ESI-MS spectrum of **1** 14
Figure S6. UV spectrum of **1** in MeOH 15
Figure S7. IR spectrum of **1** 15
Figure S8. ^{1}H NMR (600 MHz) spectrum of **1** in CD_3OD 16
Figure S9. ^{13}C NMR (150 MHz) spectrum of **1** in CD_3OD 16
Figure S10. DEPT 135 spectrum of **1** in CD_3OD 17
Figure S11. HSQC spectrum of **1** in CD_3OD 17
Figure S12. HMBC spectrum of **1** in CD_3OD 18
Figure S13. ^{1}H–^{1}H COSY spectrum of **1** in CD_3OD 18
Figure S14. ^{1}H–^{1}H NOESY spectrum of **1** in CD_3OD 19
Figure S15. (+)-HR-ESI-MS spectrum of **2** 19
Figure S16. UV spectrum of **2** in MeOH 20
Figure S17. IR spectrum of **2** 20
Figure S18. ^{1}H NMR (600 MHz) spectrum of **2** in CD_3OD 21
Figure S19. ^{13}C NMR (150 MHz) spectrumof **2** in CD_3OD 21

* Corresponding authors.

E-mail address: zhanguanqun@mail.xjtu.edu.cn. (Z. Guan), guozj@mail.xjtu.edu.cn. (Z. Guo)

Figure S20. DEPT 135 spectrum of **2** in CD_3OD 22
Figure S21. HSQC spectrum of **2** in CD_3OD 22
Figure S22. HMBC spectrum of **2** in CD_3OD 23
Figure S23. $^1H-^1H$ COSY spectrum of **2** in CD_3OD 23
Figure S24. NOESY spectrum of **2** in CD_3OD 24
Figure S25. (+)-HR-ESI-MS spectrum of **3** 24
Figure S26. UV spectrum of **3** in MeOH 25
Figure S27. ECD spectrum of **3** in MeOH 25
Figure S28. IR spectrum of **3** 26
Figure S29. ^1H NMR (600 MHz) spectrum of **3** in CD_3OD 26
Figure S30. ^{13}C NMR (150 MHz) spectrumof **3** in CD_3OD 27
Figure S31. DEPT 135 spectrum of **3** in CD_3OD 27
Figure S32. HSQC spectrum of **3** in CD_3OD 28
Figure S33. HMBC spectrum of **3** in CD_3OD 28
Figure S34. $^1H-^1H$ COSY spectrum of **3** in CD_3OD 29
Figure S35. NOESY spectrum of **3** in CD_3OD 29
Figure S36. (+)-HR-ESI-MS spectrum of **4** 30
Figure S37. UV spectrum of **4** in MeOH 30
Figure S38. ECD spectrum of **4** in MeOH 31
Figure S39. IR spectrum of **4** 31
Figure S40. ^1H NMR (600 MHz) spectrum of **4** in CD_3OD 32
Figure S41. ^{13}C NMR (150 MHz) spectrumof **4** in CD_3OD 32
Figure S42. DEPT 135 spectrum of **4** in CD_3OD 33
Figure S43. HSQC spectrum of **4** in CD_3OD 33
Figure S44. HMBC spectrum of **4** in CD_3OD 34
Figure S45. $^1H-^1H$ COSY spectrum of **4** in CD_3OD 34
Figure S46. NOESY spectrum of **4** in CD_3OD 35
Figure S47. (+)-HR-ESI-MS spectrum of **5** 35
Figure S48. UV spectrum of **5** in MeOH 36
Figure S49. ECD spectrum of **5** in MeOH 36
Figure S50. IR spectrum of **5** 37
Figure S51. ^1H NMR (600 MHz) spectrum of **5** in CD_3OD 37
Figure S52. ^{13}C NMR (150 MHz) spectrumof **5** in CD_3OD 38
Figure S53. DEPT 135 spectrum of **5** in CD_3OD 38
Figure S54. HSQC spectrum of **5** in CD_3OD 39
Figure S55. HMBC spectrum of **5** in CD_3OD 39
Figure S56. $^1H-^1H$ COSY spectrum of **5** in CD_3OD 40
Figure S57. NOESY spectrum of **5** in CD_3OD 40
Figure S58. (+)-HR-ESI-MS spectrum of **6** 41
Figure S59. UV spectrum of **6** in MeOH 41
Figure S60. IR spectrum of **6** 42
Figure S61. ^1H NMR (600 MHz) spectrum of **6** in CD_3OD 42
Figure S62. ^{13}C NMR (150 MHz) spectrum of **6** in CD_3OD 43
Figure S63. DEPT 135 spectrum of **6** in CD_3OD 43

Figure S64. HSQC spectrum of **6** in CD_3OD 44
Figure S65. HMBC spectrum of **6** in CD_3OD 44
Figure S66. $^1H-^1H$ COSY spectrum of **6** in CD_3OD 45
Figure S67. NOESY spectrum of **6** in CD_3OD 45
Figure S68. (+)-HR-ESI-MS spectrum of **7** 46
Figure S69. UV spectrum of **7** in MeOH 46
Figure S70. IR spectrum of **7** 47
Figure S71. ^1H NMR (600 MHz) spectrum of **7** in CD_3OD 47
Figure S72. ^{13}C NMR (150 MHz) spectrum of **7** in CD_3OD 48
Figure S73. DEPT 135 spectrum of **7** in CD_3OD 48
Figure S74. HSQC spectrum of **7** in CD_3OD 49
Figure S75. HMBC spectrum of **7** in CD_3OD 49
Figure S76. $^1H-^1H$ COSY spectrum of **7** in CD_3OD 50
Figure S77. NOESY spectrum of **7** in CD_3OD 50
Figure S78. (+)-HR-ESI-MS spectrum of **8** 51
Figure S79. UV spectrum of **8** in MeOH 51
Figure S80. ECD spectrum of **8** in MeOH 52
Figure S81. IR spectrum of **8** 52
Figure S82. ^1H NMR (600 MHz) spectrum of **8** in CD_3OD 53
Figure S83. ^{13}C NMR (150 MHz) spectrum of **8** in CD_3OD 53
Figure S84. DEPT 135 spectrum of **8** in CD_3OD 54
Figure S85. HSQC spectrum of **8** in CD_3OD 54
Figure S86. HMBC spectrum of **8** in CD_3OD 55
Figure S87. $^1H-^1H$ COSY spectrum of **8** in CD_3OD 55
Figure S88. NOESY spectrum of **8** in CD_3OD 56
Figure S89. (+)-HR-ESI-MS spectrum of **9** 56
Figure S90. UV spectrum of **9** in MeOH 57
Figure S91. ECD spectrum of **9** in MeOH 57
Figure S92. IR spectrum of **9** 58
Figure S93. ^1H NMR (600 MHz) spectrum of **9** in CD_3OD 58
Figure S94. ^{13}C NMR (150 MHz) spectrum of 9 in CD_3OD 59
Figure S95. DEPT 135 spectrum of **9** in CD_3OD 59
Figure S96. HSQC spectrum of **9** in CD_3OD 60
Figure S97. HMBC spectrum of **9** in CD_3OD 60
Figure S98. $^1H-^1H$ COSY spectrum of **9** in CD_3OD 61
Figure S99. NOESY spectrum of **9** in CD_3OD 61
Figure S100. (+)-HR-ESI-MS spectrum of **10** 62
Figure S101. UV spectrum of **10** in MeOH 62
Figure S102. ECD spectrum of **10** in MeOH 63
Figure S103. IR spectrum of **10** 63
Figure S104. ^1H NMR (600 MHz) spectrum of **10** in CD_3OD 64
Figure S105. ^{13}C NMR (150 MHz) spectrum of **10** in CD_3OD 64
Figure S106. DEPT 135 spectrum of **10** in CD_3OD 65
Figure S107. HSQC spectrum of **10** in CD_3OD 65

Figure S108. HMBC spectrum of **10** in CD_3OD 66
Figure S109. $^1H-^1H$ COSY spectrum of **10** in CD_3OD 66
Figure S110. NOESY spectrum of **10** in CD_3OD 67
Figure S111. (+)-HR-ESI-MS spectrum of **11** 67
Figure S112. UV spectrum of **11** in MeOH 68
Figure S113. ECD spectrum of **11** in MeOH 68
Figure S114. IR spectrum of **11** 69
Figure S115. ^1H NMR (600 MHz) spectrum of **11** in CD_3OD 69
Figure S116. ^{13}C NMR (150 MHz) spectrum of **11** in CD_3OD 70
Figure S117. DEPT 135 spectrum of **11** in CD_3OD 70
Figure S118. HSQC spectrum of **11** in CD_3OD 71
Figure S119. HMBC spectrum of **11** in CD_3OD 71
Figure S120. $^1H-^1H$ COSY spectrum of **11** in CD_3OD 72
Figure S121. NOESY spectrum of **11** in CD_3OD 72
Figure S122. (+)-HR-ESI-MS spectrum of **12** 73
Figure S123. UV spectrum of **12** in MeOH 73
Figure S124. ECD spectrum of **12** in MeOH 74
Figure S125. IR spectrum of **12** 74
Figure S126. ^1H NMR (600 MHz) spectrum of **12** in CD_3OD 75
Figure S127. ^{13}C NMR (150 MHz) spectrum of **12** in CD_3OD 75
Figure S128. DEPT 135 spectrum of **12** in CD_3OD 76
Figure S129. HSQC spectrum of **12** in CD_3OD 76
Figure S130. HMBC spectrum of **12** in CD_3OD 77
Figure S131. $^1H-^1H$ COSY spectrum of **12** in CD_3OD 77
Figure S132. NOESY spectrum of **12** in CD_3OD 78

General experimental procedures

NMR spectra were acquired with a Bruker Avance III HD600. HRESIMS spectra were measured using a Waters I-Class Vion IMS QTOF spectrometer. Optical rotations were determined in methanol using an InsMark FD polarimeter. UV and ECD spectra were obtained in methanol on a JASCO J-815 CD spectrometer. FT-IR spectra were recorded by a Bruker VERTEX70 instrument. The crystallographic data were collected on a Bruker D8 Venture diffractometer equipped with Bruker PHOTON-III detector and Ga Kα radiation (λ = 1.34139 Å). HPLC was performed on Waters 1525 fapparatus with a YMC Triart C18 column (5 μm, 10 × 250 mm) and a DAICEL CHIRALPAK IC column (5 μm, 4.6 × 250 mm). Column chromatography (CC) were carried out using silica gel (Qingdao Haiyang Chemical Co. Ltd., China), ODS (45 μm, YMC Co. Ltd., Japan), and Sephadex LH-20 (GE Healthcare Bio-Sciences AB, Sweden).

Plant material

The twigs and leaves of *Cephalotaxus sinensis* were gathered in May 2021 from Xi'an, Shaanxi Province, China. The plant was identified by Dr. Tao Zhou in School of Pharmacy, Health Science Center, Xi'an Jiaotong University, where the voucher specimen (No. 2021051501) has been stored.

Extraction and isolation

The air-dried twigs and leaves of *C. sinensis* (30 kg) were extracted using 95% ethanol by heating at 75 °C for three times (per three hours) to afford 3.50 kg crude extract. The crude extract was dispersed in water (20 L) and acidified to pH 2 with 2% HCl solution, then extracted with $CHCl_3$ (5 times). The aqueous phase was adjusted to pH 9–10 using 5% Na_2CO_3 solution, followed by extraction with $CHCl_3$ (5 × 10 L) and *n*-BuOH (5 × 10 L), respectively. After removing the organic solvents, the $CHCl_3$ extract (pH 9, 163.6 g) was subjected to a silica gel column chromatography (CC) with gradient elution of CH_2Cl_2/MeOH (from 100:1 to 12:1) to provide four subfractions (Fr.A–Fr.D) as monitored by TLC. Fr.A was fractionated on silica gel CC with a gradient elution of petroleum ether/acetone (PE/Ace, from 10:1 to 1:1) to obtain four subfractions Fr.A1−Fr.A4. Fr.A3 was loaded onto a Sephadex LH-20 (MeOH) to provide two subfractions Fr.A3a and Fr.A3b. Fr. A3a was further separated by RP HPLC (MeOH/H_2O/$NH_3 \cdot H_2O$, 55:45:0.2) to yield **13** (3.6 mg, t_R 16.1 min), **9** (7.0 mg, t_R 18.6 min), **1** (4.1 mg, t_R 21.4 min), **20** (11.6 mg, t_R 29.9 min). **1** was then performed by a chiral HPLC using a DAICEL CHIRALPAK IC column eluting at 1.0 mL/min with

MeOH to yield pure enantiomers **1a** (1.5 mg, t_R 19.9 min) and **1b** (1.2 mg, t_R 22.6 min); **13** was isolated by the same chiral column eluting at 0.8 mL/min with MeOH/H_2O/$NH_3 \cdot H_2O$ (78:22:0.03) to give **13a** (2.5 mg, t_R 20.9 min) and **13b** (1.0 mg, t_R 22.9 min). Compound **15** (0.66 g) was crystallized from Fr.A3b (0.85 g). Fr.A4 was separated by RP HPLC eluting with MeOH/H_2O/$NH_3 \cdot H_2O$ (53:47:0.2) to provide five subfractions Fr.A4a–Fr.A4e. Fr.A4b was purified by RP HPLC (MeCN/H_2O/$NH_3 \cdot H_2O$, 38:62:0.2) to yield **5** (1.7 mg, t_R 16.4 min). After filtering Fr.C, the filter residue and filtrate were obtained. The filter residue (18.5 g) was dissolved partially and purified using RP HPLC eluting with MeOH/H_2O/$NH_3 \cdot H_2O$ (60:40:0.2) to give **14** (12.9 mg, t_R 22.1 min), **14** was then isolated by chiral column mentioned above eluting with MeOH/H_2O/$NH_3 \cdot H_2O$ (78:22:0.03) at 0.8 mL/min to give **14b** (3.5 mg, t_R 13.0 min) and **14a** (7.2 mg, t_R 16.2 min). The filtrate was chromatographed on ODS CC (MeOH/H_2O, from 10:90 to 65:35) to produce five subfractions Fr.C1−Fr.C5. Fr.C1 was chromatographed on a silica gel CC, followed by purification with RP HPLC (MeCN/H_2O/$NH_3 \cdot H_2O$, 25:75:0.2) to yield **4** (3.3 mg, t_R 19.3 min). Fr.C2 was isolated sequentially by silica gel CC eluted with PE/Ace (5:1), then purified using RP HPLC eluted with MeCN/H_2O/$NH_3 \cdot H_2O$ (25:75:0.2) to give **3** (2.3 mg, t_R 22.4 min). Similar to Fr.C2, **12** (10.6 mg, t_R 19.3 min) and **21** (3.4 mg, t_R 24.1 min) were isolated from Fr.C3 by RP HPLC (MeCN/H_2O/$NH_3 \cdot H_2O$, 44:56:0.2). Fr.C5 was subjected to silica gel CC (PE/EtOAc, 5:1) and then purified by RP HPLC eluted with MeOH/H_2O/$NH_3 \cdot H_2O$ (70:30:0.2) to give five subfractions Fr.C5a−Fr.C5e. Purification of Fr.C5a by RP HPLC eluting with MeCN/H_2O/$NH_3 \cdot H_2O$ (55:45:0.2) to yield **7** (1.2 mg, t_R 37.5 min) and **19** (1.3 mg, t_R 42.0 min). Compounds **11** (1.4 mg, t_R 25.8 min) and **17** (0.8 mg, t_R 28.9 min) were obtained from Fr.C5b by RP HPLC (MeCN/H_2O/ $NH_3 \cdot H_2O$, 60:40:0.2). Similar to Fr.C5b, compounds **10** (3.2 mg, t_R 27.1 min) and **6** (2.4 mg, t_R 31.4 min) were isolated from Fr.C5c by RP HPLC eluting with MeCN/H_2O/$NH_3 \cdot H_2O$ (63:37:0.2). Compounds **18** (6.7 mg, t_R 34.4 min) and **16** (1.8 mg, t_R 38.5 min) were obtained by RP HLPC eluting with MeCN/H_2O/$NH_3 \cdot H_2O$ (64:36:0.2) and MeCN/H_2O/$NH_3 \cdot H_2O$ (65:35:0.2) from Fr.C5d to Fr.C5e, respectively. A silica gel CC was applied to purify Fr.D into two subfractions (Fr.D1 and Fr.D2). Fr. D1 was chromatographed on silica gel CC with gradient elution of CH_2Cl_2/MeOH (from 50:1 to 10:1), followed by Sephadex LH-20 CC (MeOH), and then purified by RP HPLC (MeOH/H_2O/ $NH_3 \cdot H_2O$, 63:37:0.2) to divide into four subsfractions Fr.D1a–Fr.D1d. Fr.D1b and Fr.D1c were purified by RP HPLC eluting with MeCN/H_2O/$NH_3 \cdot H_2O$ (25:75:0.2) and MeCN/H_2O/$NH_3 \cdot H_2O$

(40:60:0.2) to yield compounds **2** (5.5 mg, t_R 20.8 min) and **8** (1.3 mg, t_R 28.3 min), respectively. **2** was then separated by above mentioned chiral column (MeOH/H_2O/$NH_3 \cdot H_2O$ = 78:22:0.03, 0.8 mL/min) to acquired **2b** (2.3 mg, t_R 10.4 min) and **2a** (2.7 mg, t_R 14.6 min). All the flow rates of RP HPLC experiments were 2.0 mL/min.

Spectroscopic data

*(±) Cephlosine A (**1**)*: colorless crystals; $[\alpha]_D^{25}$ – 14.5 (*c* 0.1, MeOH); UV(MeOH) λ_{max} (log ε) 203 (4.72), 243 (4.01), 290 (3.79) nm; ECD (MeOH) 215 ($\Delta\varepsilon$, − 1.5), 251 ($\Delta\varepsilon$, − 1.2), 284 ($\Delta\varepsilon$, + 1.5), 328 ($\Delta\varepsilon$, − 0.8) nm; IR (KBr) ν_{max} 2933, 2889, 2802, 1720, 1622, 1483, 1228, 1101, 1039, 933 cm^{-1}; ^1H and ^{13}C NMR data, see Tables 1 and 2; HRESIMS *m/z* 328.1551 $[M + H]^+$ (calcd for $C_{19}H_{22}NO_4$, 328.1549).

*(−) Cephlosine A (**1a**)*: white amorphous solid; $[\alpha]_D^{25}$ – 160.5 (*c* 0.1, MeOH); ECD (MeOH) 205 ($\Delta\varepsilon$, − 13.7), 223 ($\Delta\varepsilon$, − 11.6), 251 ($\Delta\varepsilon$, − 8.6), 284 ($\Delta\varepsilon$, + 13.8), 328 ($\Delta\varepsilon$, − 5.6) nm;

*(+) Cephlosine A (**1b**)*: colorless crystals; $[\alpha]_D^{25}$ + 159.2 (*c* 0.1, MeOH); ECD (MeOH) 205 ($\Delta\varepsilon$, + 12.5), 223 ($\Delta\varepsilon$, + 10.5), 251 ($\Delta\varepsilon$, + 7.8), 284 ($\Delta\varepsilon$, – 12.7), 328 ($\Delta\varepsilon$, + 5.2) nm;

*(±) Cephlosine B (**2**)*: white amorphous solid; $[\alpha]_D^{25}$ – 19.5 (*c* 0.1, MeOH); UV(MeOH) λ_{max} (log ε) 202 (4.72), 235 (3.76), 285 (3.50) nm; ECD (MeOH) 205 ($\Delta\varepsilon$, − 5.5) nm; IR (KBr) ν_{max} 3394, 2939, 2825, 1651, 1514, 1452, 1292, 1219, 1110, 1018, 790 cm^{-1}; ^1H and ^{13}C NMR data, see Tables 1 and 2; HRESIMS *m/z* 318.1704 $[M + H]^+$ (calcd for $C_{18}H_{24}NO_4$, 318.1705).

(−) Cephlosine B (***2a***): white amorphous solid; $[\alpha]_D^{25}$ – 202.0 (*c* 0.1, MeOH); ECD (MeOH) 205 ($\Delta\varepsilon$, − 8.8), 226 ($\Delta\varepsilon$, − 1.80), 243 ($\Delta\varepsilon$, + 1.01), 280 ($\Delta\varepsilon$, − 0.38) nm.

(+) Cephlosine B (***2b***): white amorphous solid; $[\alpha]_D^{25}$ + 200.3 (*c* 0.1, MeOH); ECD (MeOH) 205 ($\Delta\varepsilon$, + 7.9), 226 ($\Delta\varepsilon$, + 1.62), 243 ($\Delta\varepsilon$, − 0.91), 280 ($\Delta\varepsilon$, + 0.36) nm.

*Cephlosine C (**3**)*: colorless crystal; $[\alpha]_D^{25}$ – 44.3 (*c* 0.1, MeOH); UV(MeOH) λ_{max} (log ε) 203 (4.71), 233 (3.76), 285 (3.64) nm; ECD (MeOH) 202 ($\Delta\varepsilon$, −7.0), 210 ($\Delta\varepsilon$, + 3.5), 220 ($\Delta\varepsilon$, + 5.1), 280 ($\Delta\varepsilon$, −1.3) nm; IR (KBr) ν_{max} 3410, 2939, 2833, 1645, 1508, 1454, 1353, 1242, 1117, 1016, 811 cm^{-1}; ^1H and ^{13}C NMR data, see Tables 1 and 2; HRESIMS *m/z* 316.1551 $[M + H]^+$ (calcd for $C_{18}H_{22}NO_4$, 316.1549).

*Cephlosine D (**4**)*: colorless crystal; $[\alpha]_D^{25}$ – 11.5 (*c* 0.1, MeOH); UV(MeOH) λ_{max} (log ε) 202 (4.75), 240 (3.71), 290 (3.82) nm; ECD (MeOH) 206 ($\Delta\varepsilon$, + 7.3), 238 ($\Delta\varepsilon$, + 2.0), 294 ($\Delta\varepsilon$, − 0.64)

nm; IR (KBr) ν_{max} 3423, 2933, 2804, 1644, 1502, 1485, 1373, 1240, 1128, 1037, 927 cm^{-1}; ^{1}H and ^{13}C NMR data, see Tables 1 and 2; HRESIMS *m/z* 332.1504 $[M + H]^+$ (calcd for $C_{18}H_{22}NO_5$, 332.1498).

*Cephlosine E (**5**)*: white amorphous solid; $[\alpha]_D^{25}$ – 13.3 (*c* 0.1, MeOH); UV(MeOH) λ_{max} (log ε) 202 (4.67), 235 (3.50), 290 (3.51) nm; ECD (MeOH) 205 ($\Delta\varepsilon$, + 7.43), 220 ($\Delta\varepsilon$, – 0.40), 240 ($\Delta\varepsilon$, + 0.85), 290 ($\Delta\varepsilon$, − 0.34) nm; IR (KBr) ν_{max} 3414, 2932, 2794, 1668, 1502,1481, 1371, 1232, 1094, 1028, 932 cm^{-1}; ^{1}H and ^{13}C NMR data, see Tables 1 and 2; HRESIMS *m/z* 332.1486 $[M + H]^+$ (calcd for $C_{18}H_{22}NO_5$, 332.1498).

*Cephlosine F (**6**)*: white amorphous solid; $[\alpha]_D^{25}$ – 145.0 (*c* 0.1, MeOH); UV(MeOH) λ_{max} (log ε) 202 (4.85), 240 (3.66), 290 (3.66) nm; ECD (MeOH) 205 ($\Delta\varepsilon$, − 33.2), 294 (− 1.4) nm; IR (KBr) ν_{max} 3447, 2949, 2881, 1740, 1649, 1502, 1488, 1271, 1221, 1113, 1036, 929, 702 cm^{-1}; ^{1}H and ^{13}C NMR data, see Table 3; HRESIMS *m/z* 536.1932 $[M – H]^-$ (calcd for $C_{29}H_{30}NO_9$, 536.1926).

*Cephlosine G (**7**)*: white amorphous solid; $[\alpha]_D^{25}$ – 170.0 (*c* 0.1, MeOH); UV(MeOH) λ_{max} (log ε) 203 (5.06), 240 (3.83), 290 (3.94) nm; ECD (MeOH) 205 ($\Delta\varepsilon$, − 23.6), 220 ($\Delta\varepsilon$, +11.9), 294 ($\Delta\varepsilon$, − 2.4) nm; IR (KBr) ν_{max} 3364, 2949, 2889, 1739, 1651, 1504, 1483, 1448, 1227, 1117, 1035, 929, 700 cm^{-1}; ^{1}H and ^{13}C NMR data, see Table 3; HRESIMS *m/z* 536.1933 $[M – H]^-$ (calcd for $C_{29}H_{30}NO_9$, 536.1926).

*Cephlosine H (**8**)*: white amorphous solid; $[\alpha]_D^{25}$ – 9.2 (*c* 0.1, MeOH); UV(MeOH) λ_{max} (log ε) 208 (4.55), 254 (4.26), 294 (3.73) nm; ECD (MeOH) 202 ($\Delta\varepsilon$, + 8.63), 226 ($\Delta\varepsilon$, + 13.62), 253 ($\Delta\varepsilon$, − 11.26) nm; IR (KBr) ν_{max} 3361, 2937, 1662, 1510, 1446, 1255, 1088, 1029 cm^{-1}; ^{1}H and ^{13}C NMR data, see Tables 2 and 4; HRESIMS *m/z* 332.1865 $[M + H]^+$ (calcd for $C_{19}H_{26}NO_4$, 332.1862).

*Cephlosine I (**9**)*: colorless crystal; $[\alpha]_D^{25}$ – 15.0 (*c* 0.1, MeOH); UV(MeOH) λ_{max} (log ε) 203 (4.91), 244 (4.10), 285 (3.95) nm; ECD (MeOH) 212 ($\Delta\varepsilon$, − 15.28), 244 ($\Delta\varepsilon$, − 2.26) nm; IR (KBr) ν_{max} 2924, 2818, 1504,1488, 1238, 1233, 1095, 1039, 929, 598 cm^{-1}; ^{1}H and ^{13}C NMR data, see Tables 2 and 4; HRESIMS *m/z* 328.1551 $[M + H]^+$ (calcd for $C_{19}H_{22}NO_4$, 328.1543).

*Cephlosine J (**10**)*: colorless crystal; $[\alpha]_D^{25}$ + 76.9 (*c* 0.1, MeOH); UV(MeOH) λ_{max} (log ε) 202 (4.75), 235 (3.84), 289 (3.74) nm; ECD (MeOH) 206 ($\Delta\varepsilon$, + 6.75), 243 ($\Delta\varepsilon$, + 4.37), 286 ($\Delta\varepsilon$, + 0.86) nm; IR (KBr) ν_{max} 3418, 2935, 2866, 1502, 1483, 1230, 1097, 1043, 936 cm^{-1}; ^{1}H and ^{13}C NMR data, see Tables 2 and 4; HRESIMS *m/z* 330.1710 $[M + H]^+$ (calcd for $C_{19}H_{24}NO_4$, 330.1705).

*Cephlosine K (**11**)*: light yellow powder; $[\alpha]_D^{25}$ + 51.4 (*c* 0.1, MeOH); UV(MeOH) λ_{max} (log ε)

204 (4.85), 230 (4.14), 283 (3.67) nm; ECD (MeOH) 206 ($\Delta\varepsilon$, + 10.55), 233 ($\Delta\varepsilon$, + 5.99) nm; IR (KBr) ν_{max} 3419, 2937, 2841, 1606, 1514, 1259, 1093, 1025, 752 cm^{-1}; ^{1}H and ^{13}C NMR data, see Tables 2 and 4; HRESIMS *m/z* 346.2021 $[M + H]^+$ (calcd for $C_{20}H_{28}NO_4$, 346.2013).

*Cephlosine L (**12**)*: light yellow powder; $[\alpha]_D^{25}$ + 126.8 (*c* 0.1, MeOH); UV(MeOH) λ_{max} (log ε) 203 (4.63), 234 (3.81), 285 (3.51) nm; ECD (MeOH) 203 ($\Delta\varepsilon$, + 50.83), 223 ($\Delta\varepsilon$, – 2.56), 240 ($\Delta\varepsilon$, + 1.44) nm; IR (KBr) ν_{max} 3354, 2920, 2841, 1585, 1508, 1448, 1280, 1257, 1105, 1039, 795 cm^{-1}; ^{1}H and ^{13}C NMR data, see Tables 2 and 4; HRESIMS *m/z* 316.1917 $[M + H]^+$ (calcd for $C_{19}H_{26}NO_3$, 316.1913).

Single-crystal X-ray diffraction analysis

Crystal X-ray diffraction data for compounds **1b**, **3**–**4**, **9**–**10**, **18,** and **1** were collected on a Bruker APEX-II diffractometer equipped with graphite-monochromatized Ga Kα radiation (λ = 1.34139 Å). The structures were refined and solved based on previously described procedures.[1,2] The crystallographic data of compounds **1b**, **3**–**4**, **9**–**10**, **18**, and **1** were deposited at the Cambridge Crystallographic Data Centre with the deposition numbers of 2213948–2213954, respectively.

*Crystallographic Data of **1b**:* $C_{19}H_{21}NO_4$, M = 327.37, T = 200 (2) K, orthorhombic, $P2_12_12_1$, a = 8.0253 (4) Å, b = 10.2408 (5) Å, c = 20.0504 (10) Å, $\alpha = \beta = \gamma = 90^{\circ}$, V = 1647.85 (14) $Å^3$, Z = 4, D_{calcd} = 1.320 g/cm^3, crystal size 0.12 × 0.10 × 0.10 mm^3, F(000) = 696, absorption coefficient 0.481 mm^{-1}, reflections collected 32663, 8.434° < 2θ < 144.622°, −11 ≤ h ≤ 11, −14 ≤ k ≤ 12, −28 ≤ l ≤28, independent reflections, 4751 [R(int) = 0.0387], final R indices [I > 2σ(I)], R_1 = 0.0326, wR_2 = 0.0885, R indices (all data), R_1 = 0.0327, wR_2 = 0.0886. Flack structure parameter: 0.04 (3).

*Crystallographic Data of **3**:* $C_{18}H_{21}NO_4$, M = 315.36, T = 100 (2) K, orthorhombic, $P2_12_12_1$, a = 8.3100 (17) Å, b = 10.917 (2) Å, c = 17.120 (4) Å, $\alpha = \beta = \gamma = 90^{\circ}$, V = 1553.1 (5) $Å^3$, Z = 4, D_{calcd} = 1.349 g/cm^3, crystal size 0.3 × 0.2 × 0.12 mm^3, F(000) = 672, absorption coefficient 0.495 mm^{-1}, reflections collected 32663, 8.988° < 2θ < 144.964°, −11 ≤ h ≤ 11, −15 ≤ k ≤ 15, −19 ≤ l ≤24, independent reflections, 4627 [R(int) = 0.0733], final R indices [I > 2σ(I)], R_1 = 0.0352, wR_2 = 0.0947, R indices (all data), R_1 = 0.0353, wR_2 = 0.0948. Flack structure parameter: 0.11 (5).

*Crystallographic Data of **4** :* $C_{18}H_{21}NO_5$, M = 331.36, T = 200 (2) K, monoclinic, $P2_1$, a = 6.6976 (4) Å, b = 10.7016 (6) Å, c = 11.0783 (6) Å, $\alpha = \gamma = 90^{\circ}$, β = 94.0760 (10), V = 792.03 (8) $Å^3$, Z = 2,

D_{calcd} = 1.389 g/cm^3, crystal size 0.30 × 0.15 × 0.12 mm^3, F(000) = 352, absorption coefficient 0.535 mm^{-1}, reflections collected 30485, 11.524° < 2θ < 144.588°, −9 ≤ h ≤ 9, −14 ≤ k ≤ 15, −15 ≤ l ≤15, independent reflections, 4610 [R(int) = 0.0299], final R indices [I > 2σ(I)], R_1 = 0.0310, wR_2 = 0.0923, R indices (all data), R_1 = 0.0311, wR_2 = 0.0925. Flack structure parameter: 0.03 (5).

Crystallographic Data of ***9*** *:* $C_{19}H_{21}NO_4$, M = 327.37, T = 100 (1) K, orthorhombic, $P2_12_12_1$, a = 8.4578 (8) Å, b = 9.5190 (9) Å, c = 19.2209 (18) Å, α =β =γ = 90°, V = 1547.5 (3) Å^3, Z = 4, D_{calcd} = 1.405 g/cm^3, crystal size 0.30 × 0.20 × 0.20 mm^3, F(000) = 696, absorption coefficient 0.512 mm^{-1}, reflections collected 25285, 12.824° < 2θ < 109.984°, −10 ≤ h ≤ 10, −11 ≤ k ≤ 11, −23 ≤ l ≤18, independent reflections, 2915 [R(int) = 0.0445], final R indices [I > 2σ(I)], R_1 = 0.0316, wR_2 = 0.0817, R indices (all data), R_1 = 0.0317, wR_2 = 0.0818. Flack structure parameter: 0.15 (5).

Crystallographic Data of ***10*** *:* $C_{19}H_{23}NO_4$, M = 329.38, T = 200 (2) K, orthorhombic, $P2_12_12_1$, a = 7.5187 (5) Å, b = 9.2274 (9) Å, c = 23.3001 (16) Å, α =β =γ = 90°, V = 1616.52 (19) Å^3, Z = 4, D_{calcd} = 1.353 g/cm^3, crystal size 0.20 × 010 × 0.10 mm^3, F(000) = 704, absorption coefficient 0.490 mm^{-1}, reflections collected 40611, 8.968° < 2θ < 144.738°, −10 ≤ h ≤ 10, −13 ≤ k ≤ 13, −33 ≤ l ≤33, independent reflections, 4813 [R(int) = 0.0316], final R indices [I > 2σ(I)], R_1 = 0.0298, wR_2 = 0.0836, R indices (all data), R_1 = 0.0299, wR_2 = 0.0839. Flack structure parameter: 0.06 (3).

Crystallographic Data of ***18*** *:* $C_{27}H_{35}NO_9 \cdot H_2O$, M = 553.59, T = 200 (2) K, monoclinic, $P2_1$, a = 9.4013 (5) Å, b = 26.2244 (16) Å, c = 12.2587 (7) Å, α =γ = 90°, β = 90.836 (2), V = 3022 (3) Å^3, Z = 4, D_{calcd} = 1.217 g/cm^3, crystal size 0.20 × 0.10 × 0.10 mm^3, F(000) = 1184, absorption coefficient 0.503 mm^{-1}, reflections collected 81736, 6.274° < 2θ < 126.264°, −12 ≤ h ≤ 12, −34 ≤ k ≤ 34, −16 ≤ l ≤16, independent reflections, 14799 [R(int) = 0.0457], final R indices [I > 2σ(I)], R_1 = 0.0490, wR_2 = 0.1472, R indices (all data), R_1 = 0.0549, wR_2 = 0.1512. Flack structure parameter: − 0.02 (4).

Crystallographic Data of ***1****:* $C_{19}H_{21}NO_4$, M = 327.37, T = 200 (2) K, monoclinic, $P2_1$/c, a = 6.6669 (6) Å, b = 21.971 (2) Å, c = 11.9519 (12) Å, α =γ = 90°, β =103.559 (4), V = 1701.9 (3) Å^3, Z = 4, D_{calcd} = 1.278 g/cm^3, crystal size 0.12 × 0.10 × 0.10 mm^3, F(000) = 696, absorption coefficient 0.466 mm^{-1}, reflections collected 65775, 7° < 2θ < 144.718°, −9 ≤ h ≤ 9, −31 ≤ k ≤ 29, −16 ≤ l ≤ 16, independent reflections, 5114 [R(int) = 0.0455], final R indices [I > 2σ(I)], R_1 = 0.0431, wR_2 = 0.1152, R indices (all data), R_1 = 0.0542, wR_2 = 0.1217.

Cytotoxicity evaluation

The cytotoxicity of isolated compounds against five human cancer cell lines (HL-60, A-549, SMMC-7721, MDA-MB-231, and SW480 cell lines) was evaluated using the MTT method as previously described. [3]

SARS-CoV-2 3CL^{pro} enzyme inhibition assay

The SARS-CoV-2 3CL^{pro} inhibitory activity of the isolated compounds was evaluated using an enhanced SARS-CoV-2 3CL^{pro} inhibiter screening kit (P0315S, Beyotime Biotechnology). MCA-AVLQSGFR-Lys(Dnp)-Lys-NH_2 solution was used as the fluorogenic substrate. According to the screening kit, a FRET-based protease assay was carried out. Briefly, 91 μL of assay reagent (each containing 90 μL assay buffer and 1 μL SARS-CoV-2 3CL^{pro}) and 5 μL of a series of test compound solutions dissolved in DMSO were added in each well of 96-well black plates. Then, 4 μL peptide substrates were added and incubated for 10 min at 37 °C. The relative fluorescence units (RFU) were recorded with 325 nm excitation and 393 nm emission wavelengths by using a FlexStation 3 Multi-Mode Microplate Reader (Molecular Devices, USA). Each experiment was performed in triplicate. Ebselen was used as a positive control. The percent of inhibition was calculated using the equation as follows: Inhibition activity % = $(RFU_{3CL^{pro}} - RFU_{sample})/(RFU_{3CL^{pro}} - RFU_{blank}) \times 100\%$. $RFU_{3CL^{pro}}$, RFU_{sample}, and RFU_{blank} were the relative fluorescence unit of SARS-CoV-2 3CL^{pro} control, tested compounds, and blank control, respectively.

Reference

1 G. Zhan, R. Miao, F. Zhang, G. Chang, L. Zhang, X. Zhang, and Z. Guo, Monoterpene indole alkaloids with acetylcholinesterase inhibitory activity from the leaves of *Rauvolfia vomitoria*, *Bioorg. Chem.*, **2020**, *102*, 104136.

2 G. Zhan, J. Zhou, R. Liu, T. Liu, G. Guo, J. Wang, M. Xiang, Y. Xue, Z. Luo, Y. Zhang, and G. Yao, Galanthamine, plicamine, and secoplicamine alkaloids from *Zephyranthes candida* and their anti-acetylcholinesterase and anti-inflammatory activities, *J. Nat. Prod.*, **2016**, *79*, 760–766.

3 G. Zhan, X. Qu, J. Liu, Q. Tong, J. Zhou, B. Sun, and G. Yao, Zephycandidine A, the first naturally occurring imidazo[1,2-*f*]phenanthridine alkaloid from *Zephyranthes candida*, exhibits significant anti-tumor and anti-acetylcholinesterase activities, *Sci. Rep.*, **2016**, *6*, 33990.

Table S1. SARS-CoV-2 3CL^{pro} inhibitory activities of alkaloids **1-21**

Compounds	Inhibition (%)[a]	Compounds	Inhibition (%)	Compounds	Inhibition (%)
1a	5.99±0.16	**8**	ND	**16**	ND
1b	ND[b]	**9**	ND	**17**	ND
2a	ND	**10**	ND	**18**	11.21±1.24
2b	ND	**11**	6.63±1.42	**19**	ND
3	1.47±1.06	**12**	ND	**20**	ND
4	ND	**13a**	ND	**21**	ND
5	ND	**13b**	ND	**HHT**	1.25±0.87
6	ND	**14**	6.43±0.57		
7	ND	**15**	ND		

[a] Inhibition rate (%) at 40 μM are expressed as the mean ± SD (n = 3); [b] Not detectable.
positive control: Ebselen (IC_{50} = 0.38 ± 0.05 μM).

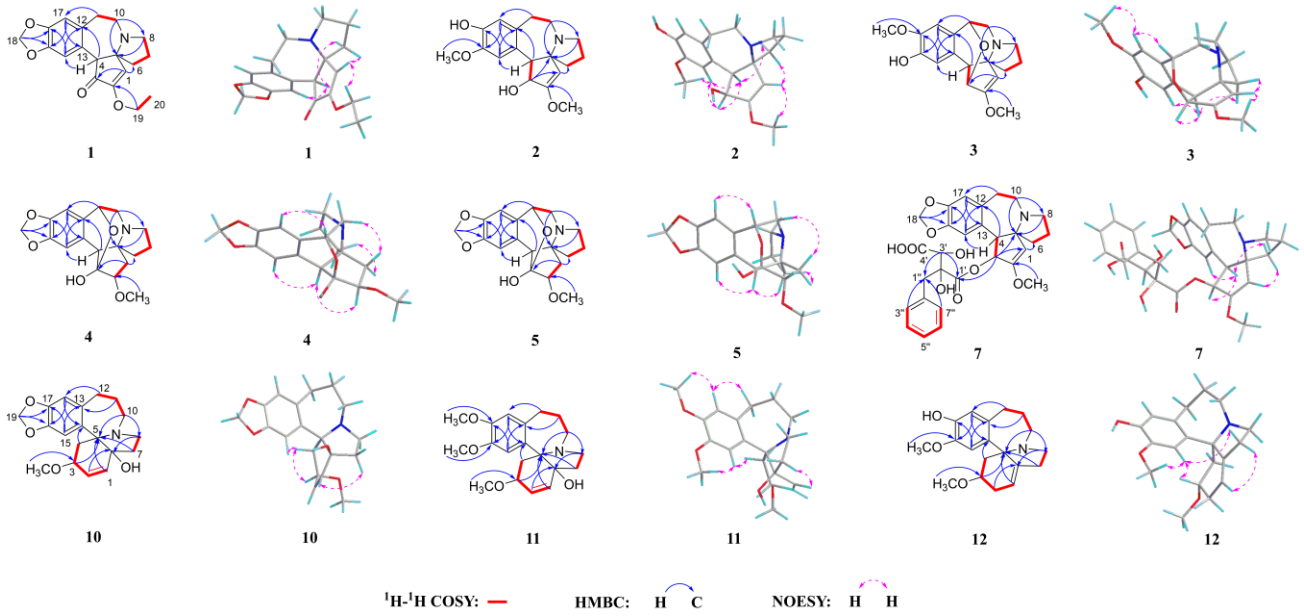

Figure S1. ^{1}H–^{1}H COSY, key HMBC, and NOESY correlations of **1–4**, **5**, **7**, and **10–12**.

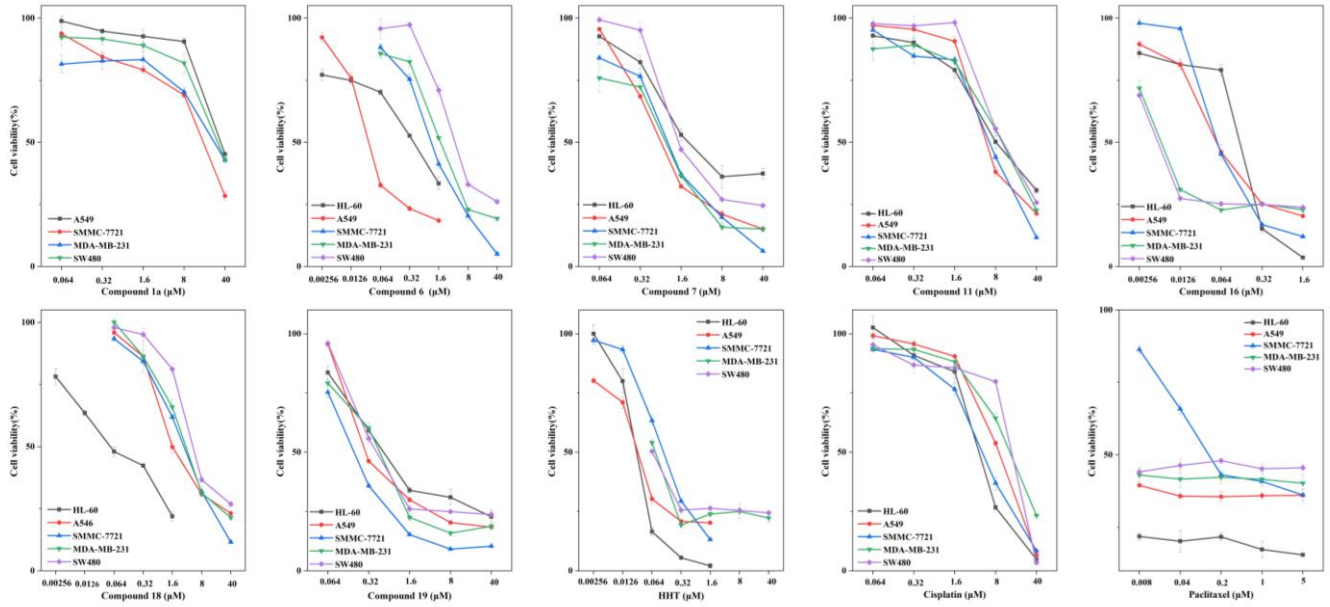

Figure S2. Concentration–response curves of cytotoxic compounds and positive control against five human cancer cell lines.

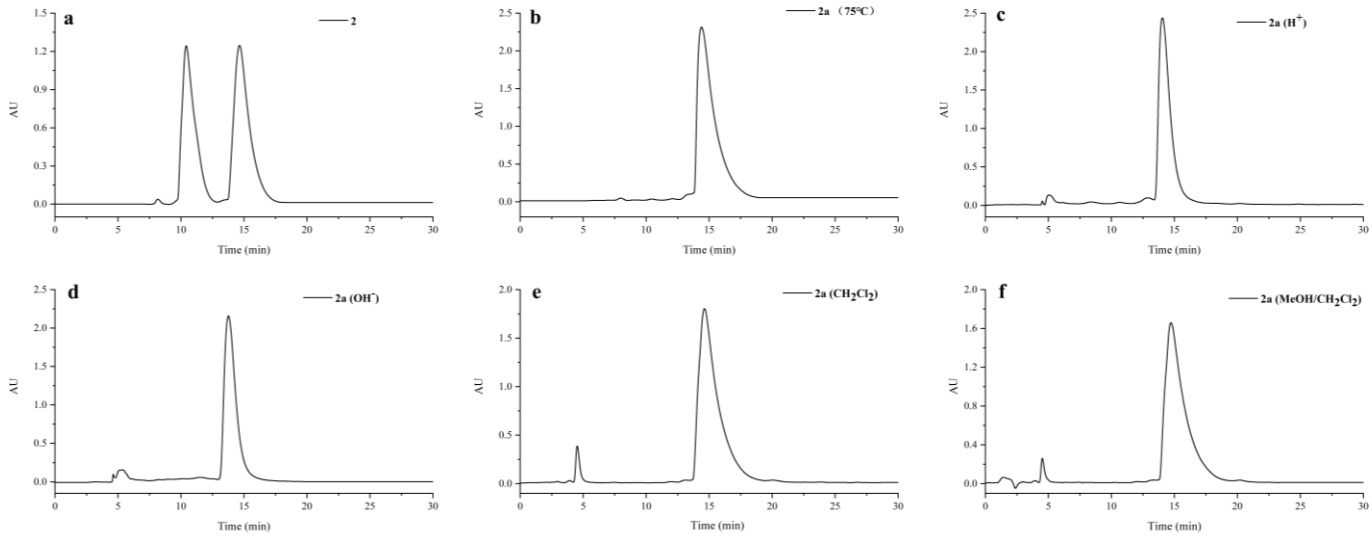

Figure S3. HPLC analysis for racemization of compound **2a** using a chiral column (Daicel Chiralpak IC, MeOH/H_2O/$NH_3 \cdot H_2O$, 78:22:0.03, 0.8 mL/min).

Condition: a): Natural mixure of compound **2**; b): Heating in 95 % ethanol at 75 °C for 9 hours; c): Dispersing in hydrochloric acid solution (pH = 2) for 24 h; d): Placing in alkaline solution (pH = 9) for 24 h; e): Placing in the dichloromethane solution for 24 h; f): Placing in the mixed solutions (CH_2Cl_2:MeOH:Et_2NH = 5:1:0.02) for 24 h.

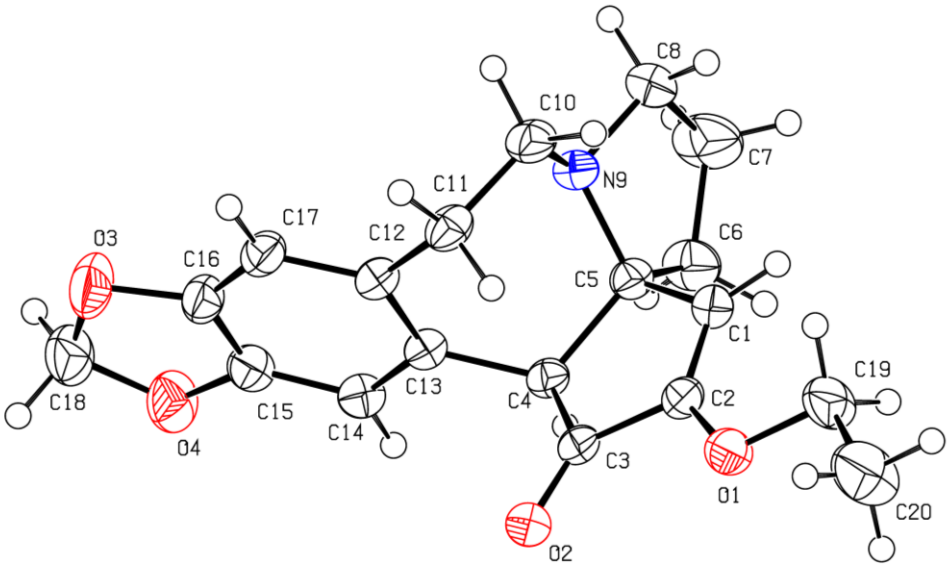

Figure S4. ORTEP drawing of **1**

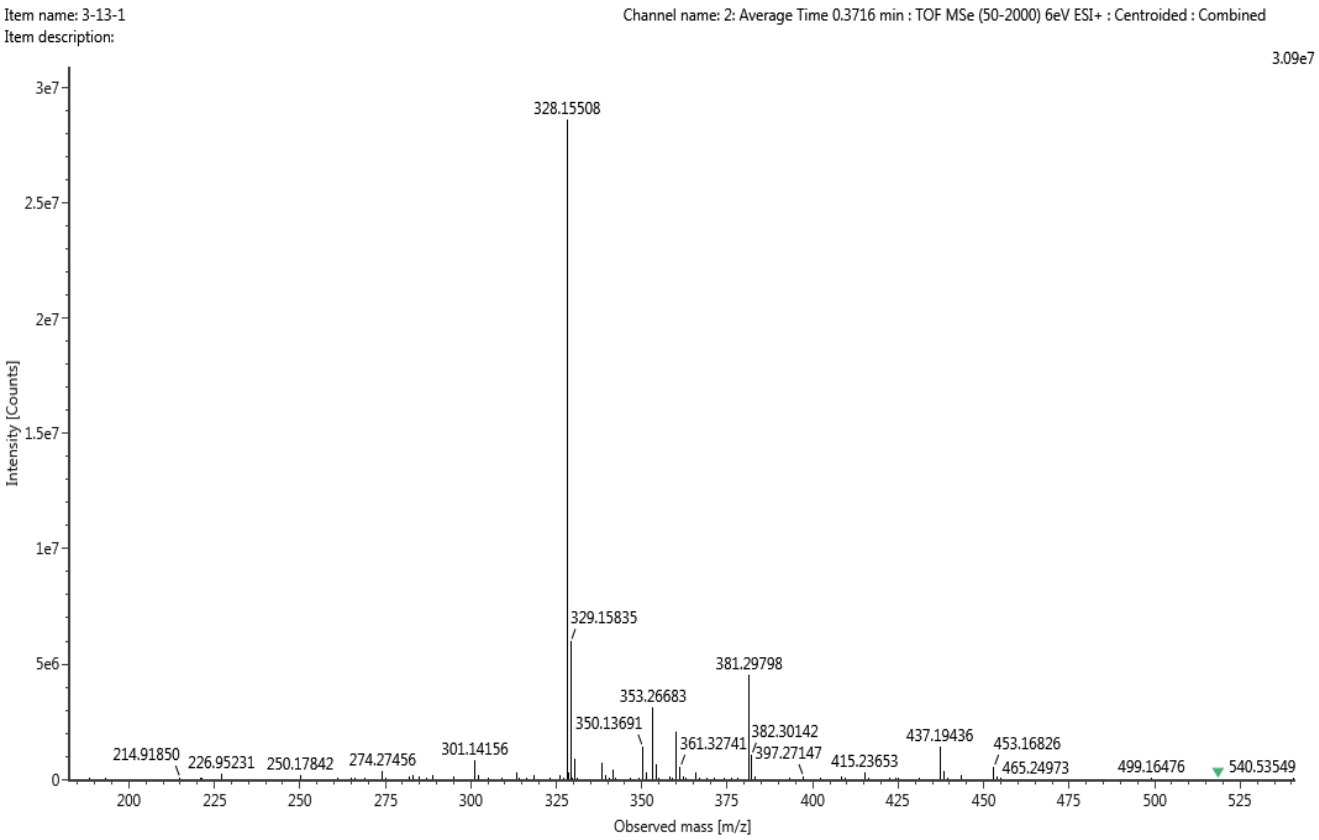

Figure S5. (+)-HR-ESI-MS spectrum of **1**

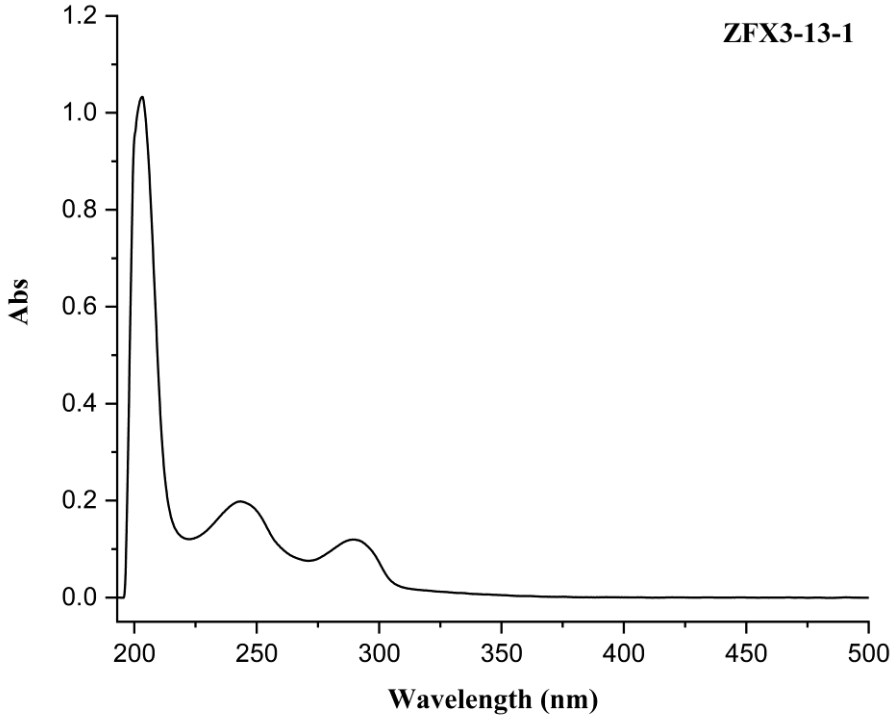

Figure S6. UV spectrum of **1** in MeOH

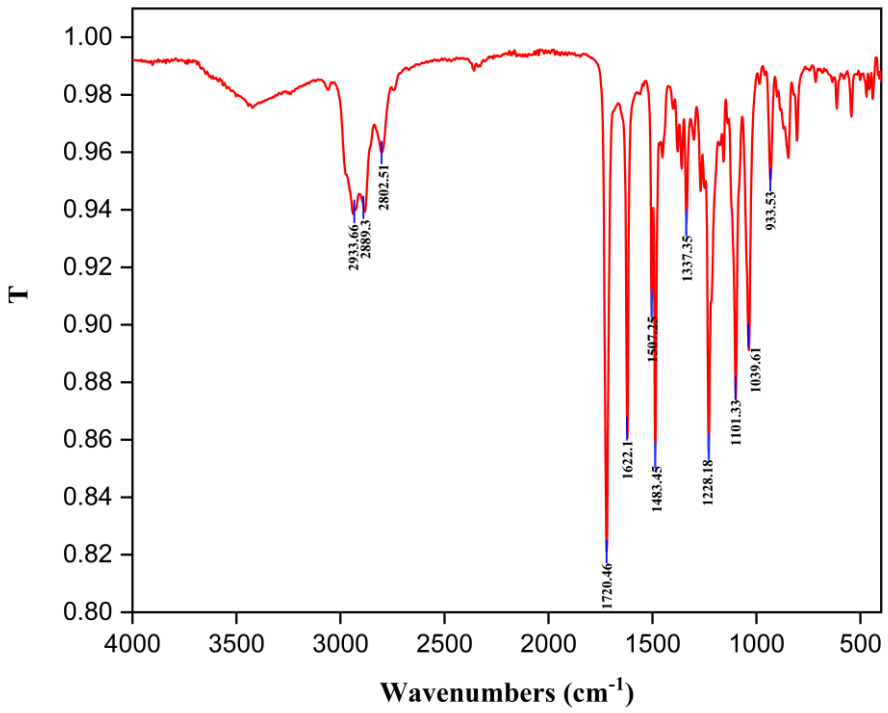

Figure S7. IR spectrum of **1**

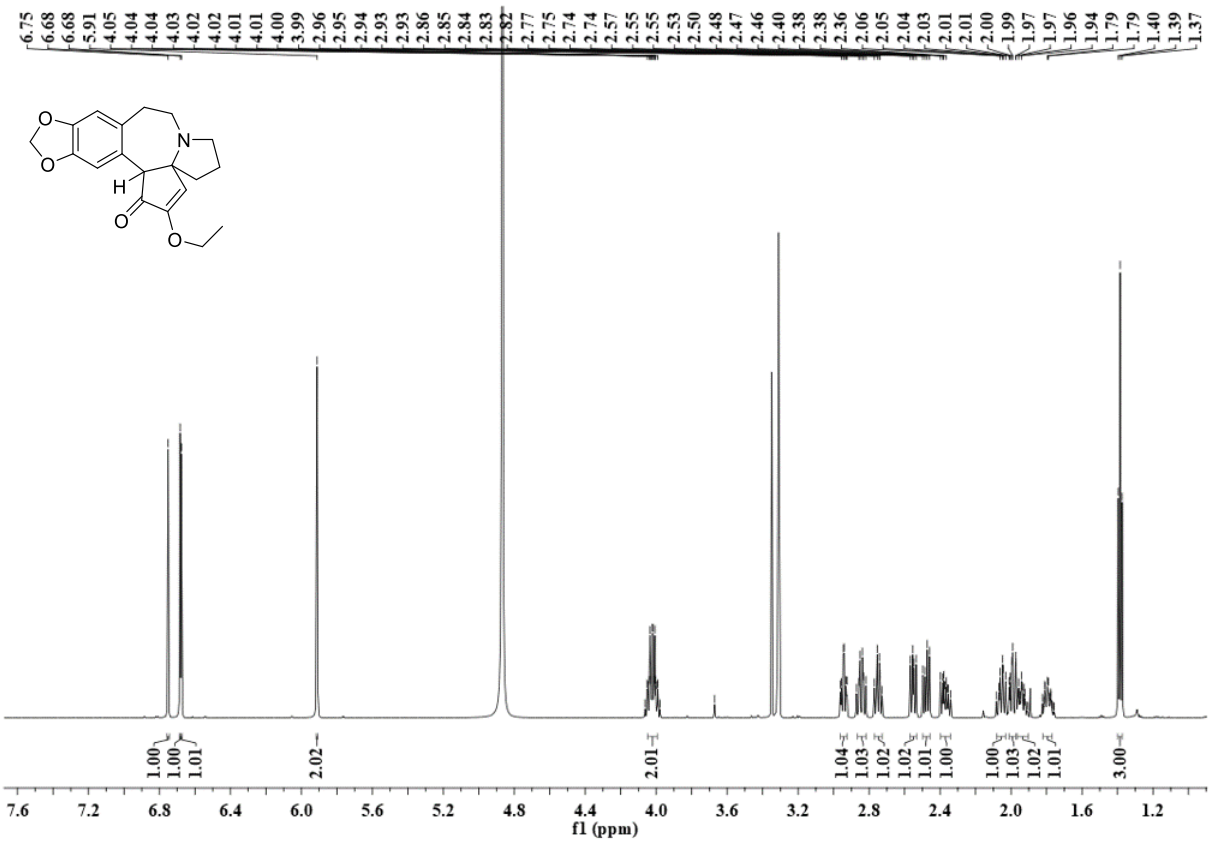

Figure S8. ^{1}H NMR (600 MHz) spectrum of **1** in CD_3OD

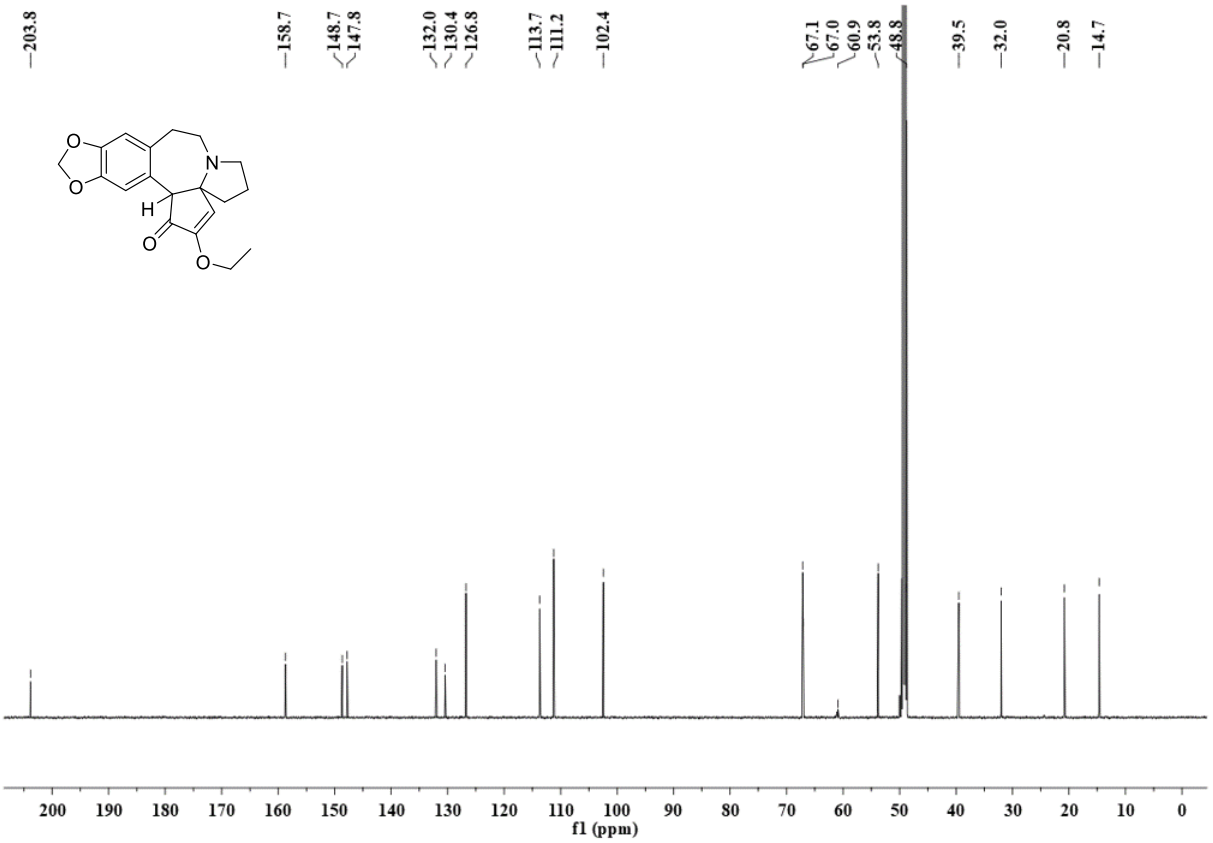

Figure S9. ^{13}C NMR (150 MHz) spectrum of **1** in CD_3OD

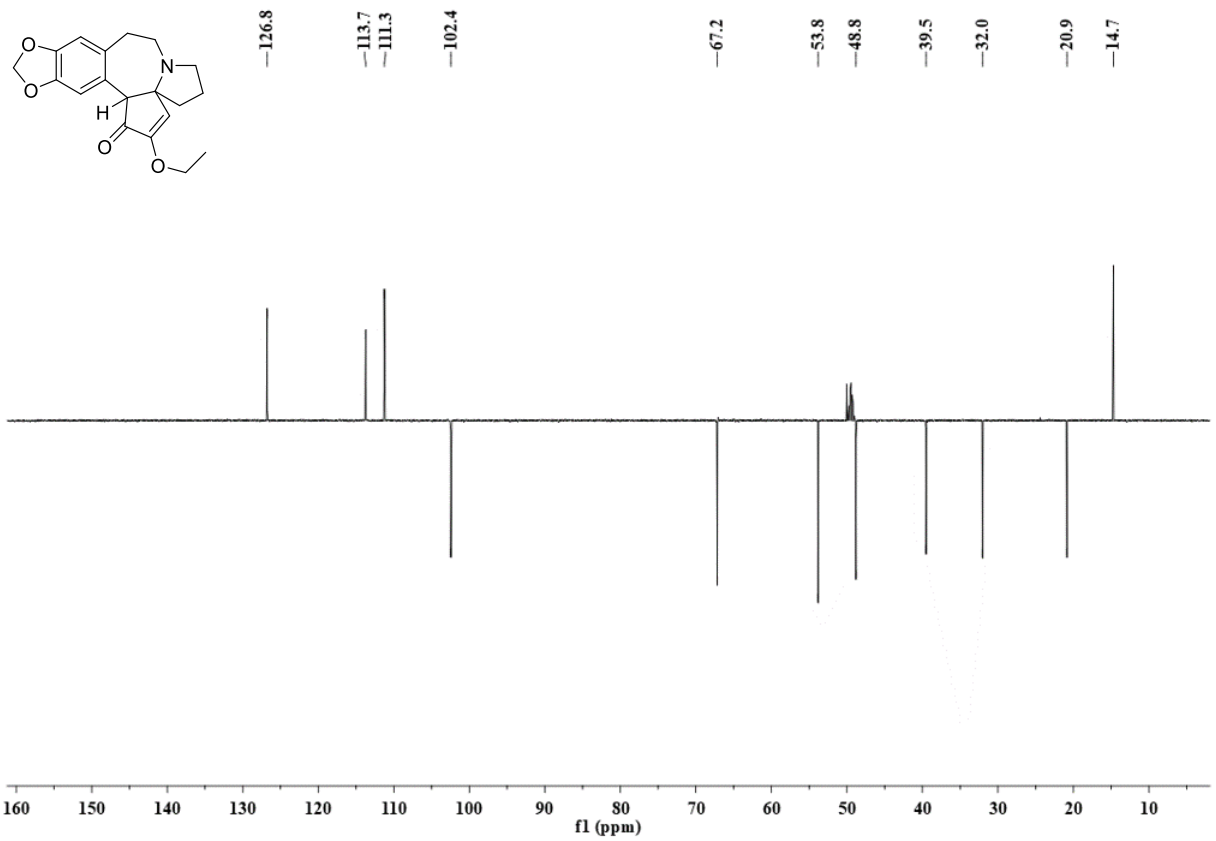

Figure S10. DEPT 135 spectrum of **1** in CD_3OD

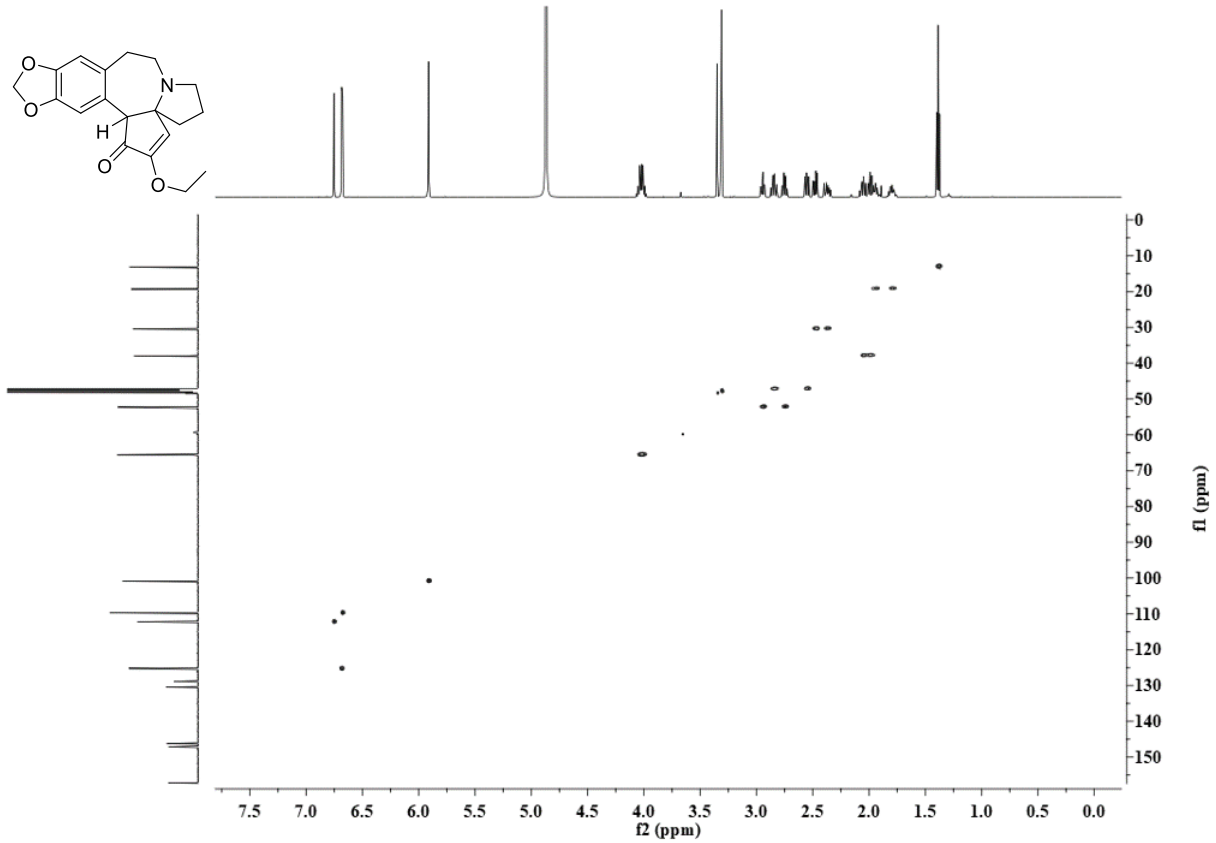

Figure S11. HSQC spectrum of **1** in CD_3OD

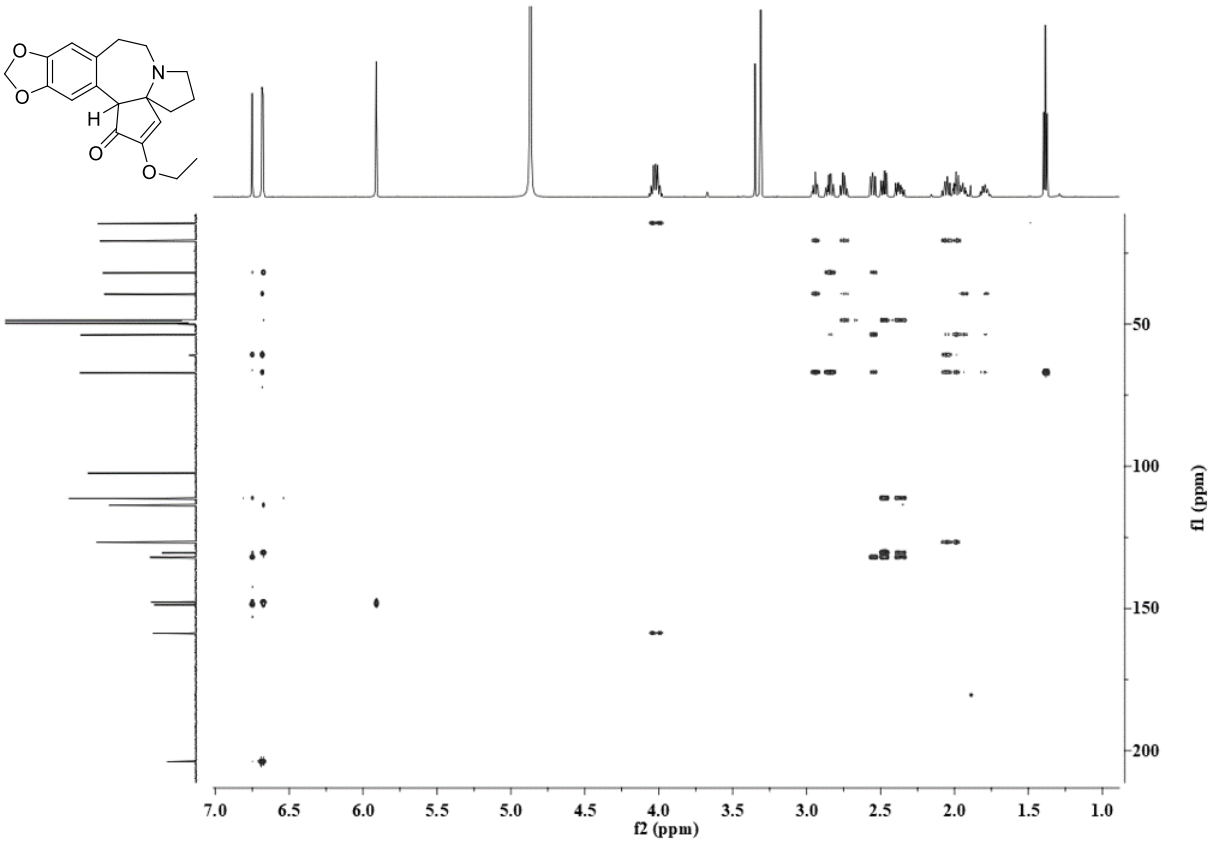

Figure S12. HMBC spectrum of **1** in CD_3OD

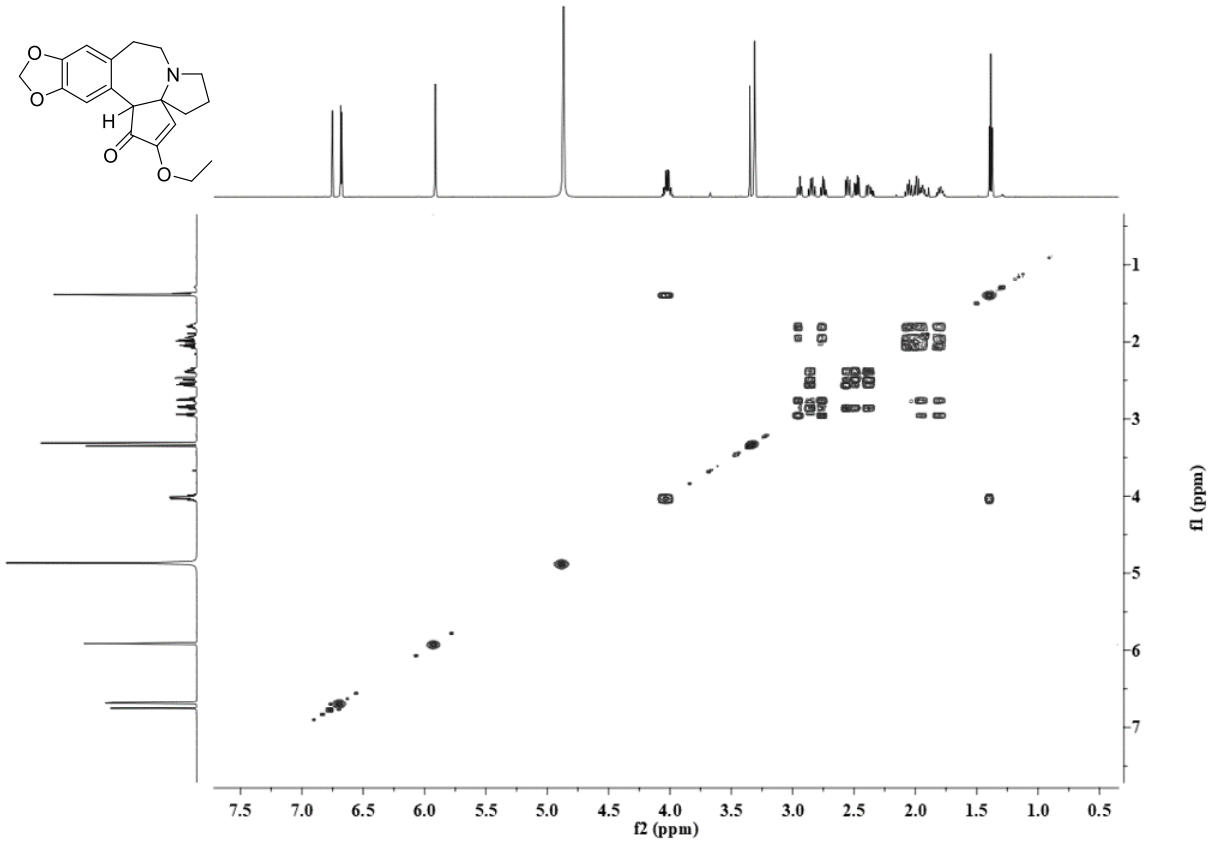

Figure S13. $^{1}H–^{1}H$ COSY spectrum of **1** in CD_3OD

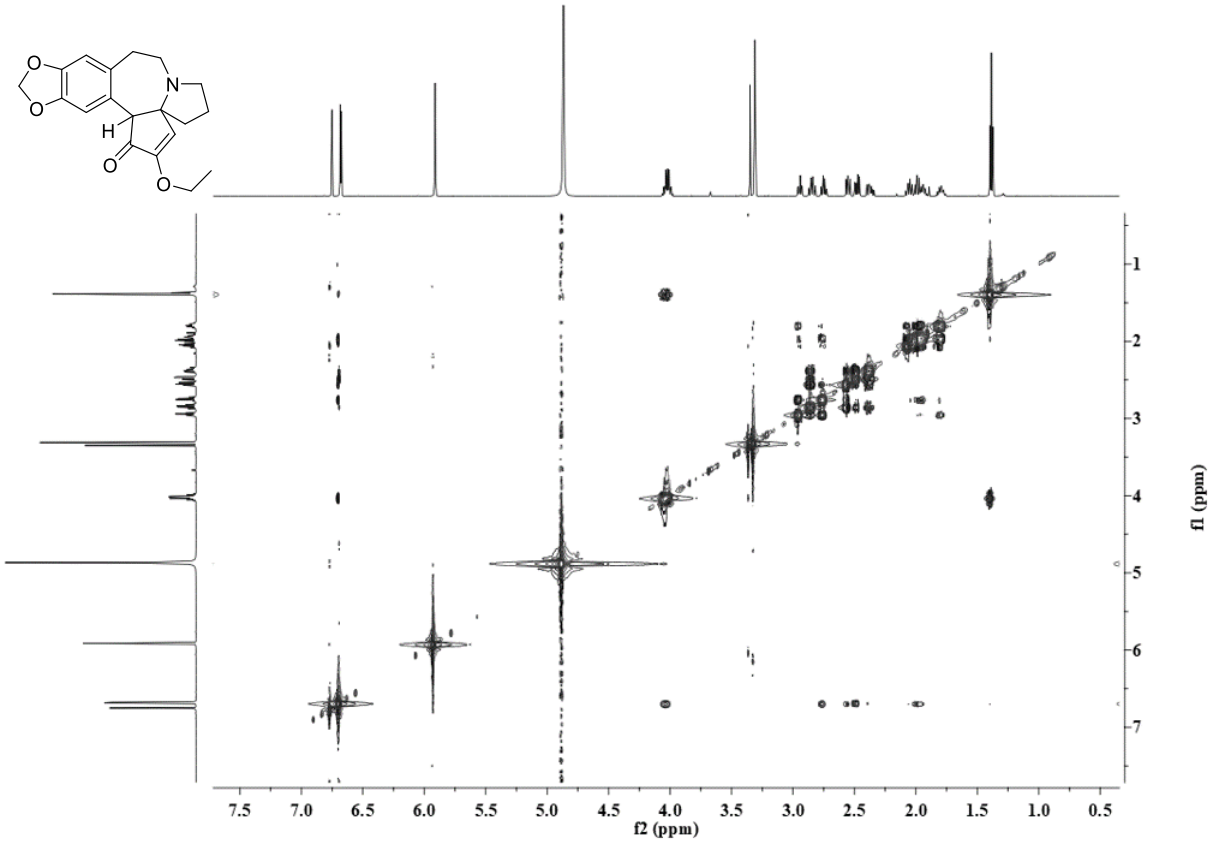

Figure S14. $^{1}H–^{1}H$ NOESY spectrum of **1** in CD_3OD

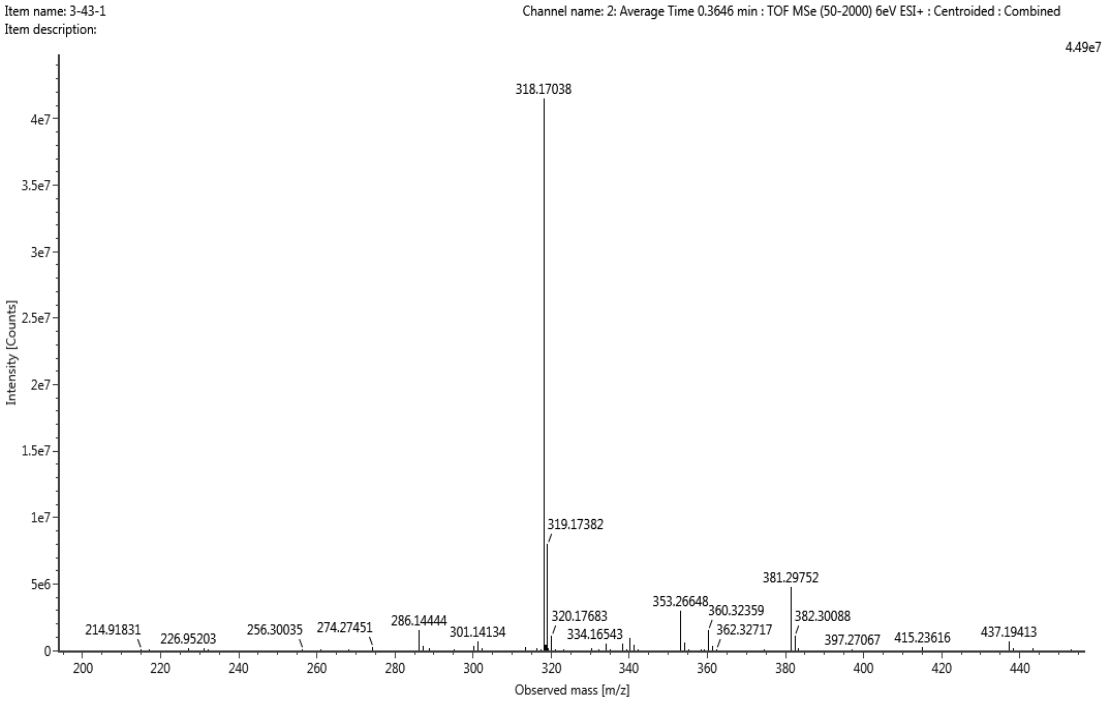

Figure S15. (+)-HR-ESI-MS spectrum of **2**

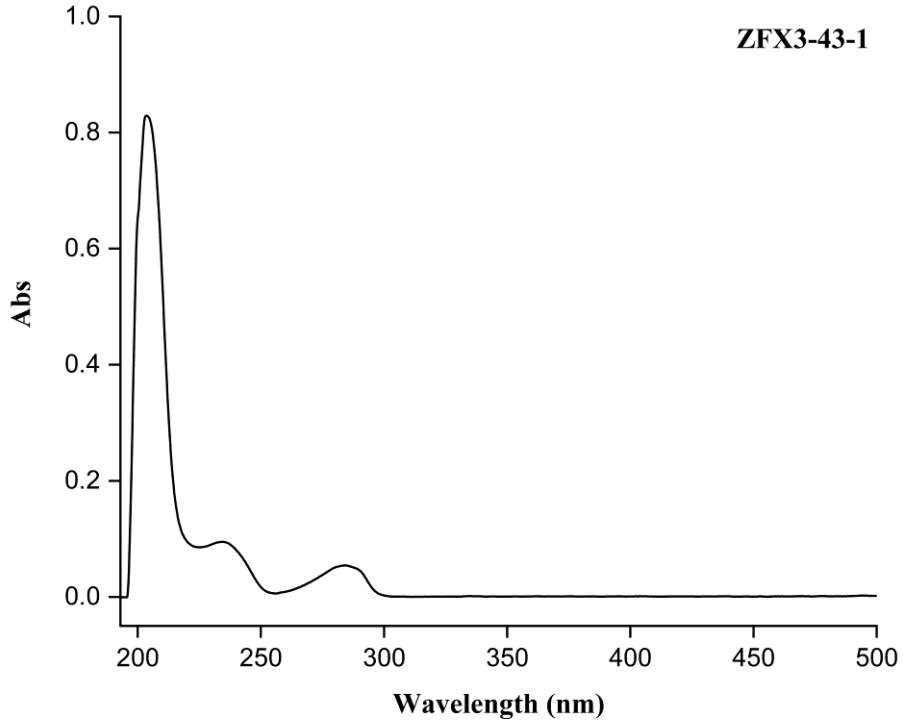

Figure S16. UV spectrum of **2** in MeOH

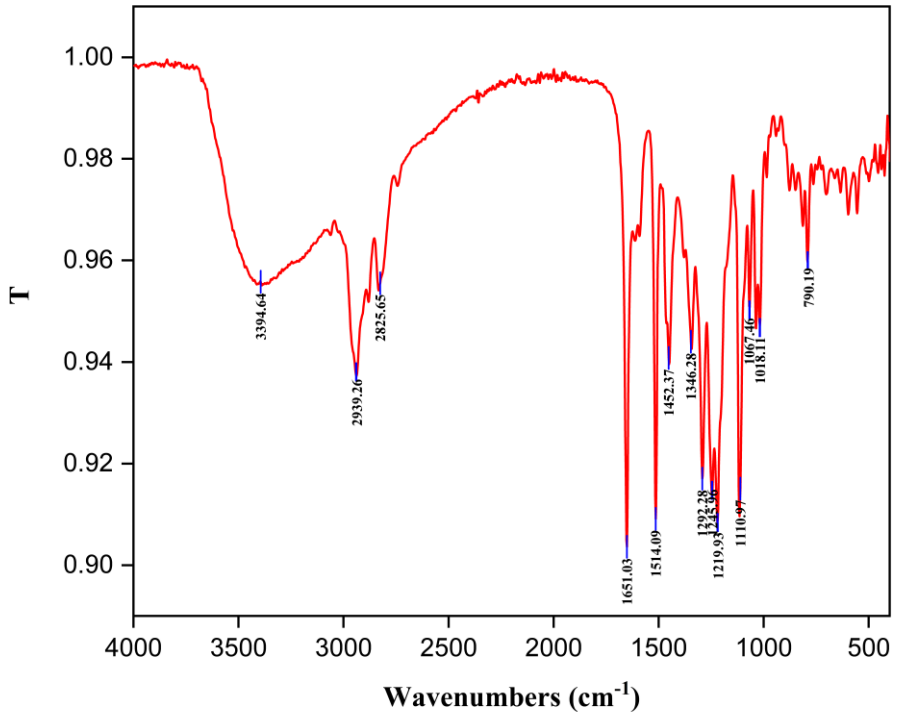

Figure S17. IR spectrum of **2**

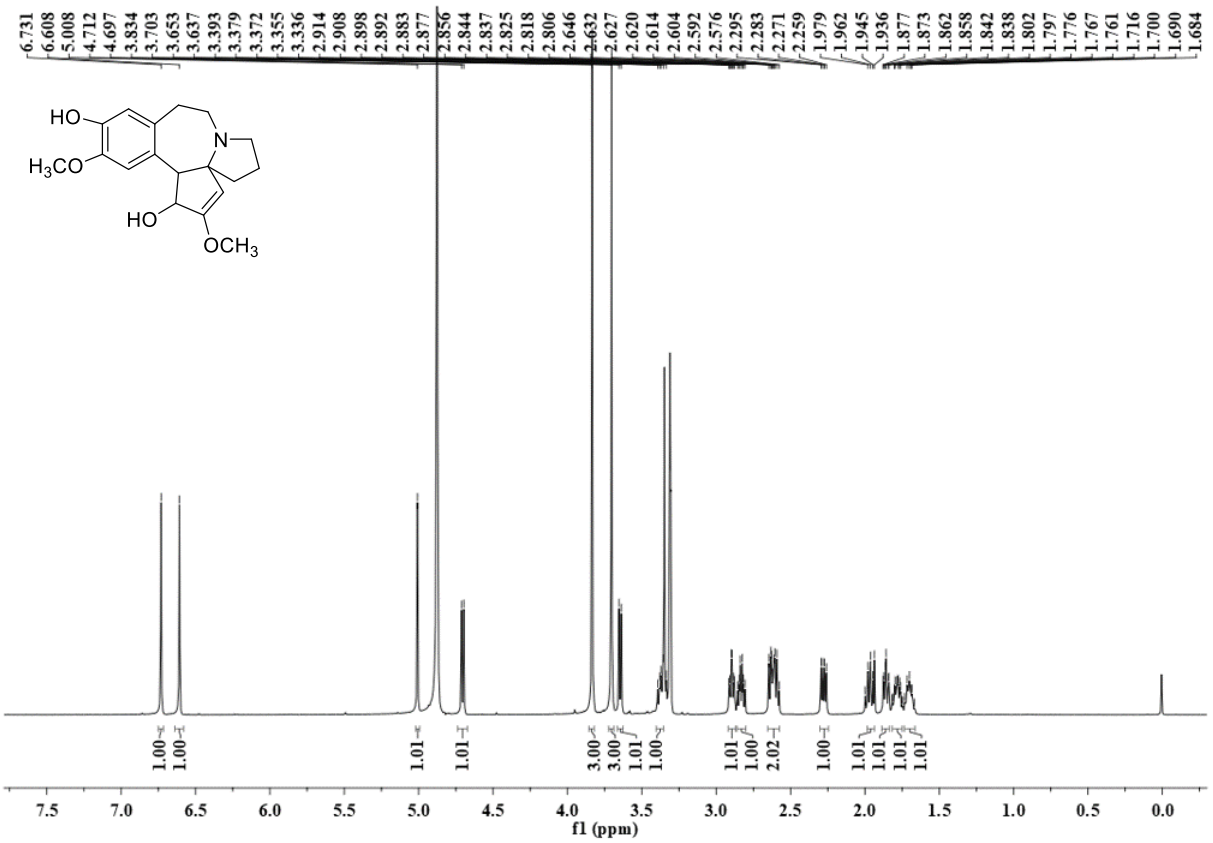

Figure S18. ^{1}H NMR (600 MHz) spectrum of **2** in CD_3OD

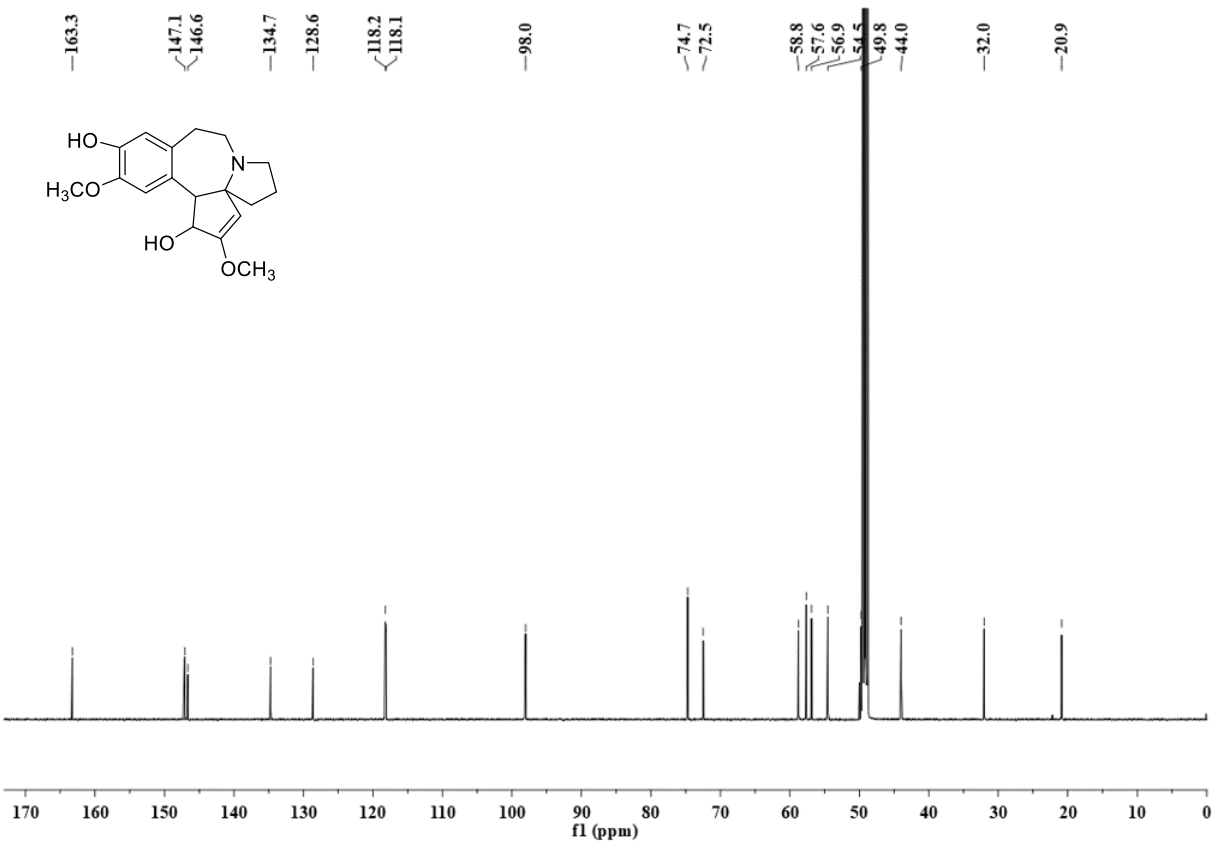

Figure S19. ^{13}C NMR (150 MHz) spectrumof **2** in CD_3OD

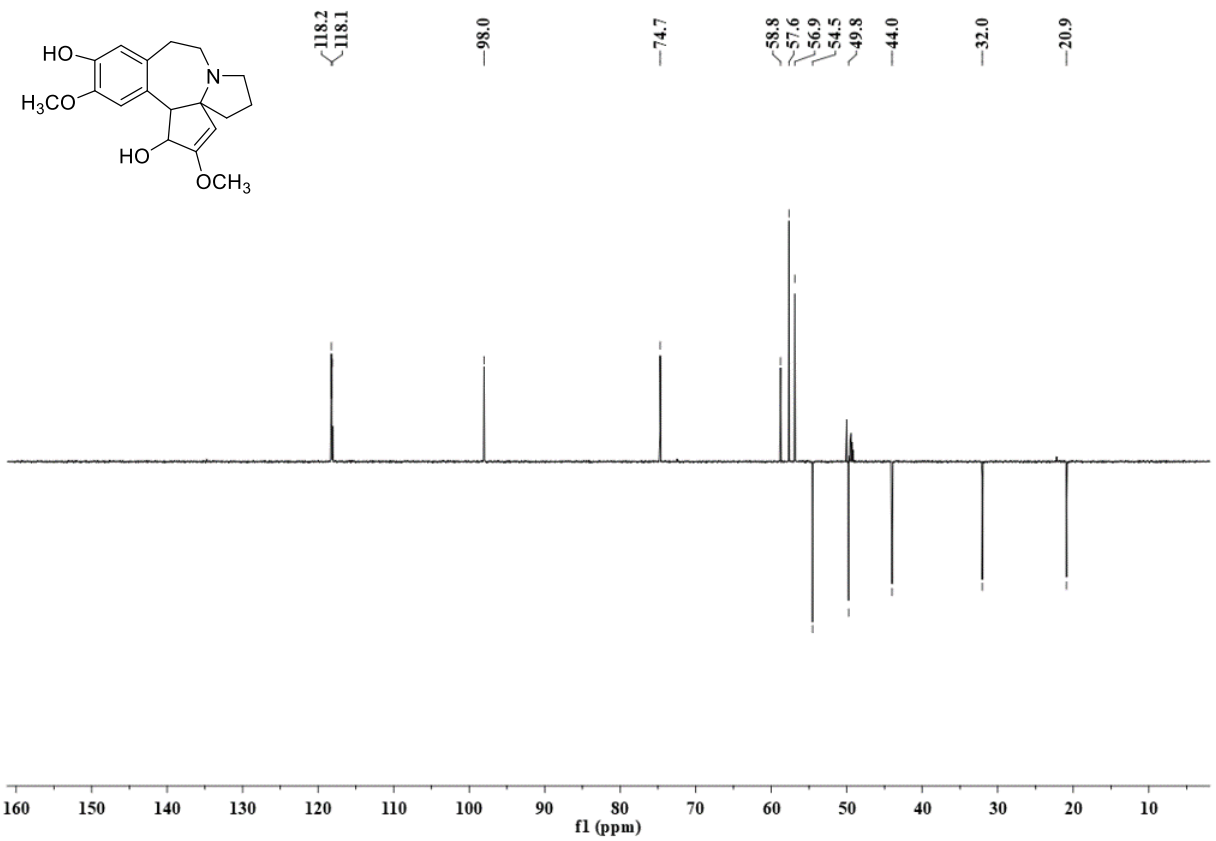

Figure S20. DEPT 135 spectrum of **2** in CD_3OD

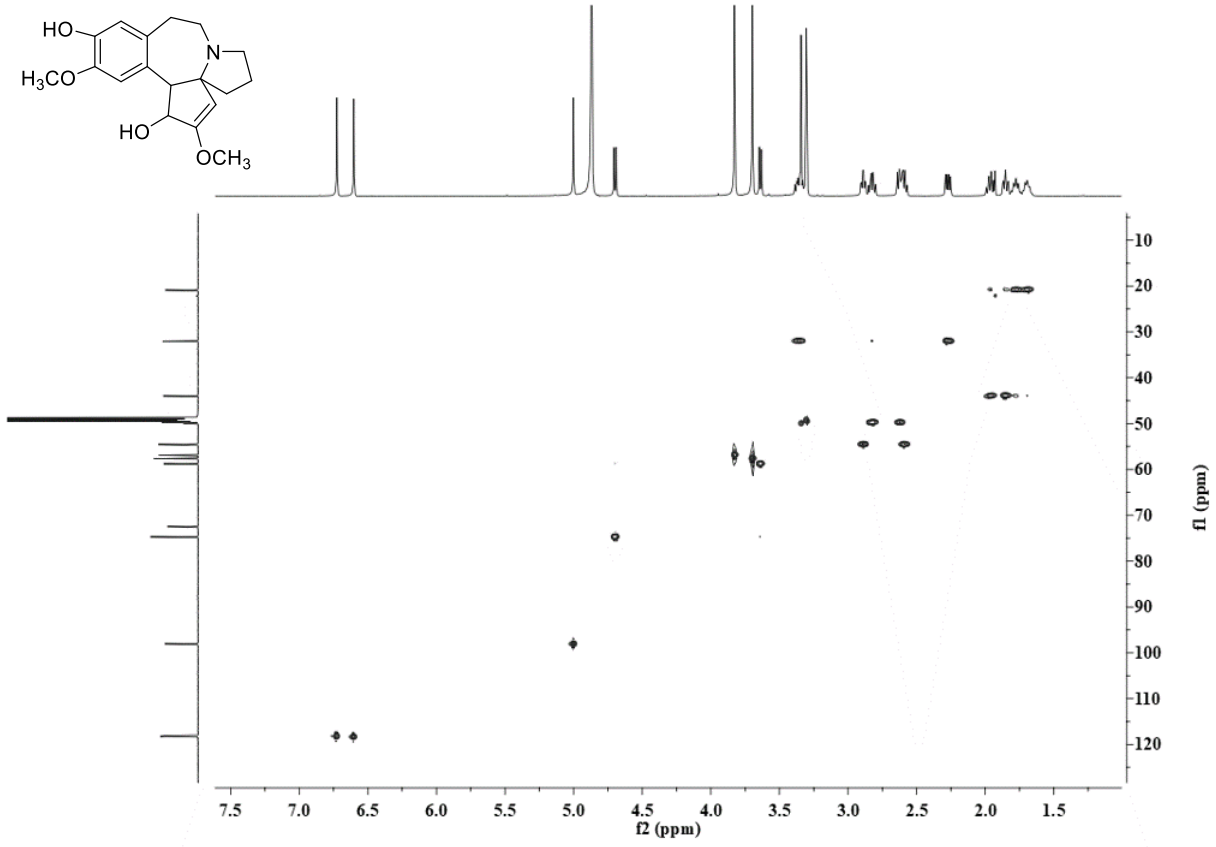

Figure S21. HSQC spectrum of **2** in CD_3OD

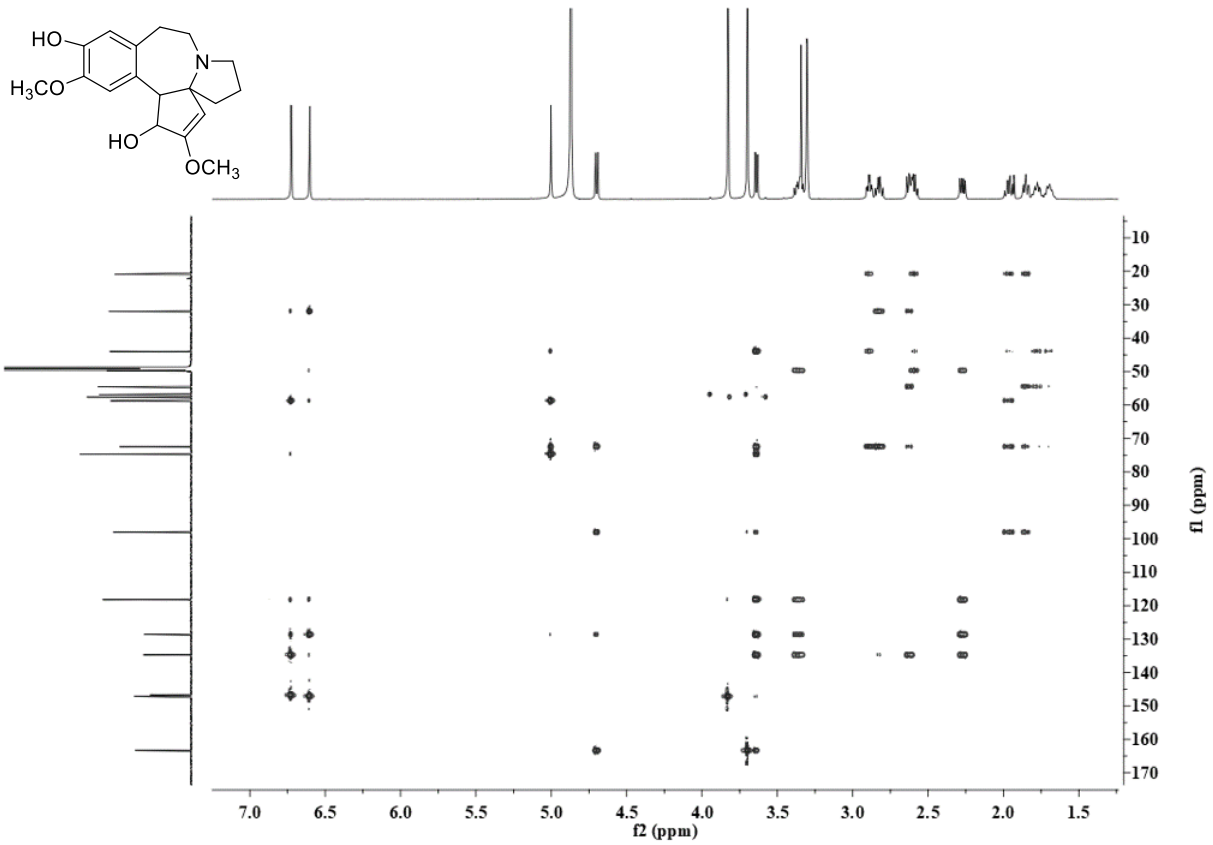

Figure S22. HMBC spectrum of **2** in CD_3OD

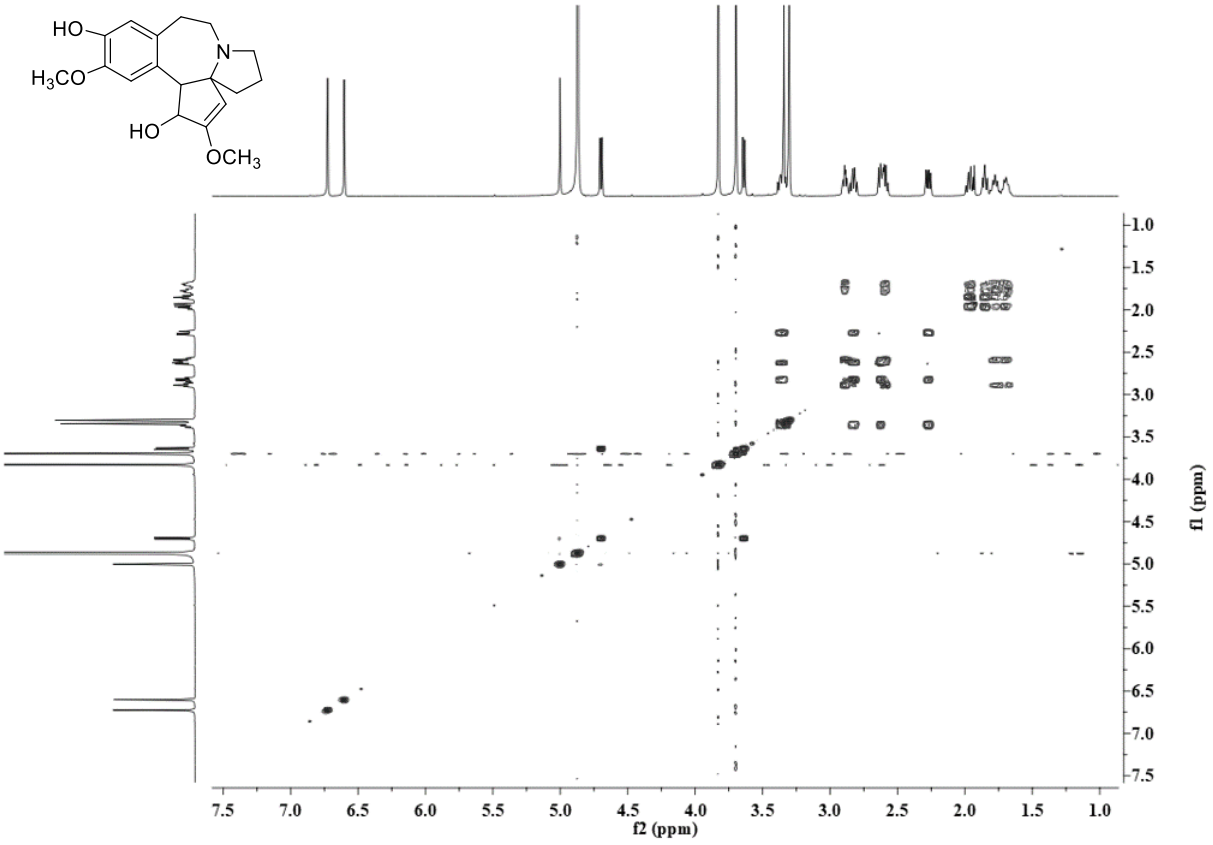

Figure S23. ^{1}H–^{1}H COSY spectrum of **2** in CD_3OD

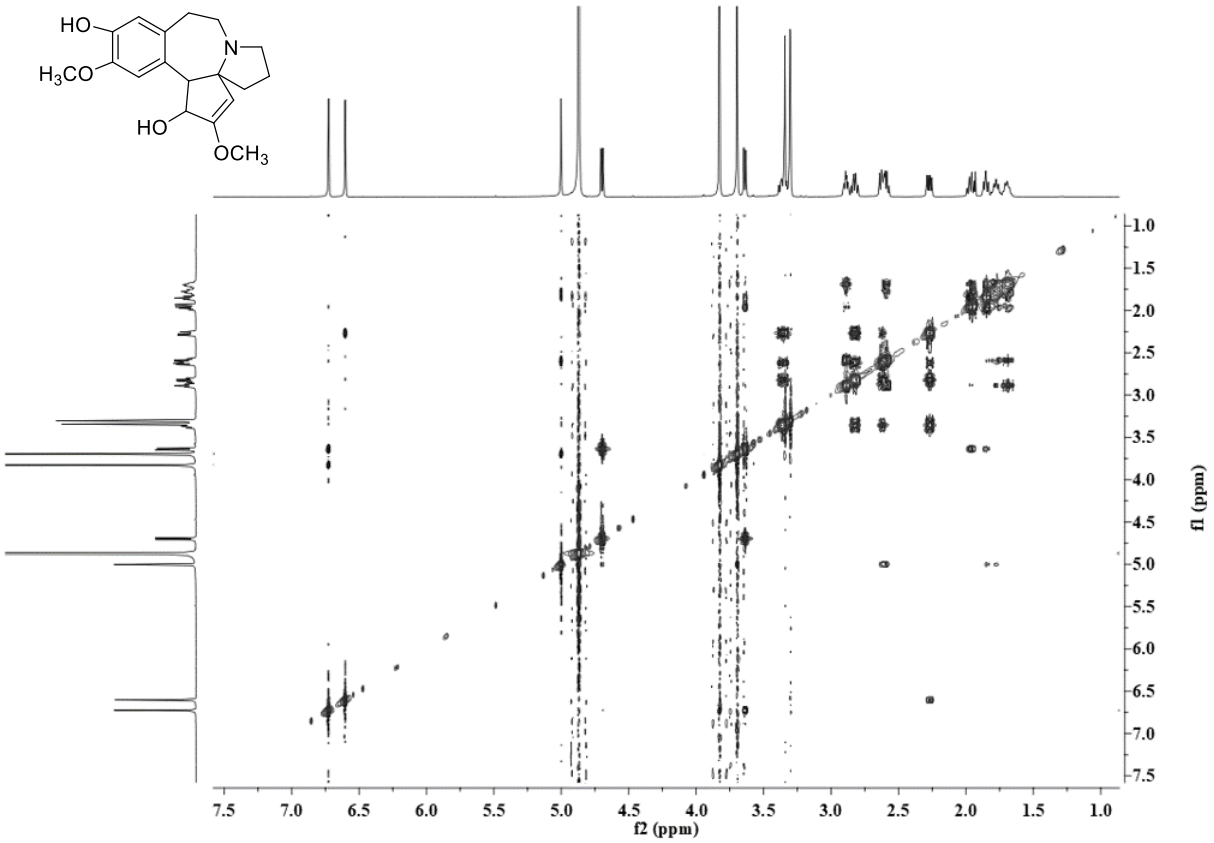

Figure S24. NOESY spectrum of **2** in CD_3OD

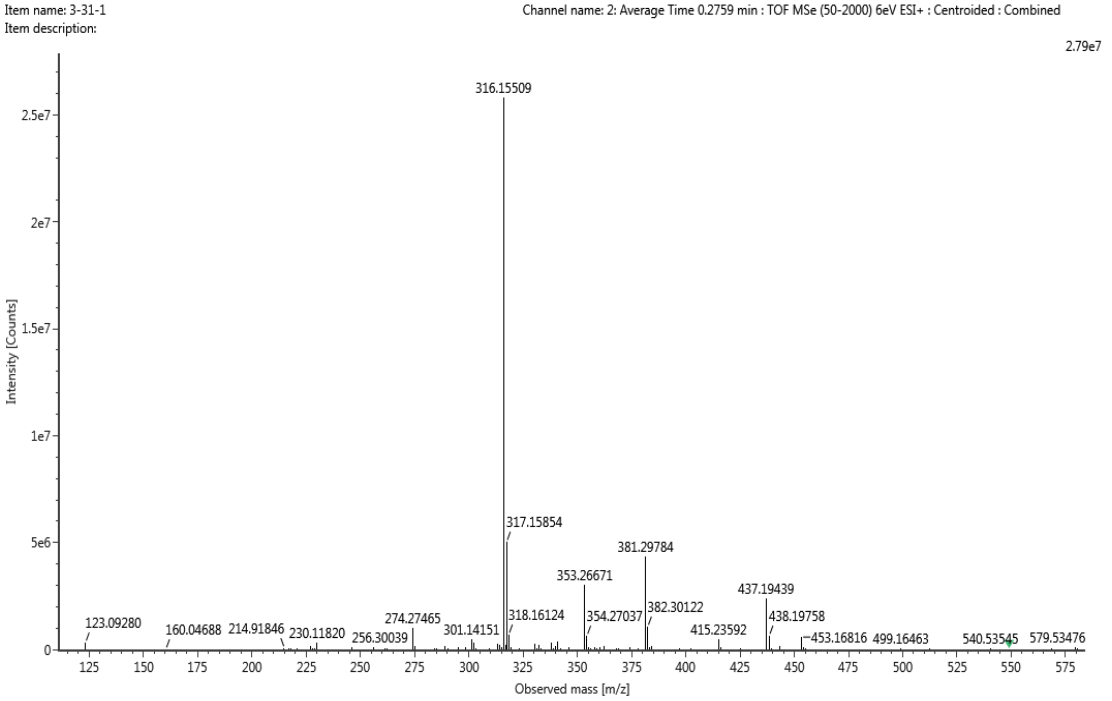

Figure S25. (+)-HR-ESI-MS spectrum of **3**

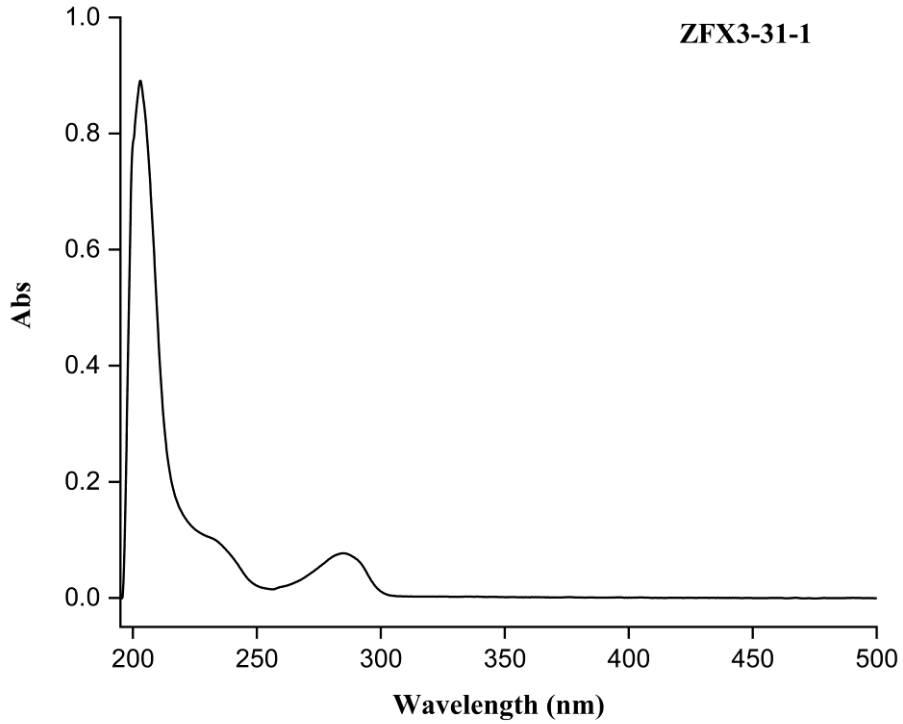

Figure S26. UV spectrum of **3** in MeOH

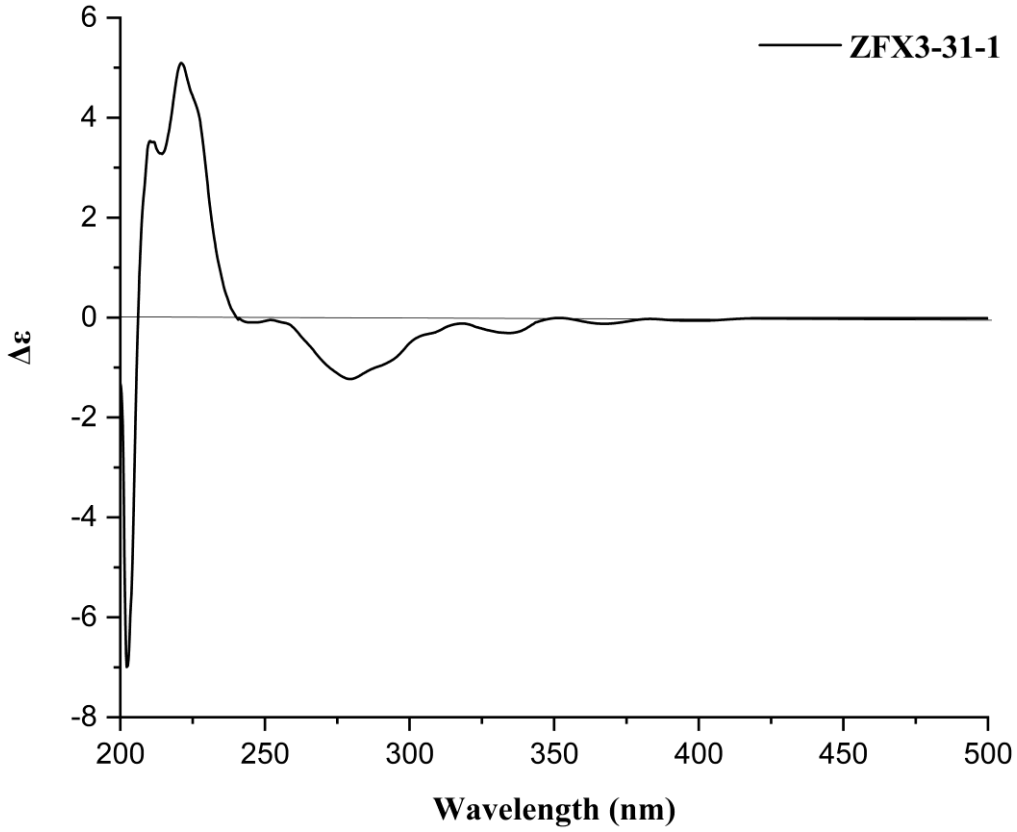

Figure S27. ECD spectrum of **3** in MeOH

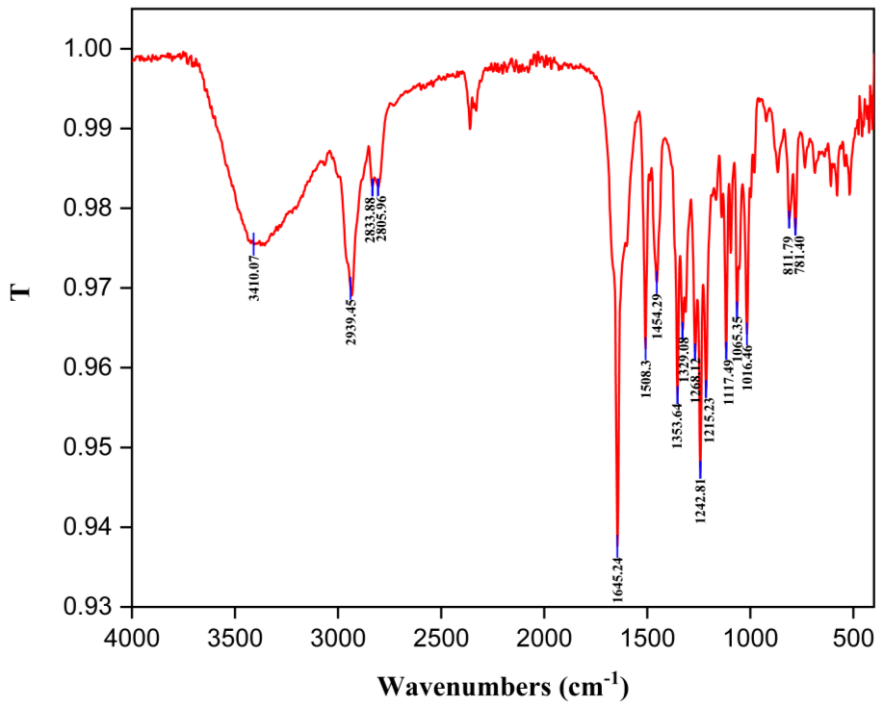

Figure S28. IR spectrum of **3**

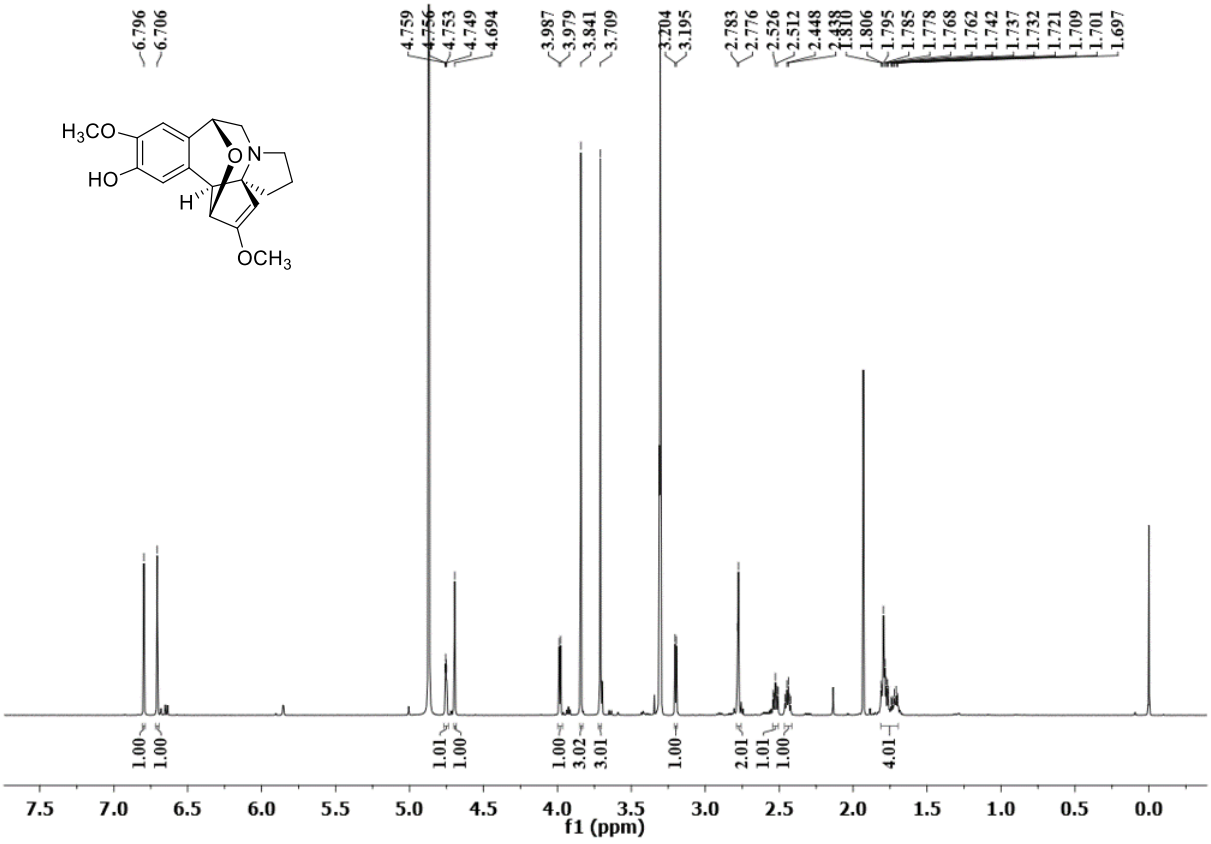

Figure S29. ^{1}H NMR (600 MHz) spectrum of **3** in CD_3OD

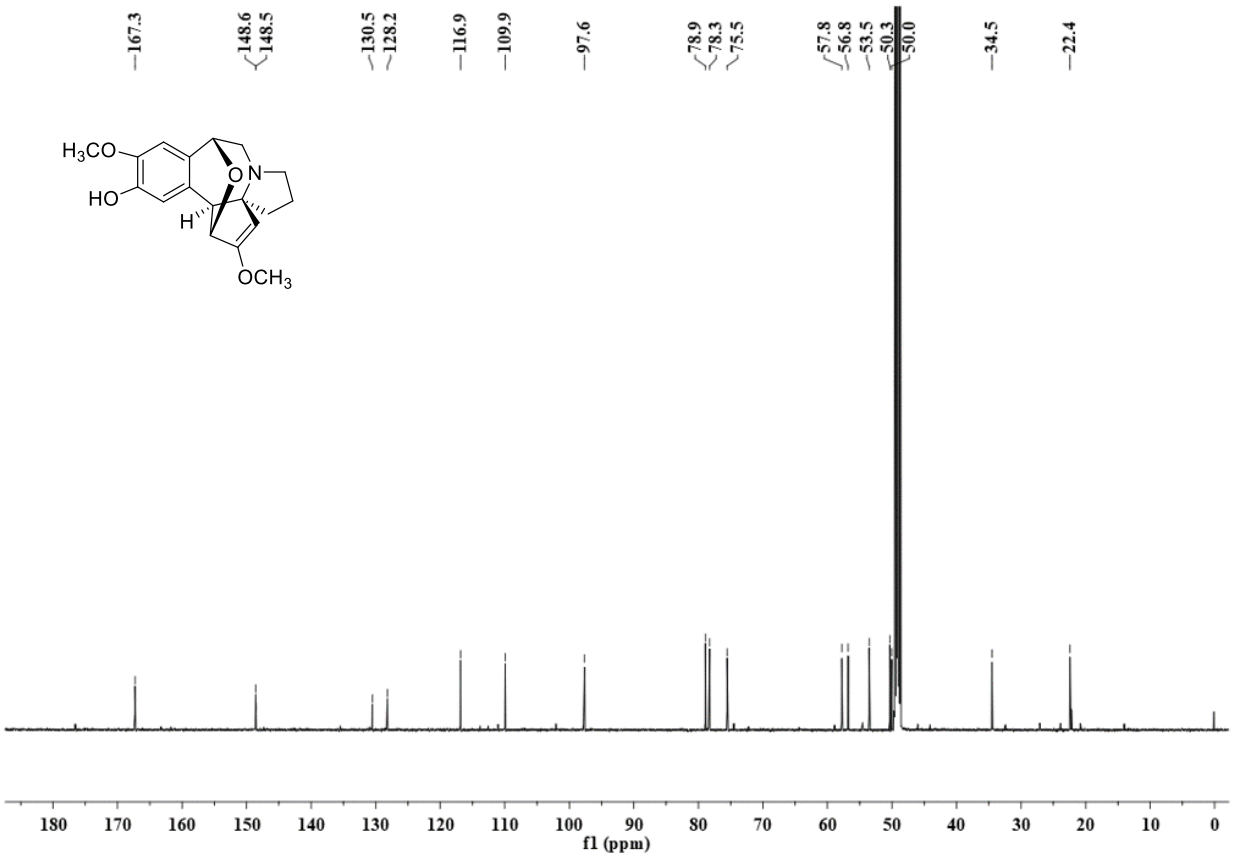

Figure S30. ^{13}C NMR (150 MHz) spectrumof **3** in CD_3OD

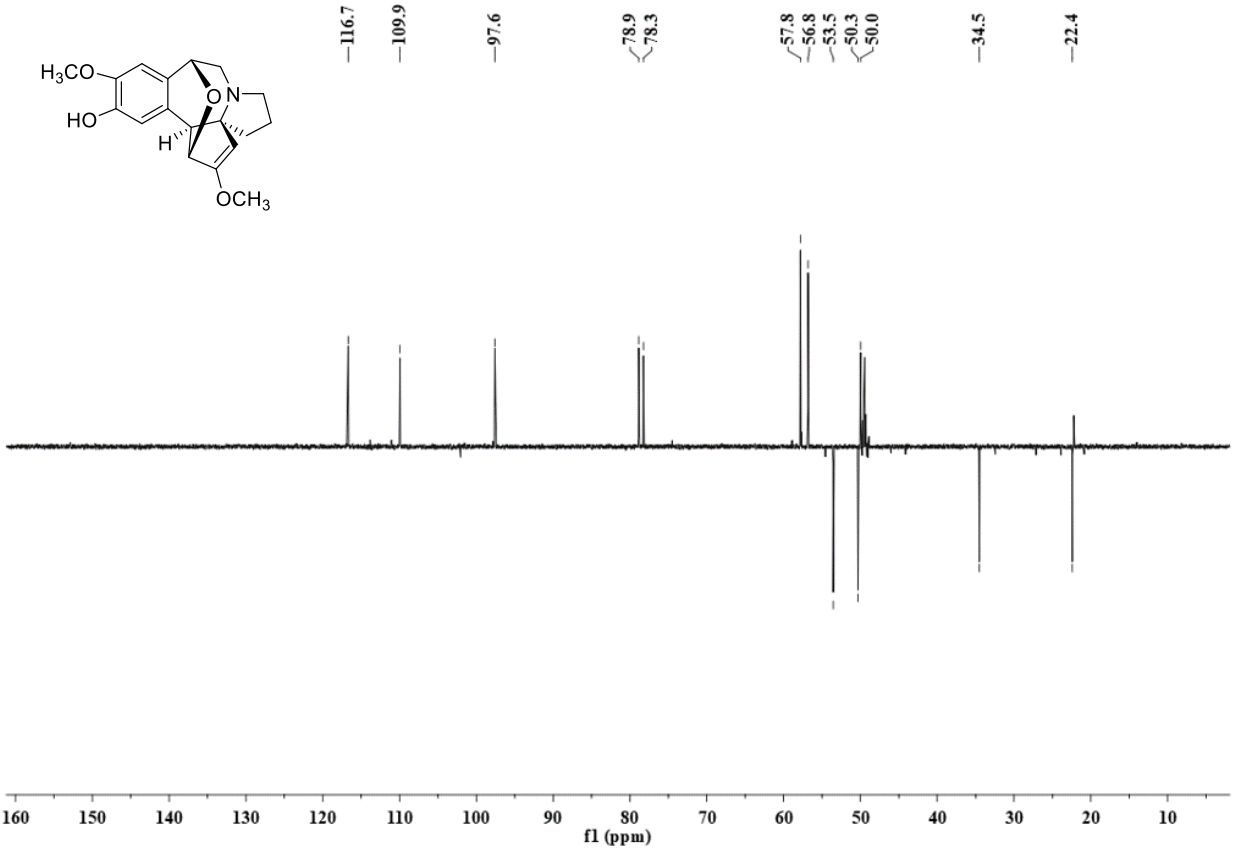

Figure S31. DEPT 135 spectrum of **3** in CD_3OD

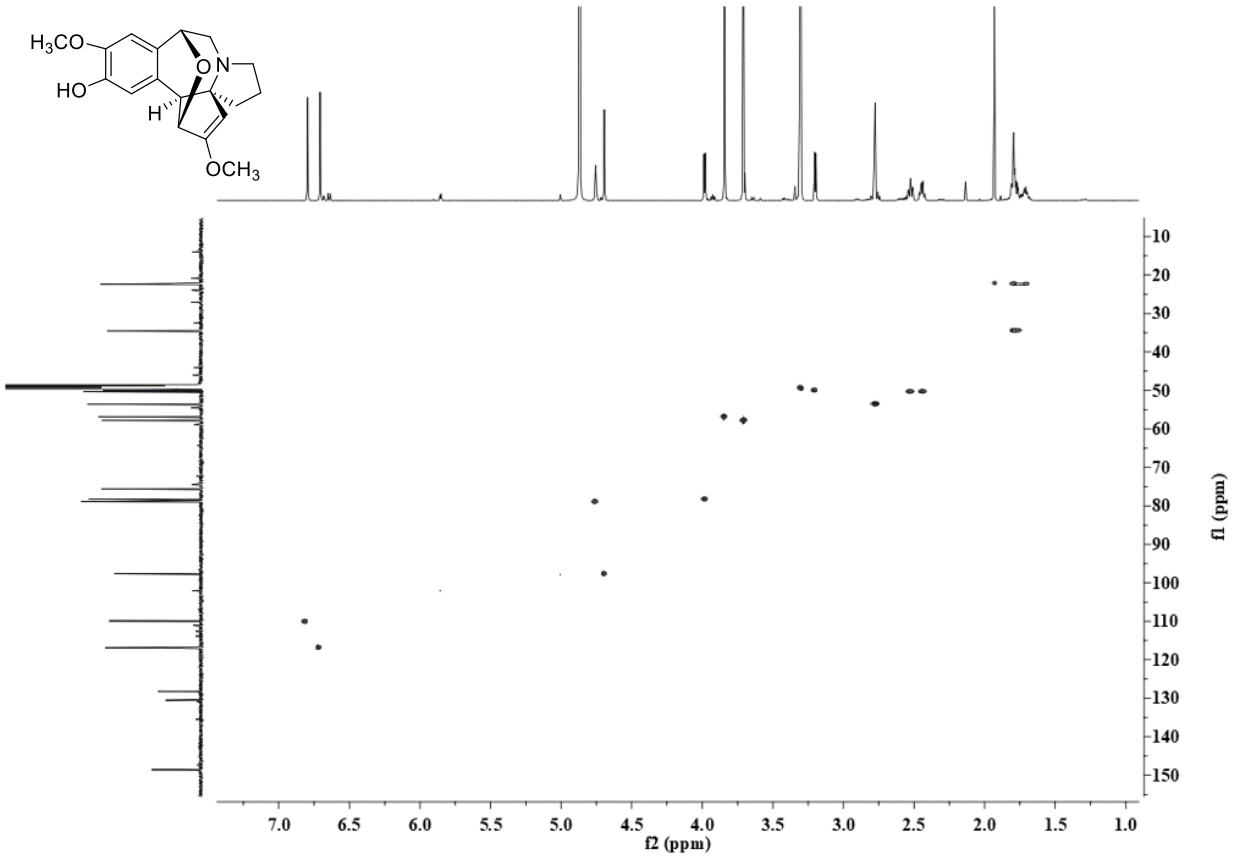

Figure S32. HSQC spectrum of **3** in CD_3OD

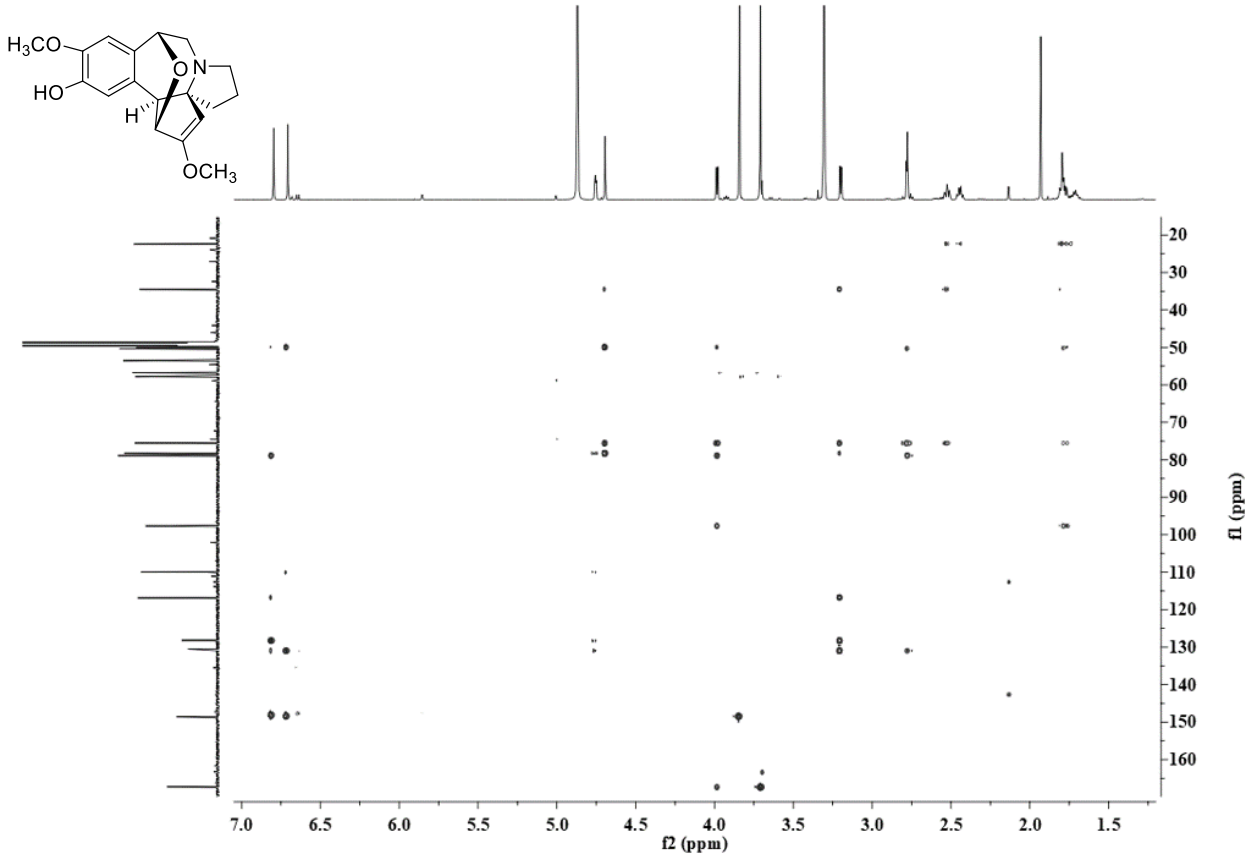

Figure S33. HMBC spectrum of **3** in CD_3OD

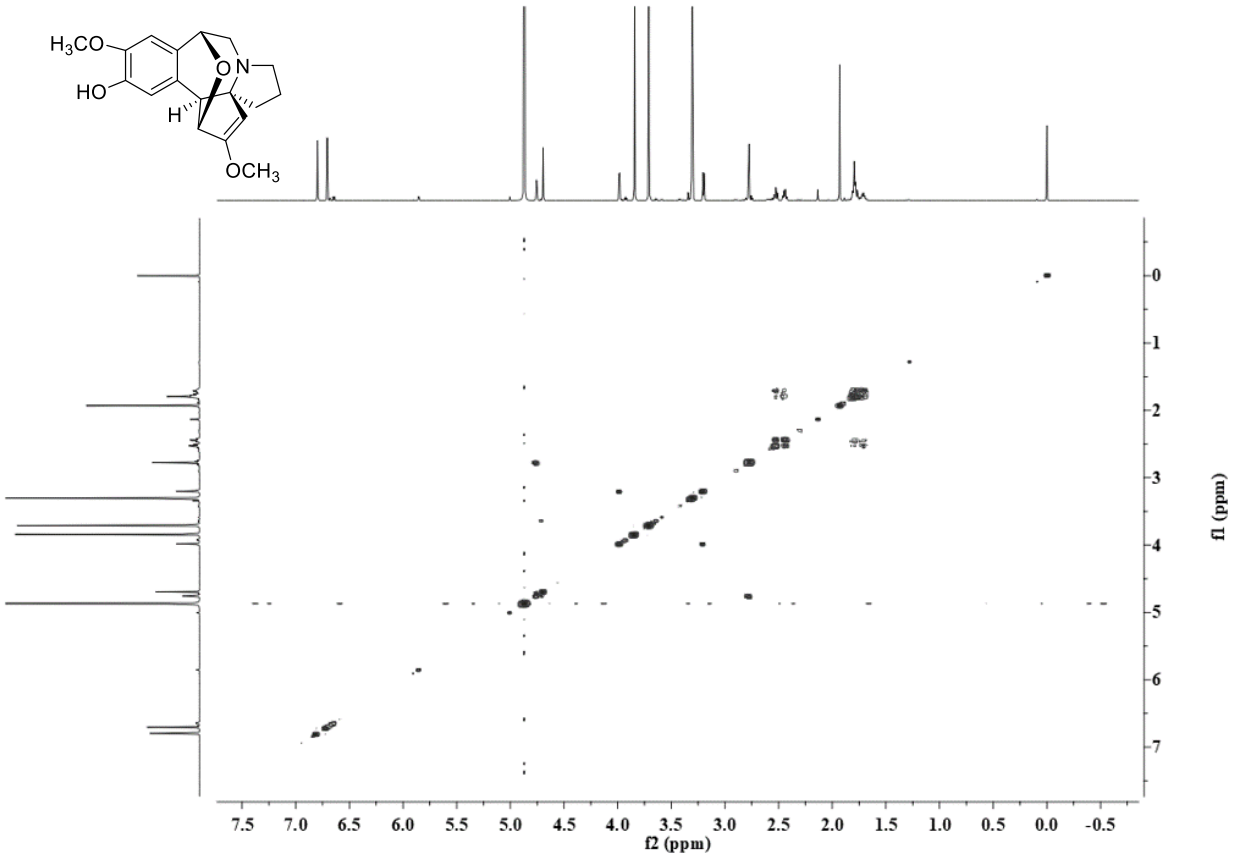

Figure S34. $^{1}H–^{1}H$ COSY spectrum of **3** in CD_3OD

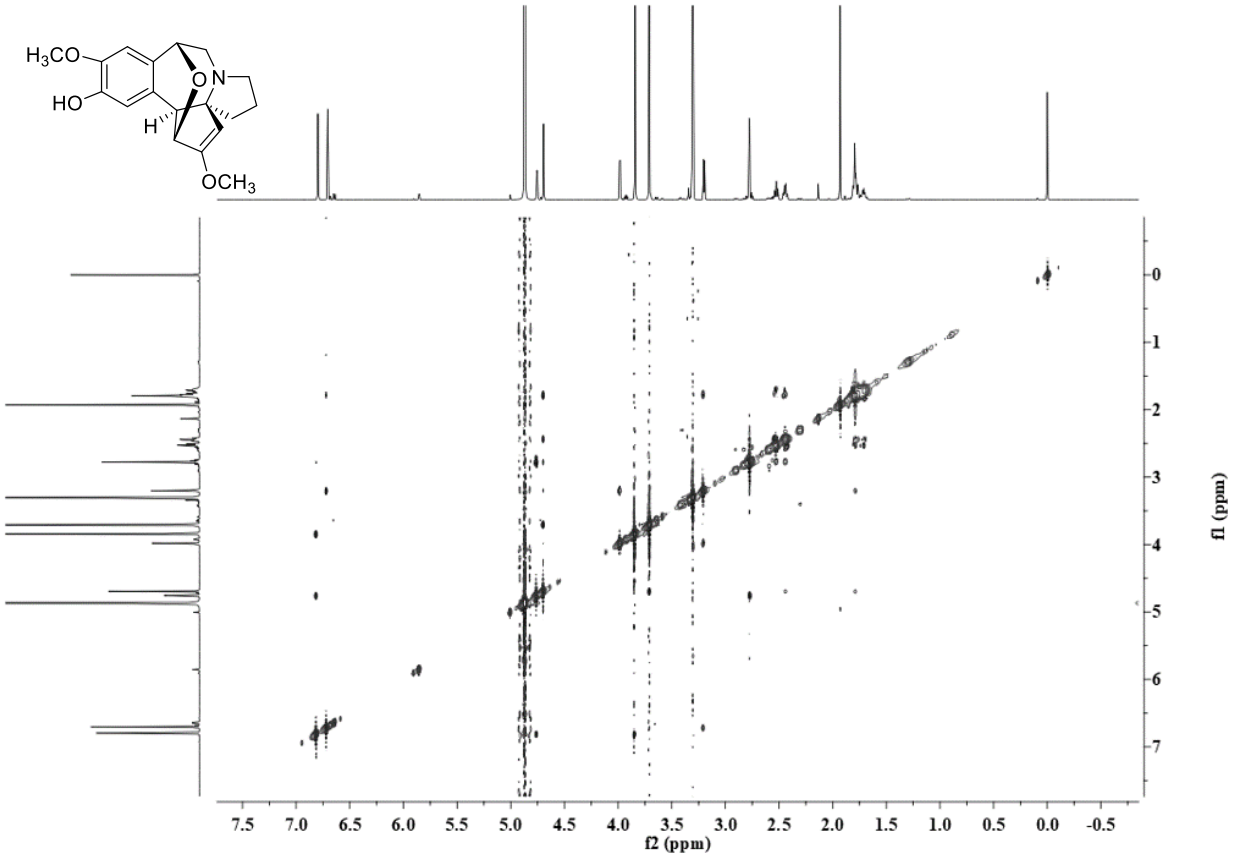

Figure S35. NOESY spectrum of **3** in CD_3OD

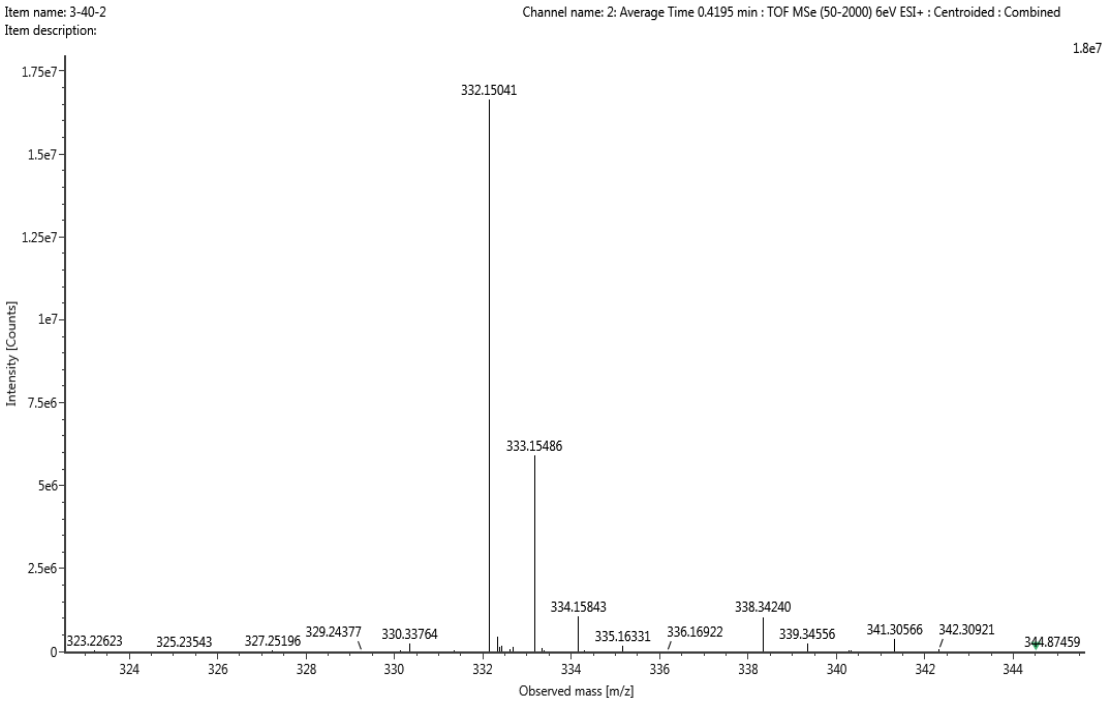

Figure S36. (+)-HR-ESI-MS spectrum of **4**

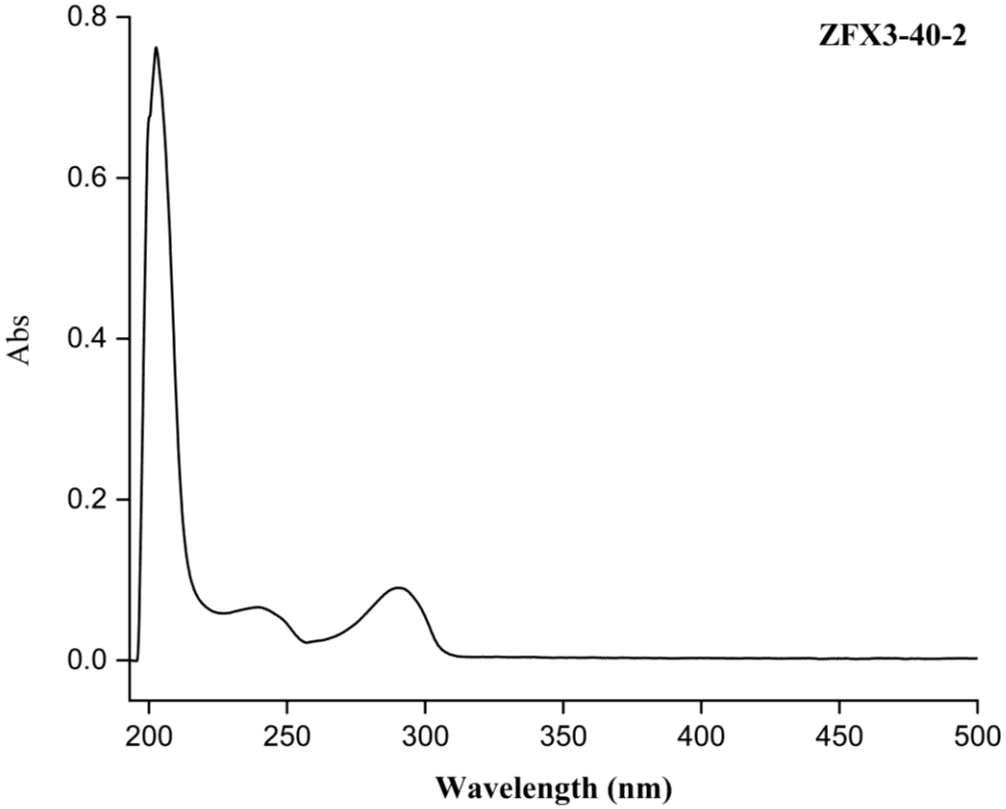

Figure S37. UV spectrum of **4** in MeOH

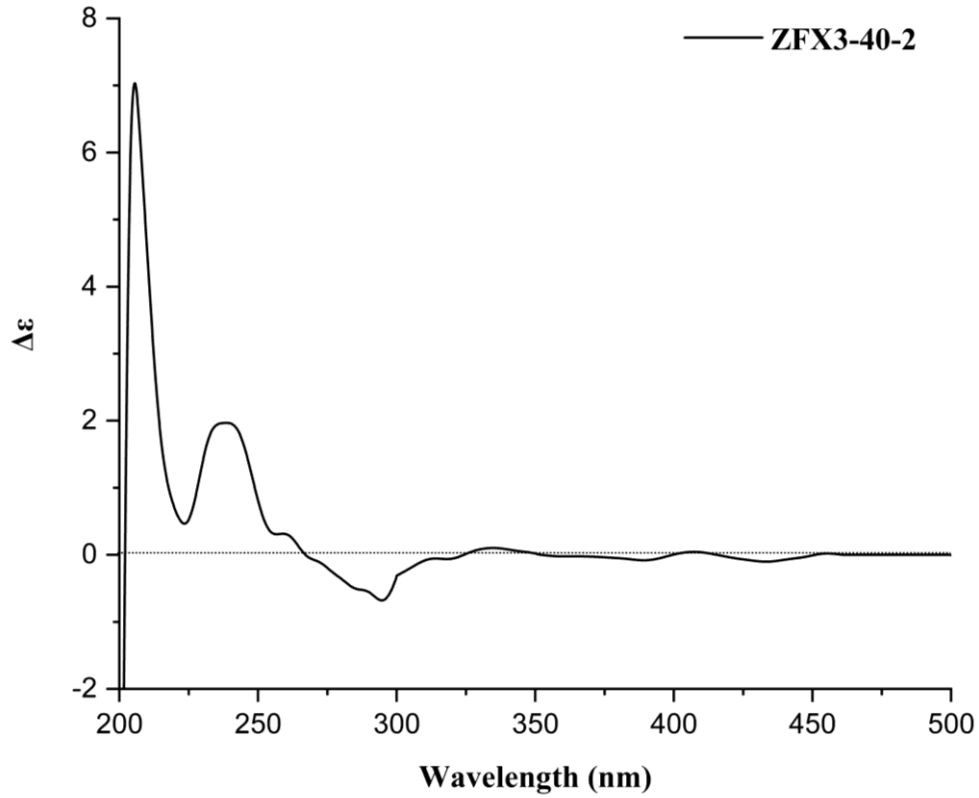

Figure S38. ECD spectrum of **4** in MeOH

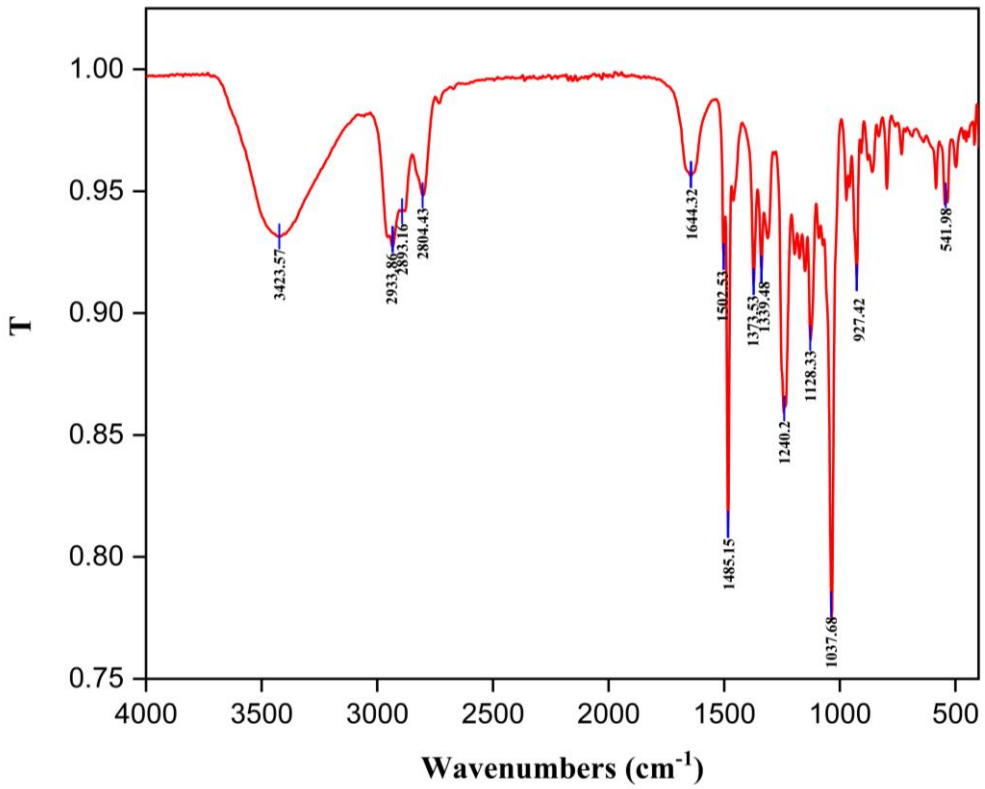

Figure S39. IR spectrum of **4**

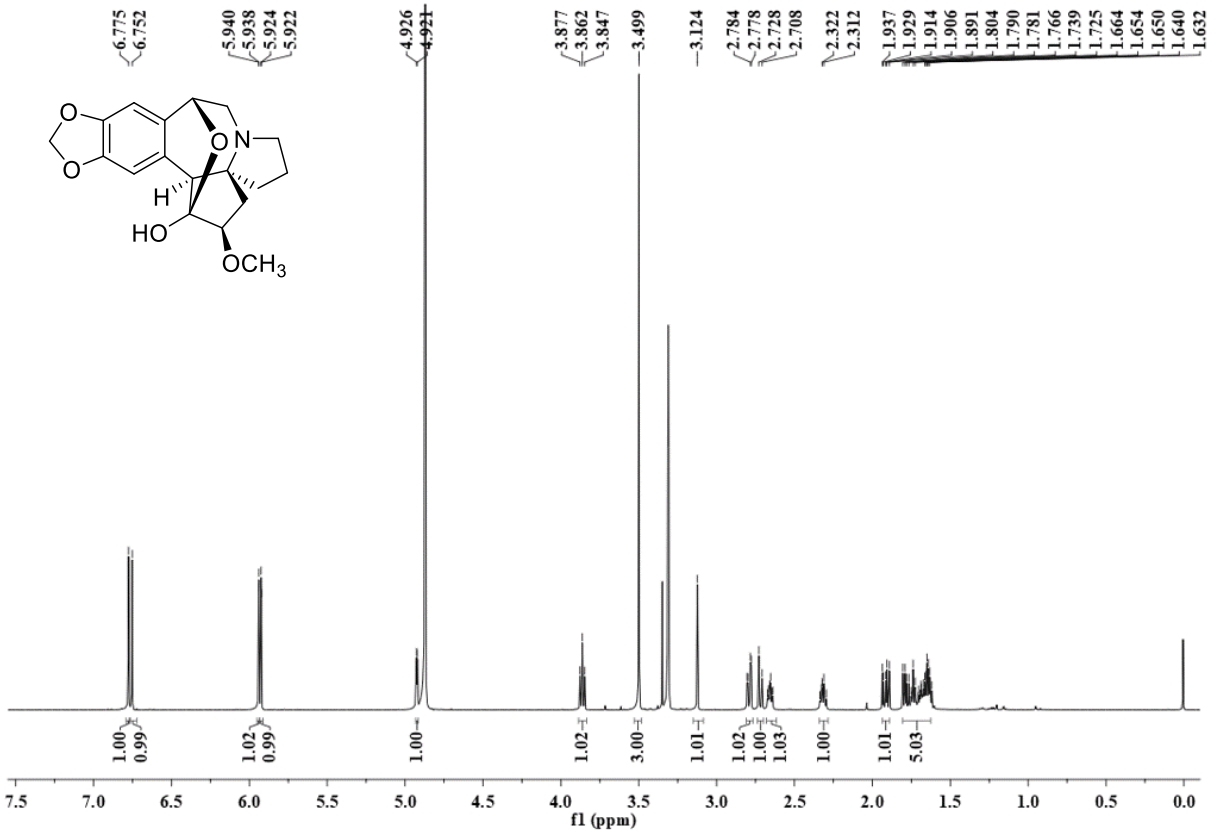

Figure S40. ^{1}H NMR (600 MHz) spectrum of **4** in CD_3OD

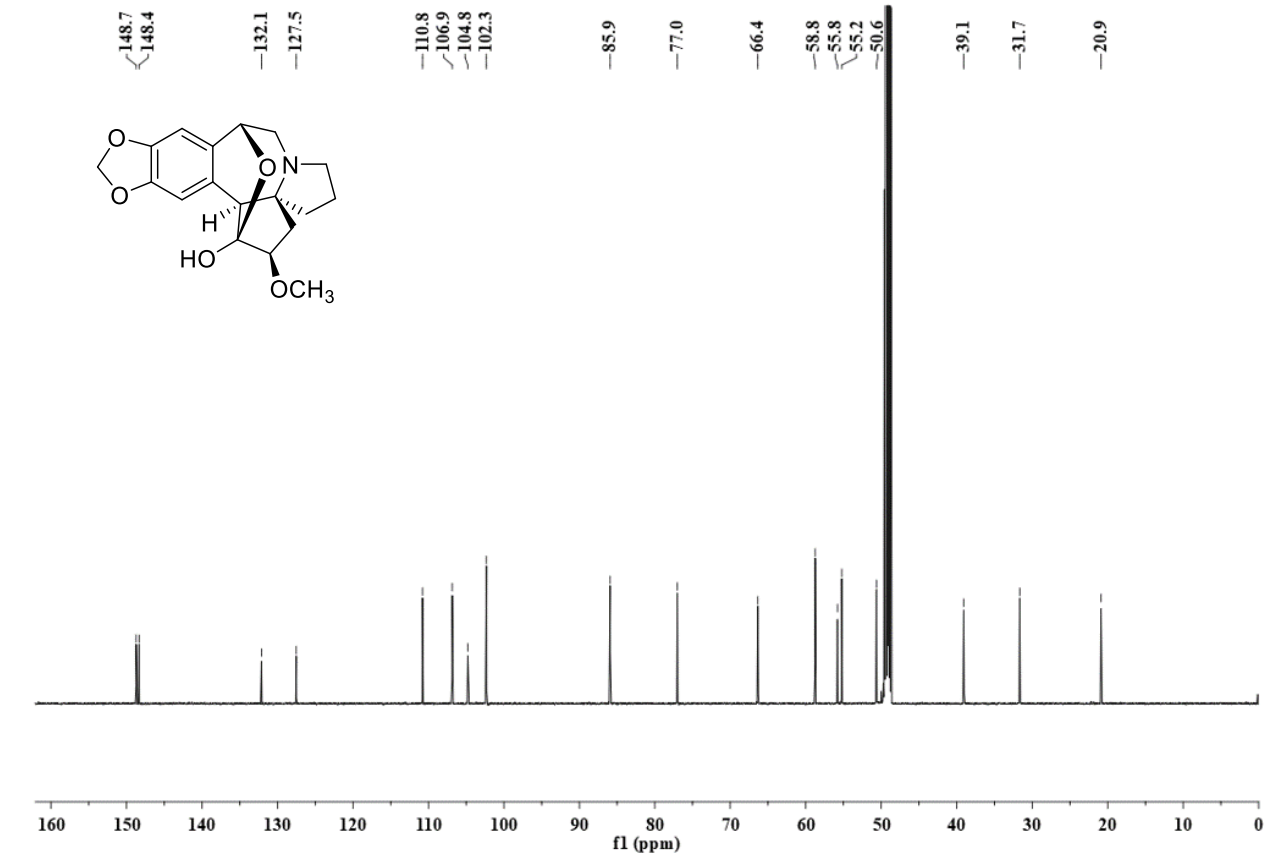

Figure S41. ^{13}C NMR (150 MHz) spectrumof **4** in CD_3OD

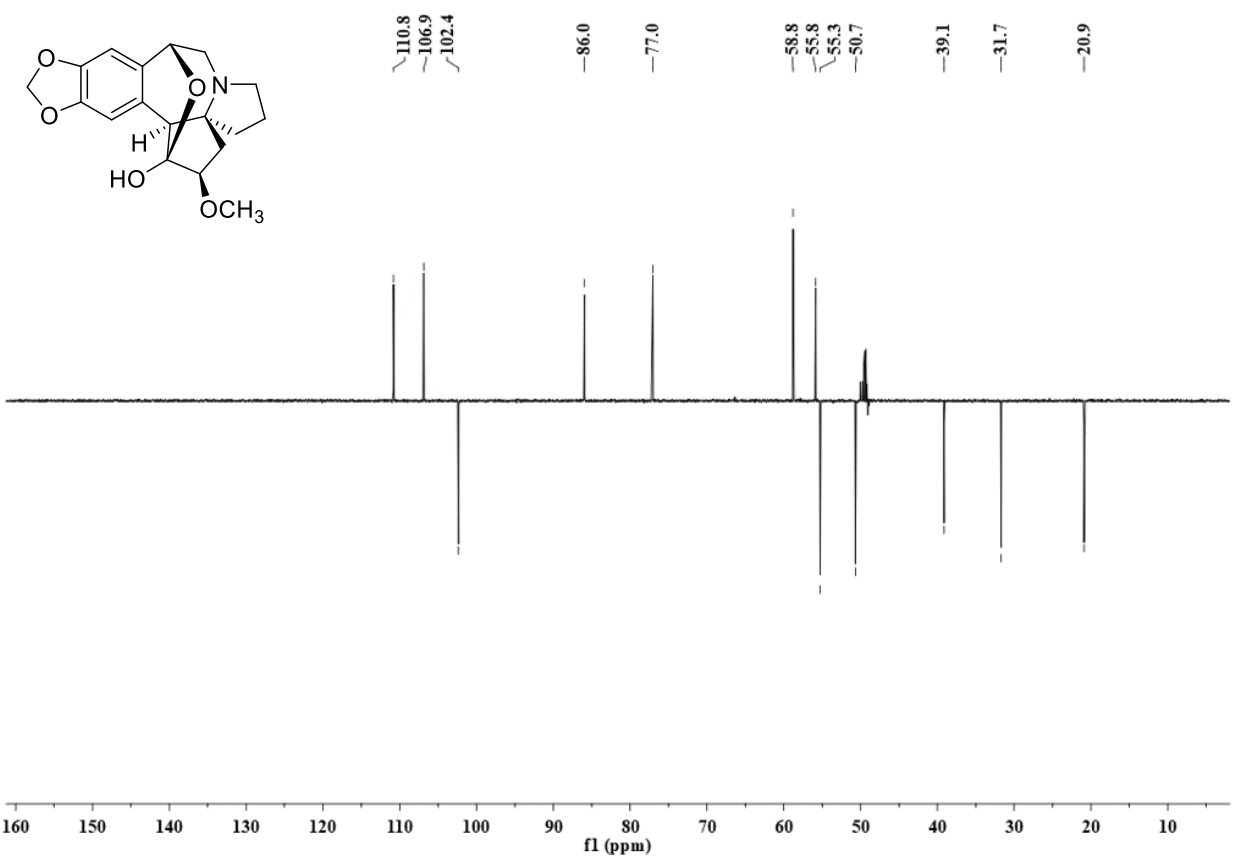

Figure S42. DEPT 135 spectrum of **4** in CD_3OD

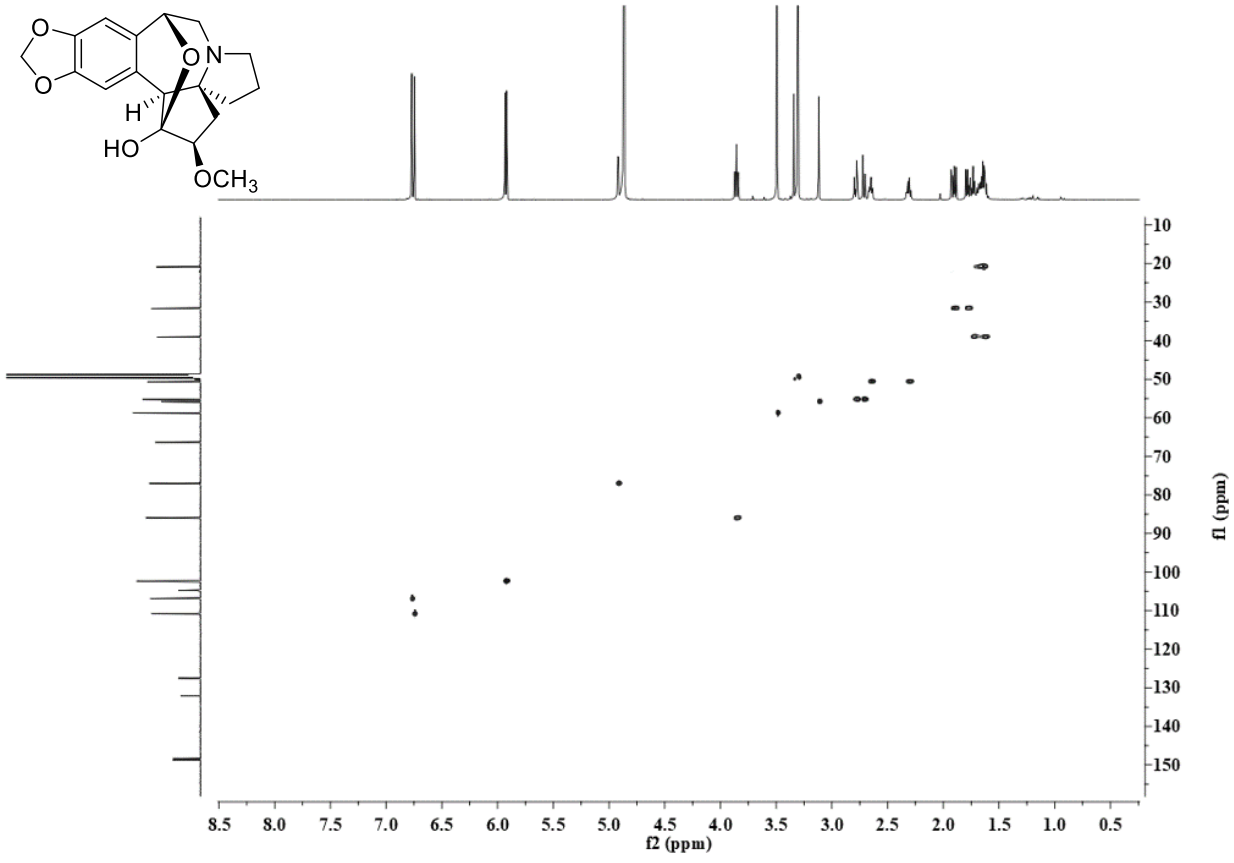

Figure S43. HSQC spectrum of **4** in CD_3OD

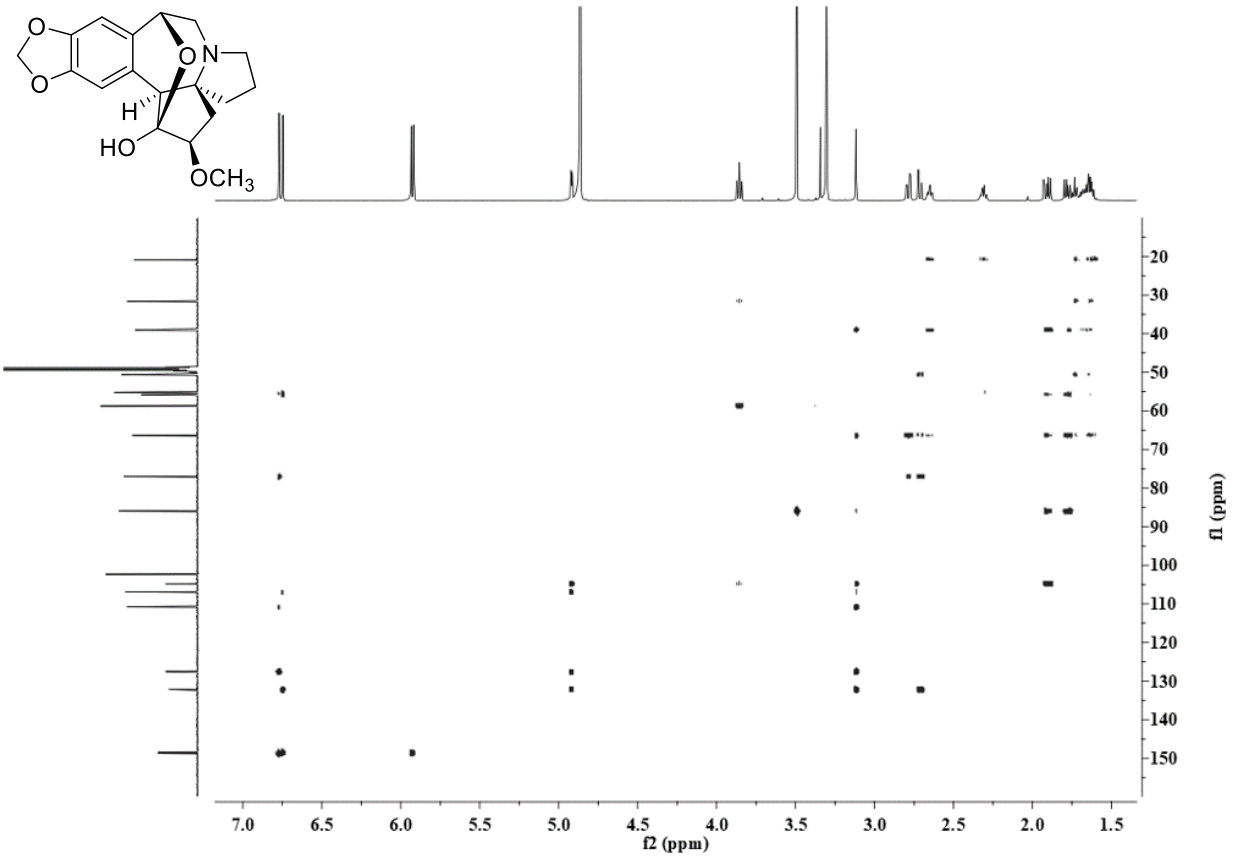

Figure S44. HMBC spectrum of **4** in CD_3OD

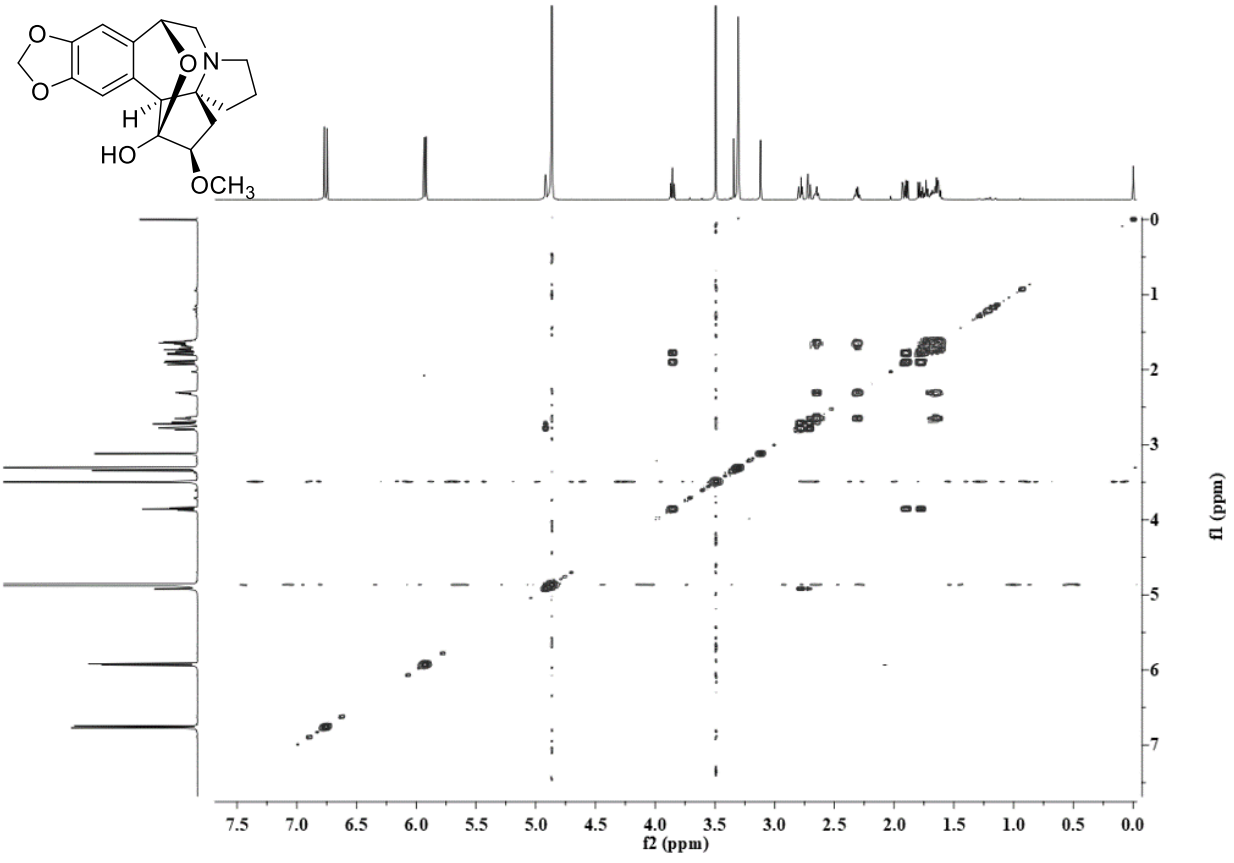

Figure S45. ^{1}H-^{1}H COSY spectrum of **4** in CD_3OD

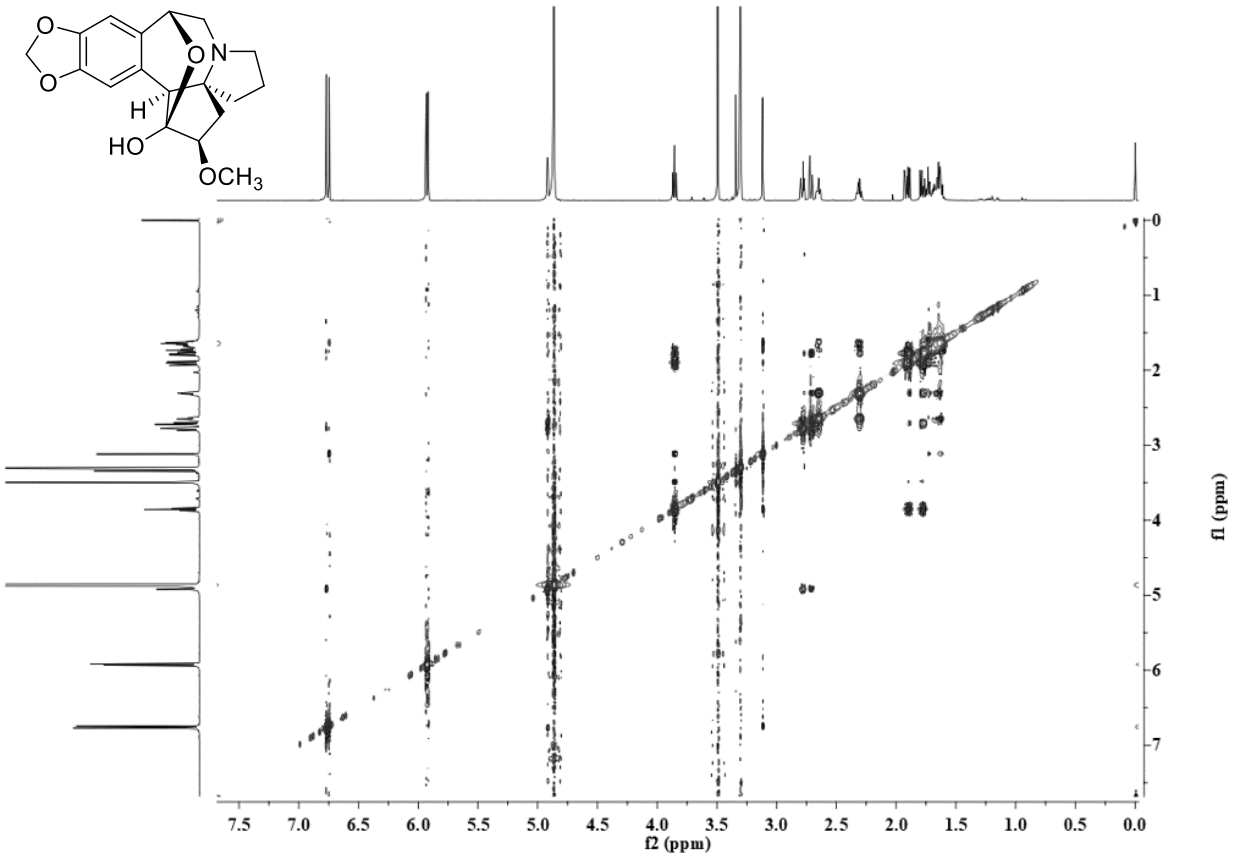

Figure S46. NOESY spectrum of **4** in CD_3OD

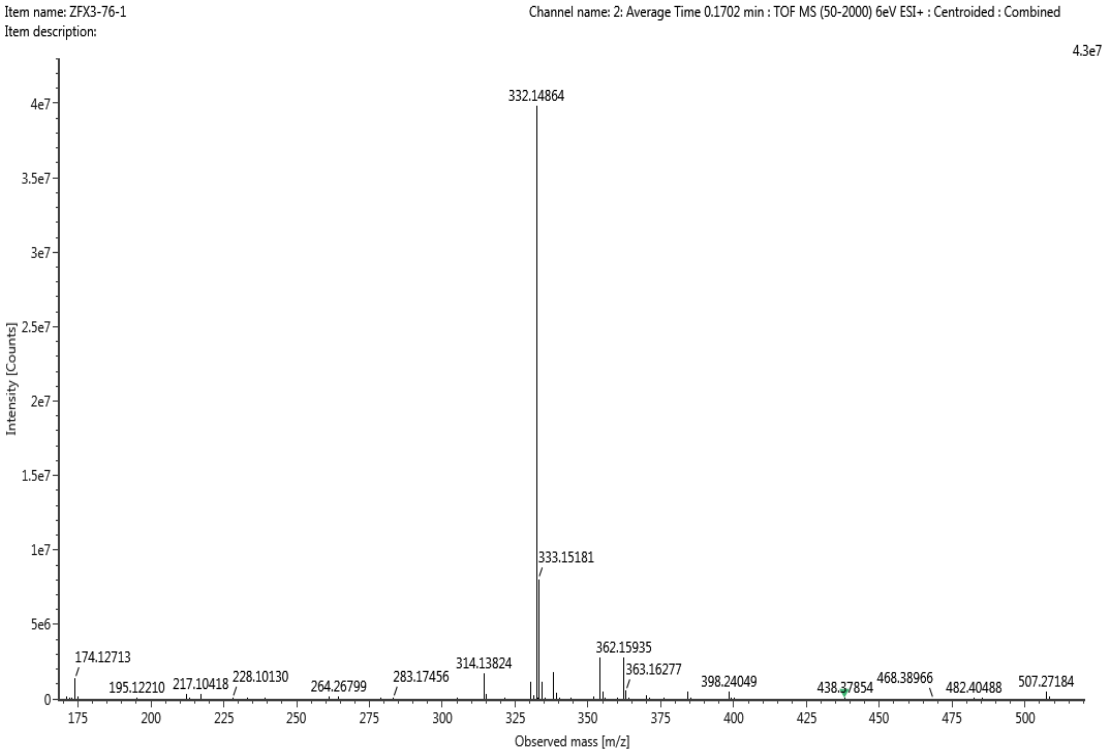

Figure S47. (+)-HR-ESI-MS spectrum of **5**

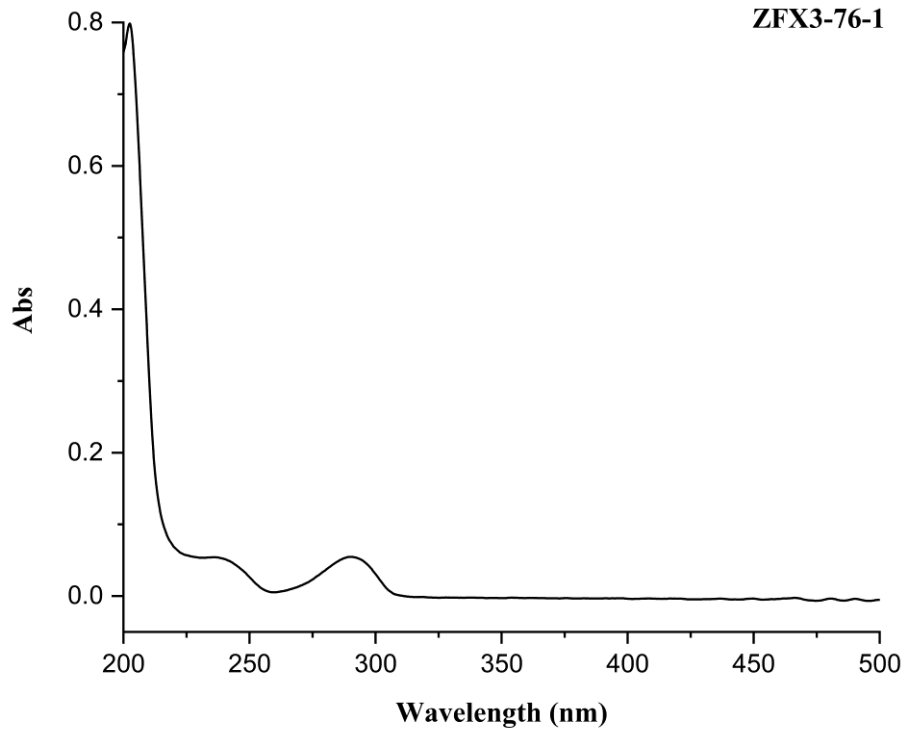

Figure S48. UV spectrum of **5** in MeOH

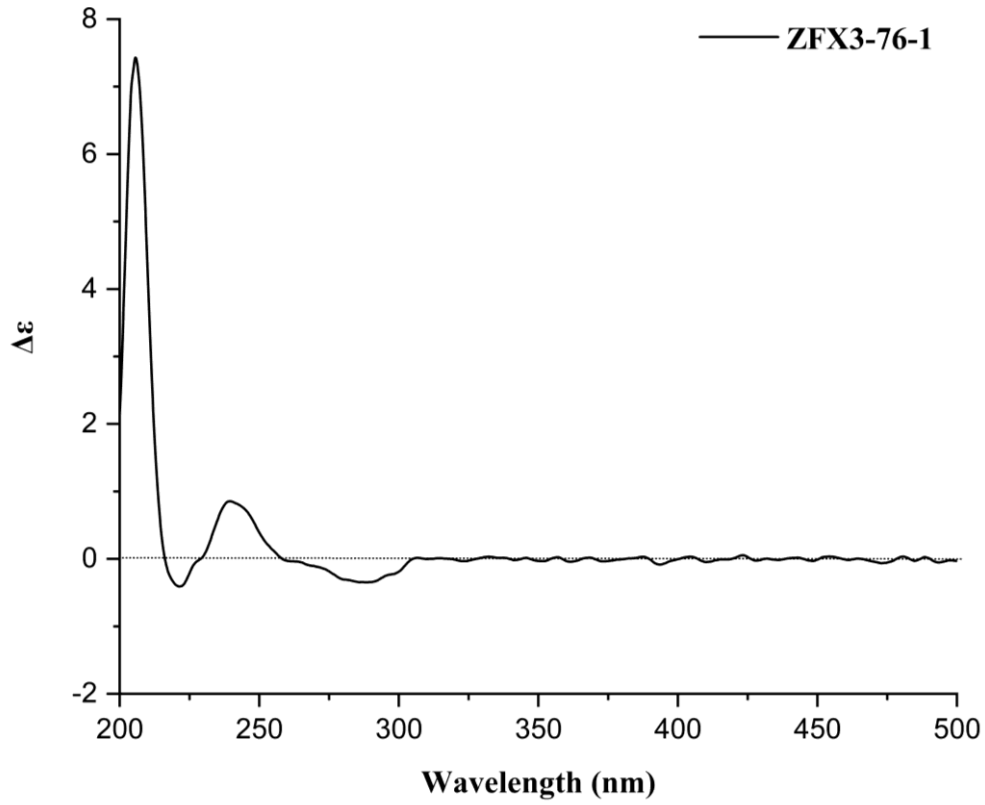

Figure S49. ECD spectrum of **5** in MeOH

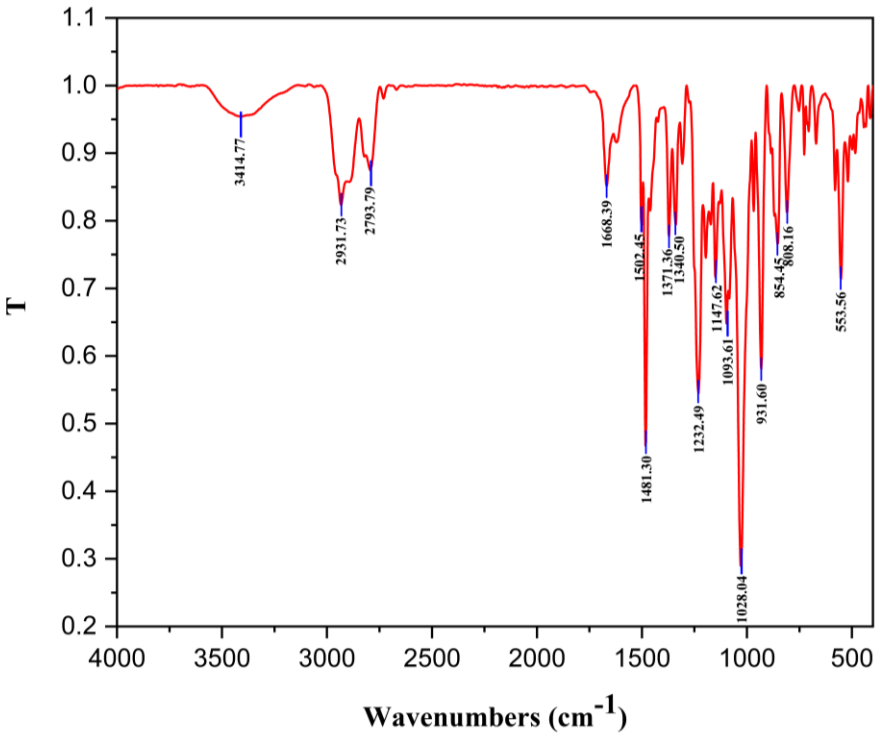

Figure S50. IR spectrum of **5**

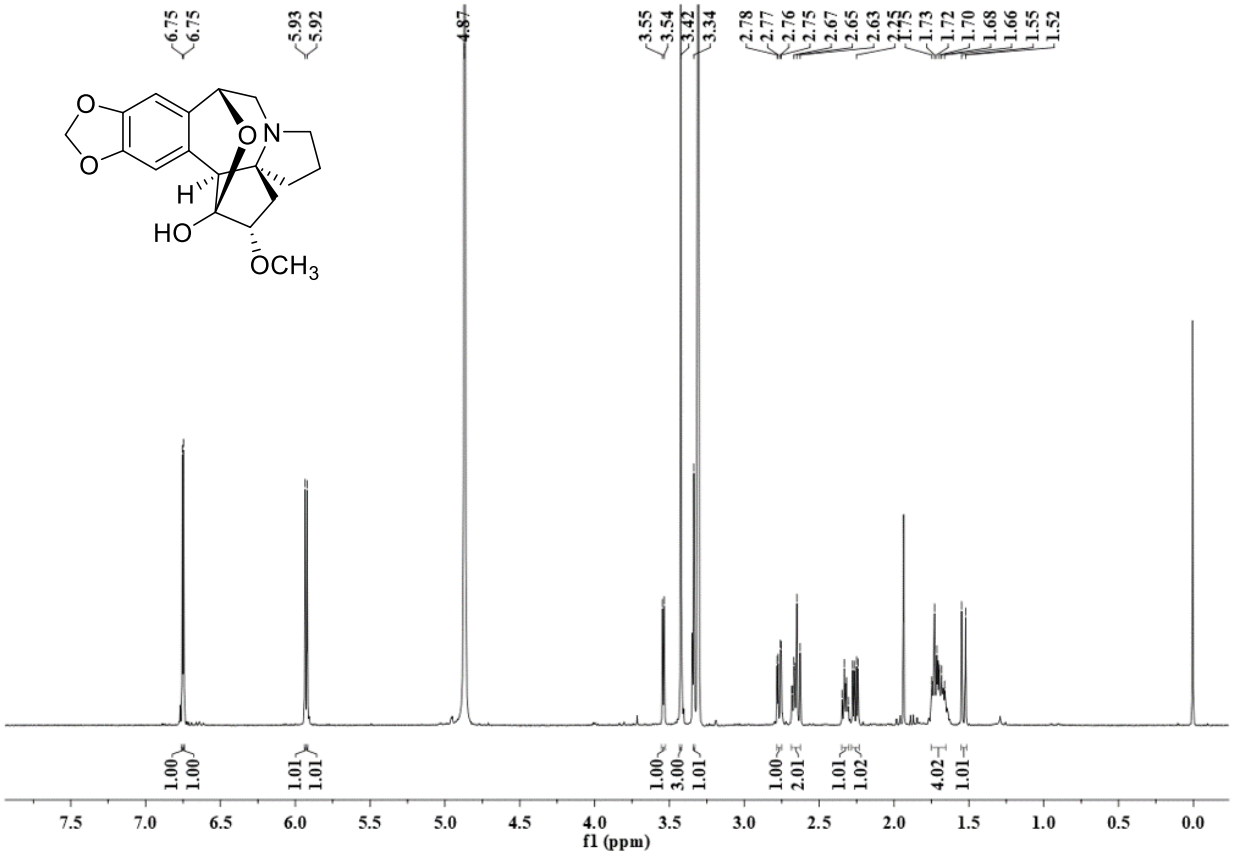

Figure S51. ^{1}H NMR (600 MHz) spectrum of **5** in CD_3OD

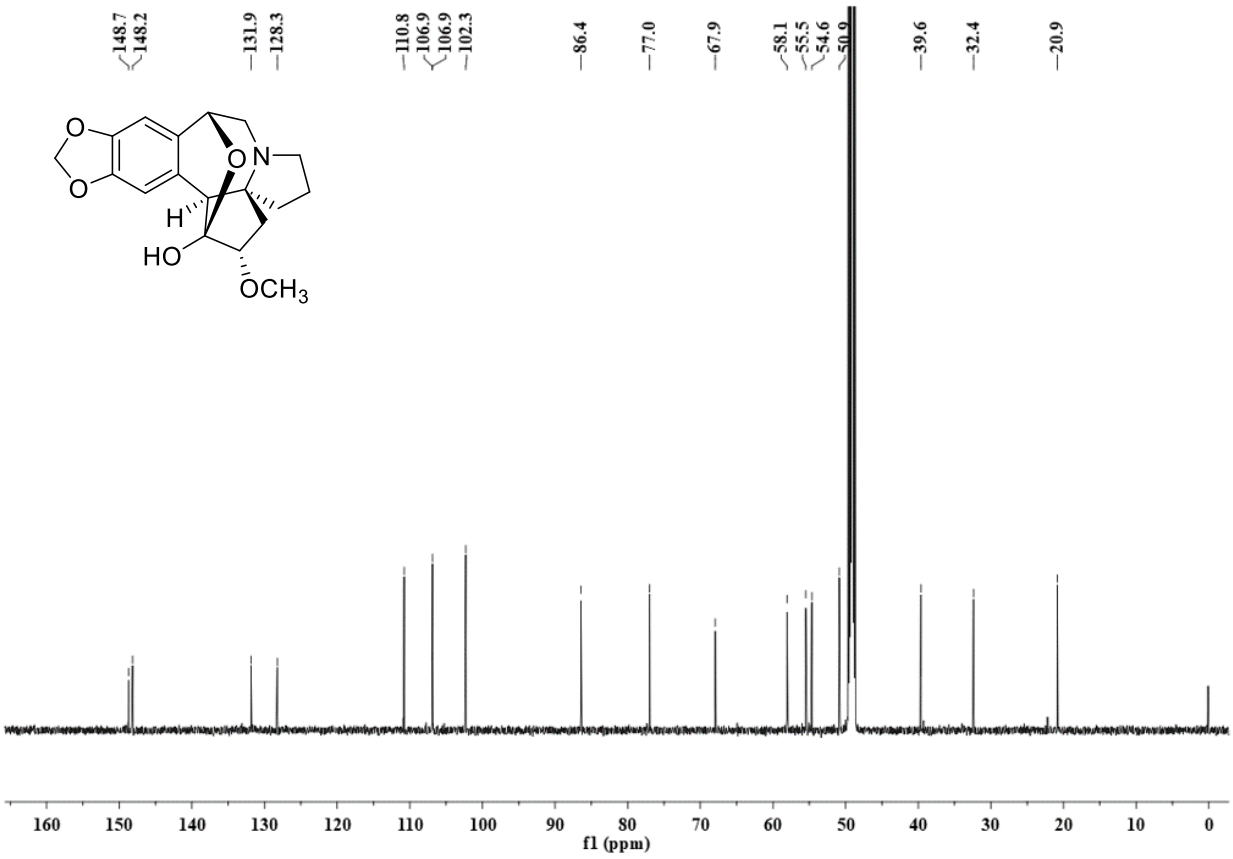

Figure S52. ^{13}C NMR (150 MHz) spectrumof **5** in CD_3OD

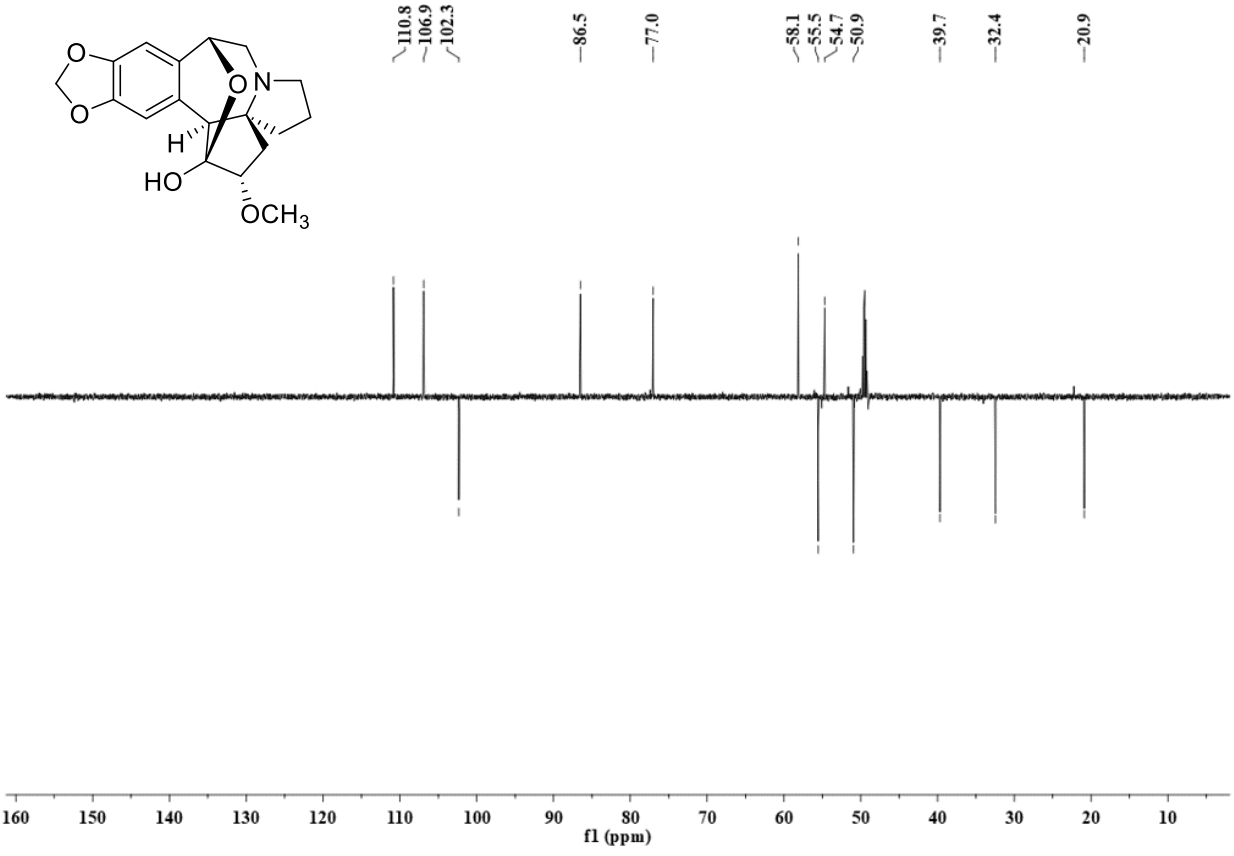

Figure S53. DEPT 135 spectrum of **5** in CD_3OD

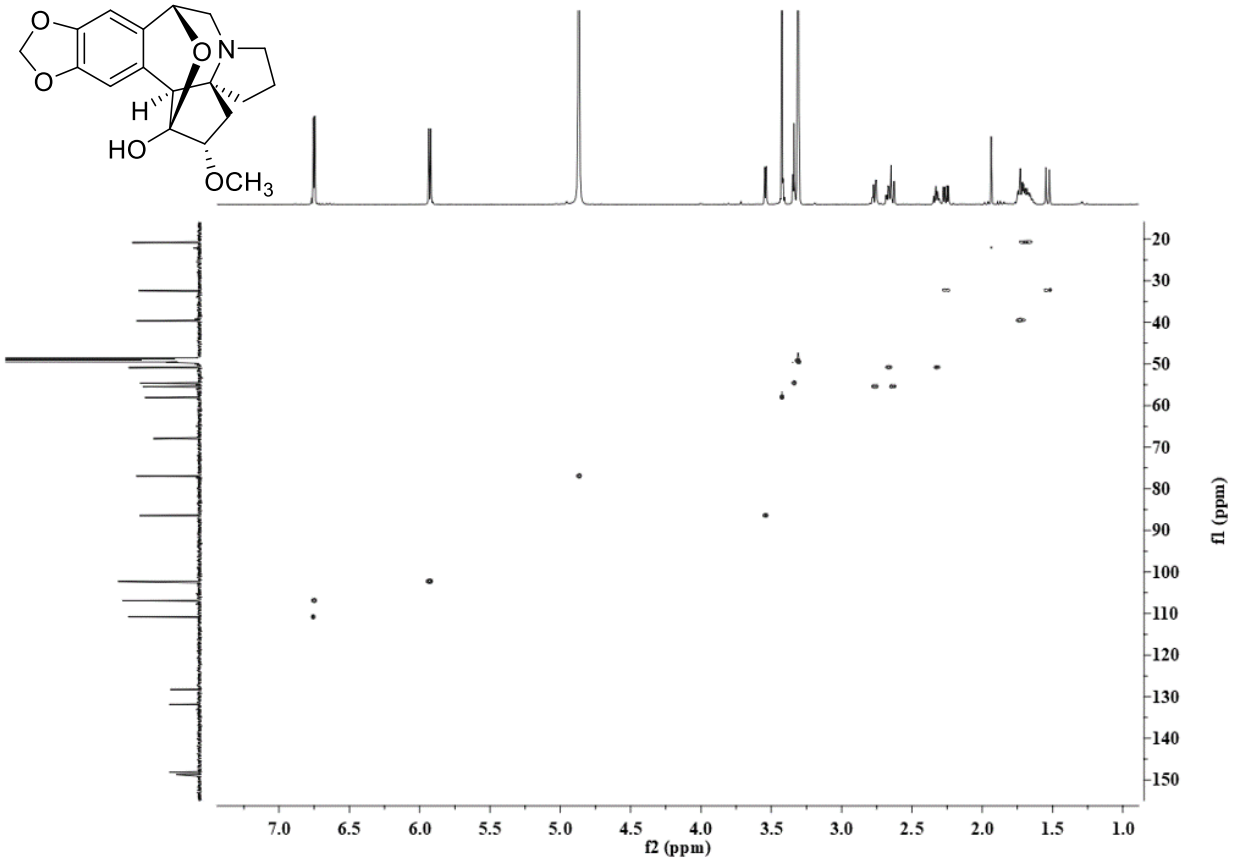

Figure S54. HSQC spectrum of **5** in CD_3OD

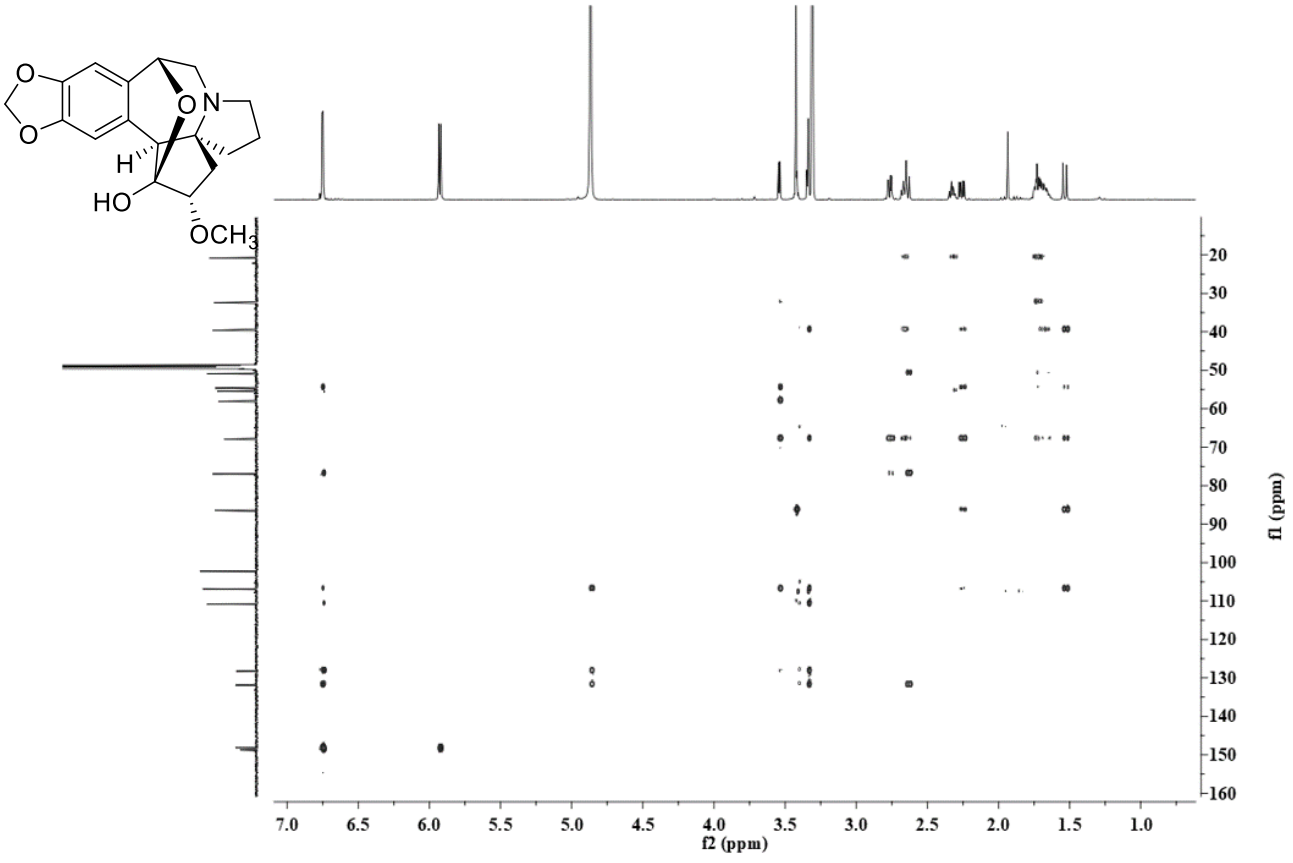

Figure S55. HMBC spectrum of **5** in CD_3OD

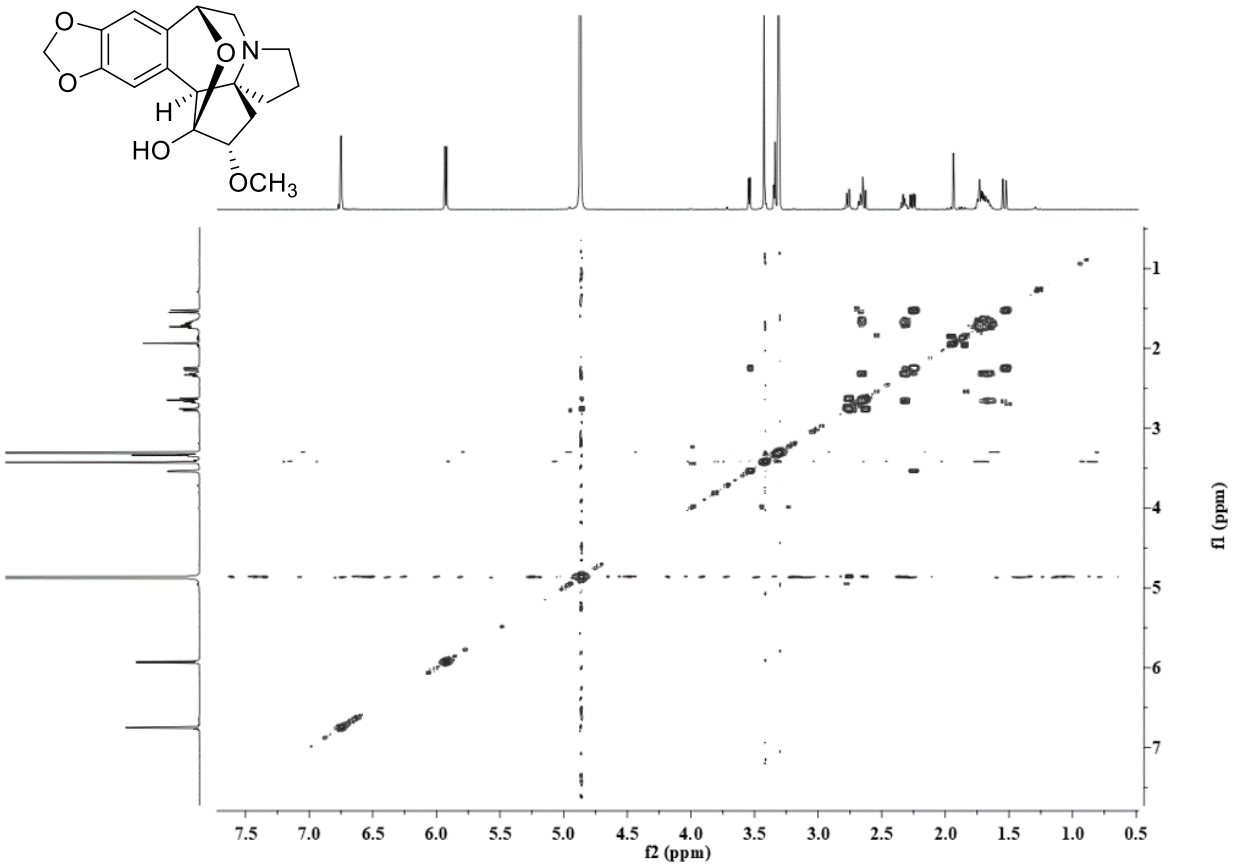

Figure S56. $^{1}H–^{1}H$ COSY spectrum of **5** in CD_3OD

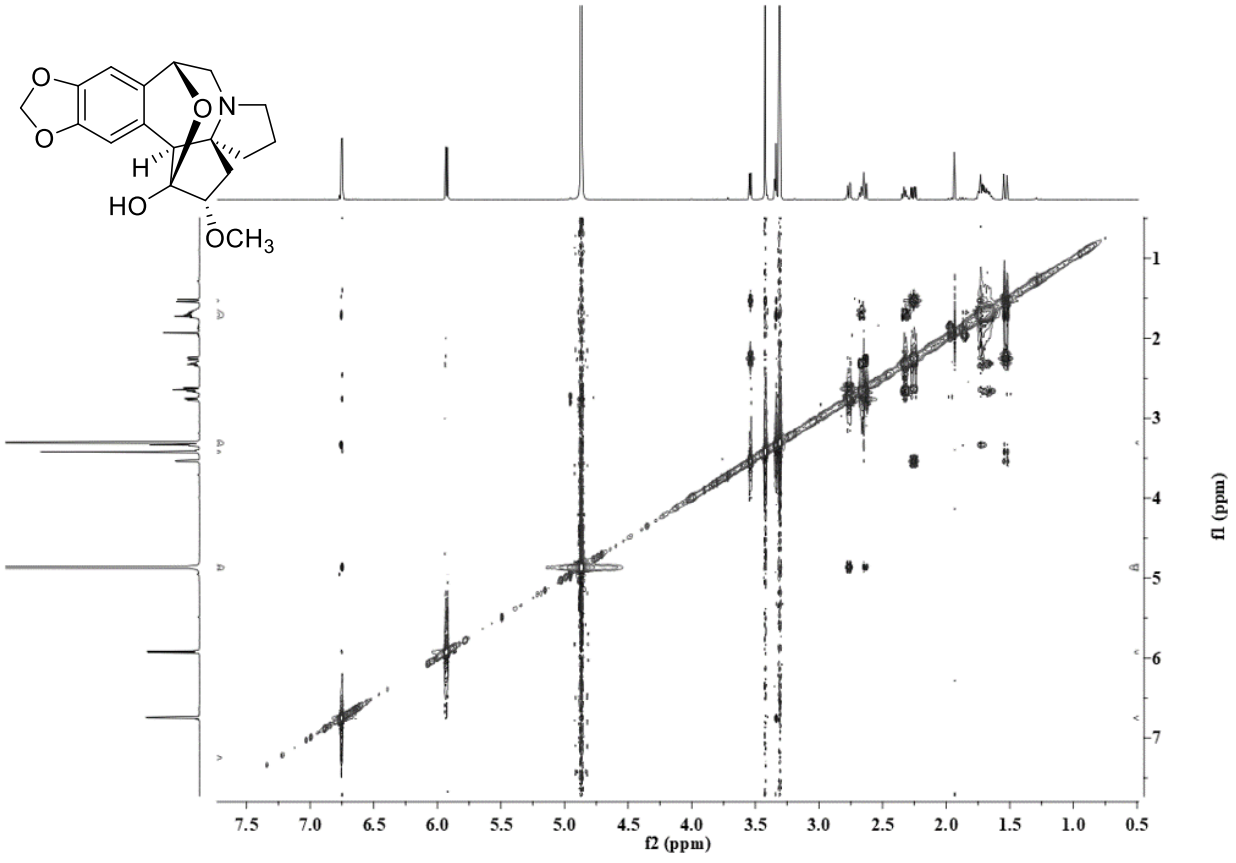

Figure S57. NOESY spectrum of **5** in CD_3OD

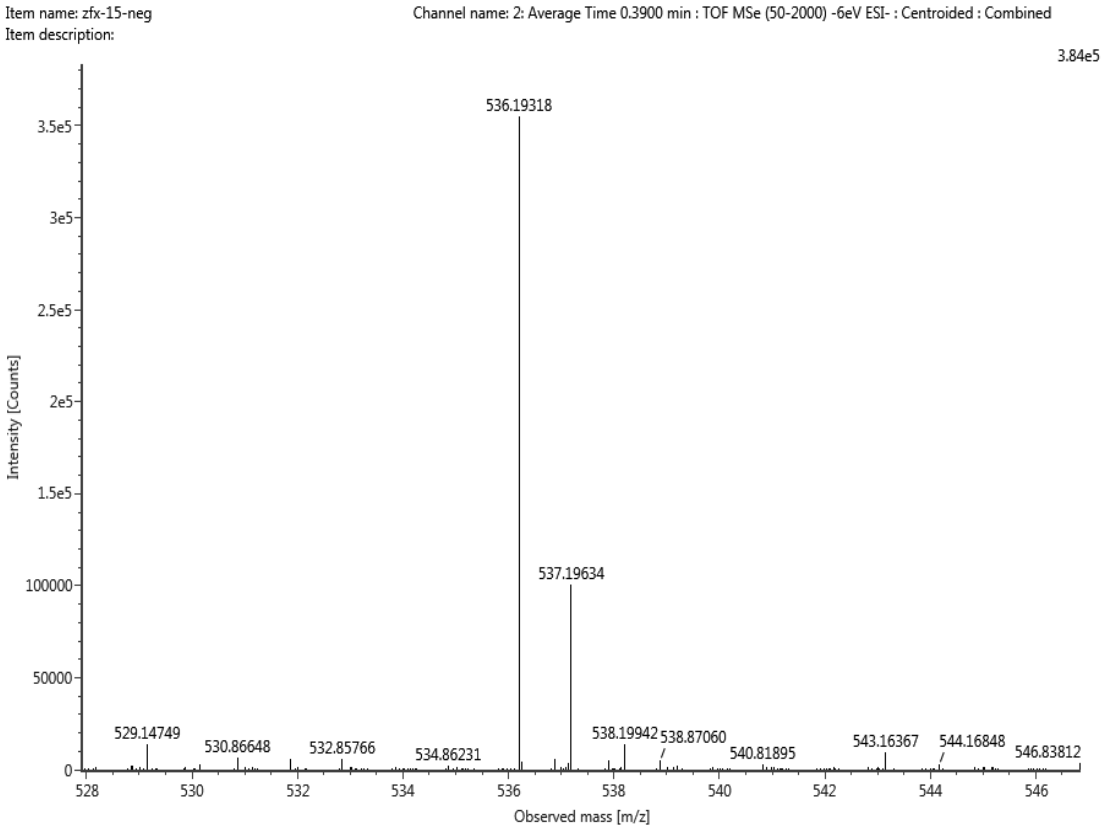

Figure S58. (+)-HR-ESI-MS spectrum of **6**

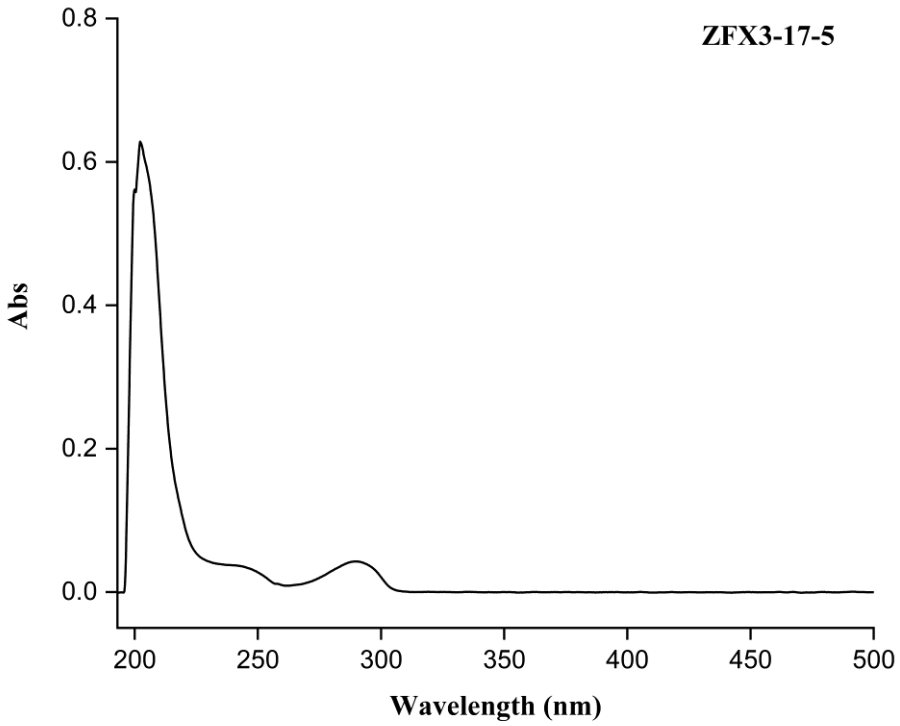

Figure S59. UV spectrum of **6** in MeOH

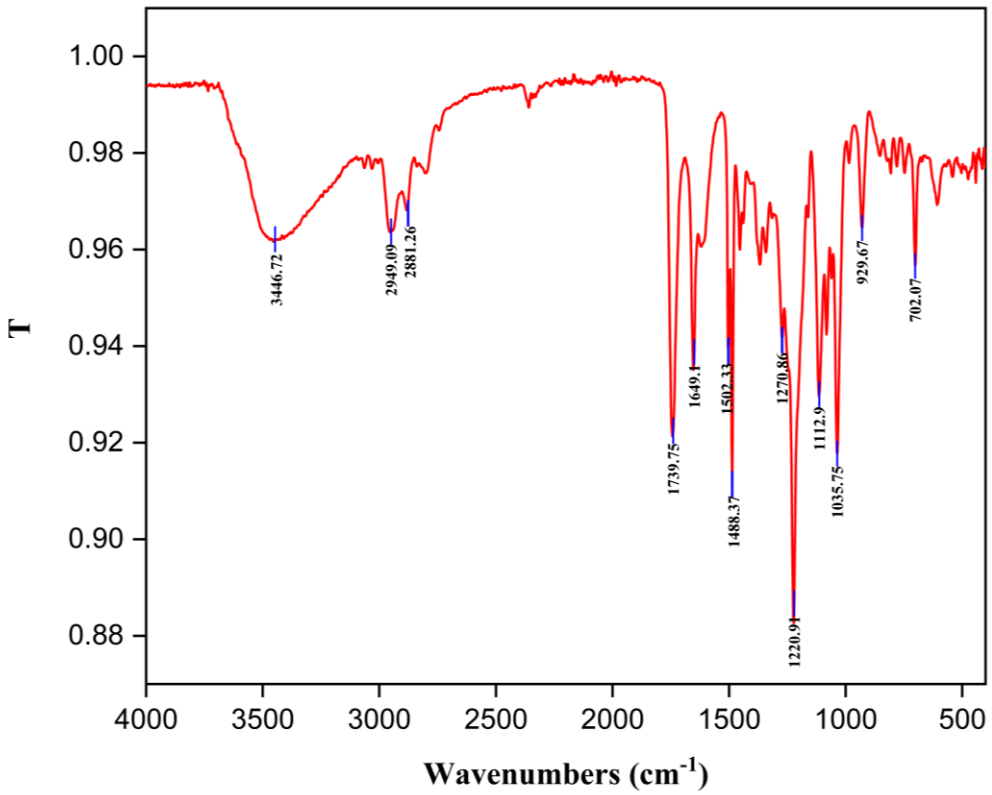

Figure S60. IR spectrum of **6**

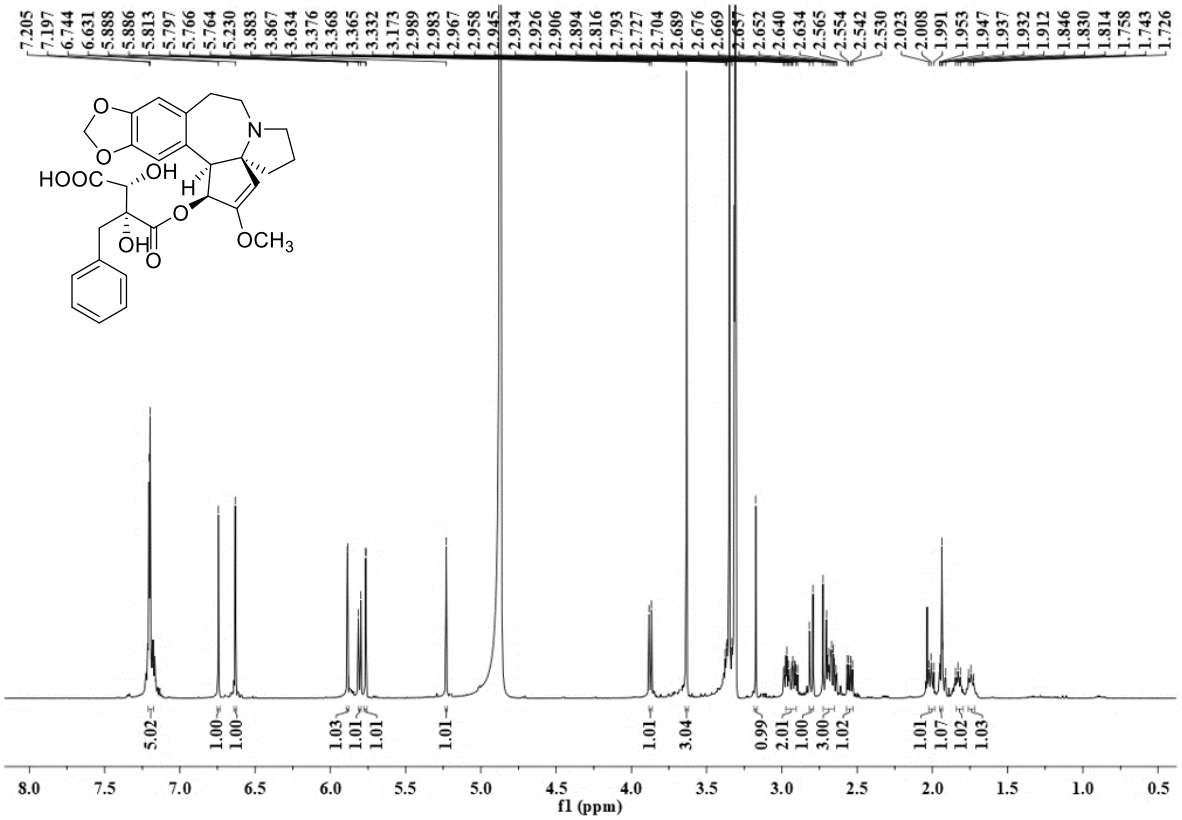

Figure S61. ^{1}H NMR (600 MHz) spectrum of **6** in CD_3OD

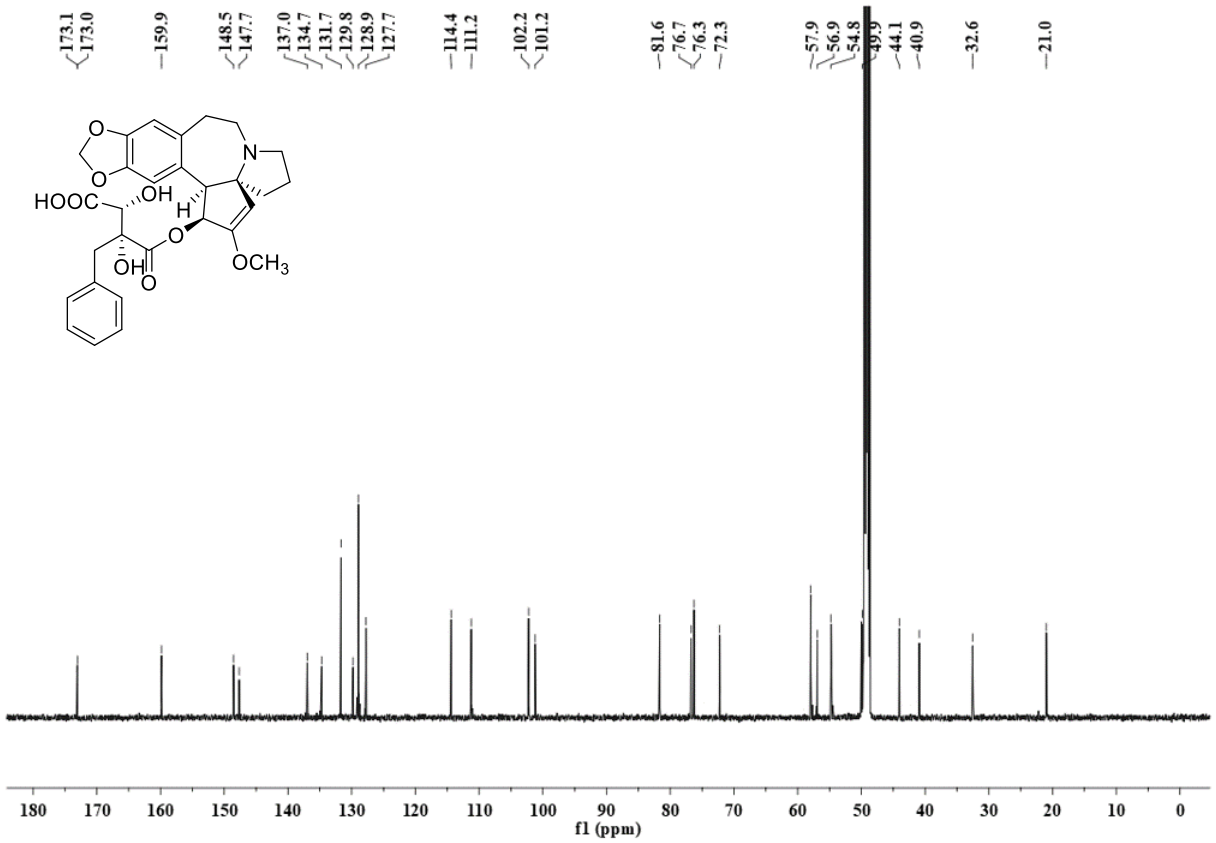

Figure S62. ^{13}C NMR (150 MHz) spectrum of **6** in CD_3OD

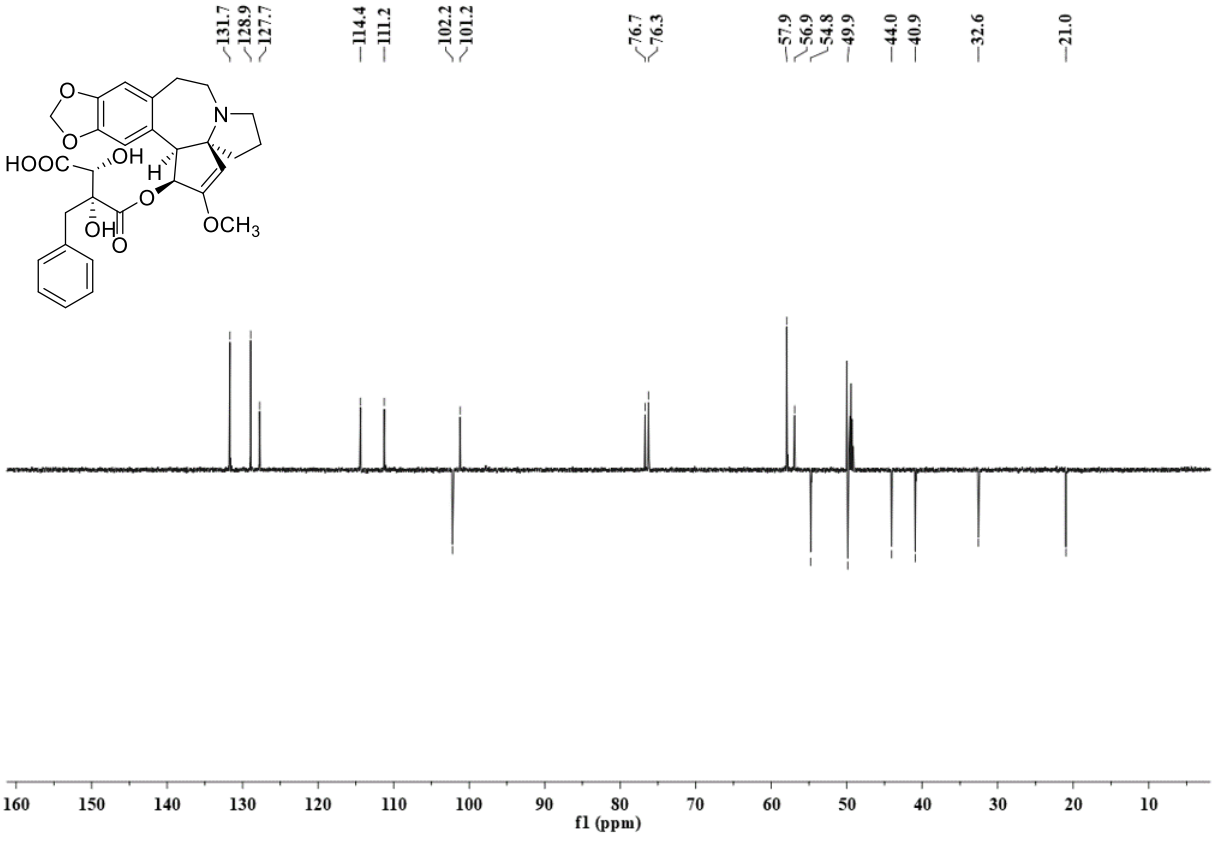

Figure S63. DEPT 135 spectrum of **6** in CD_3OD

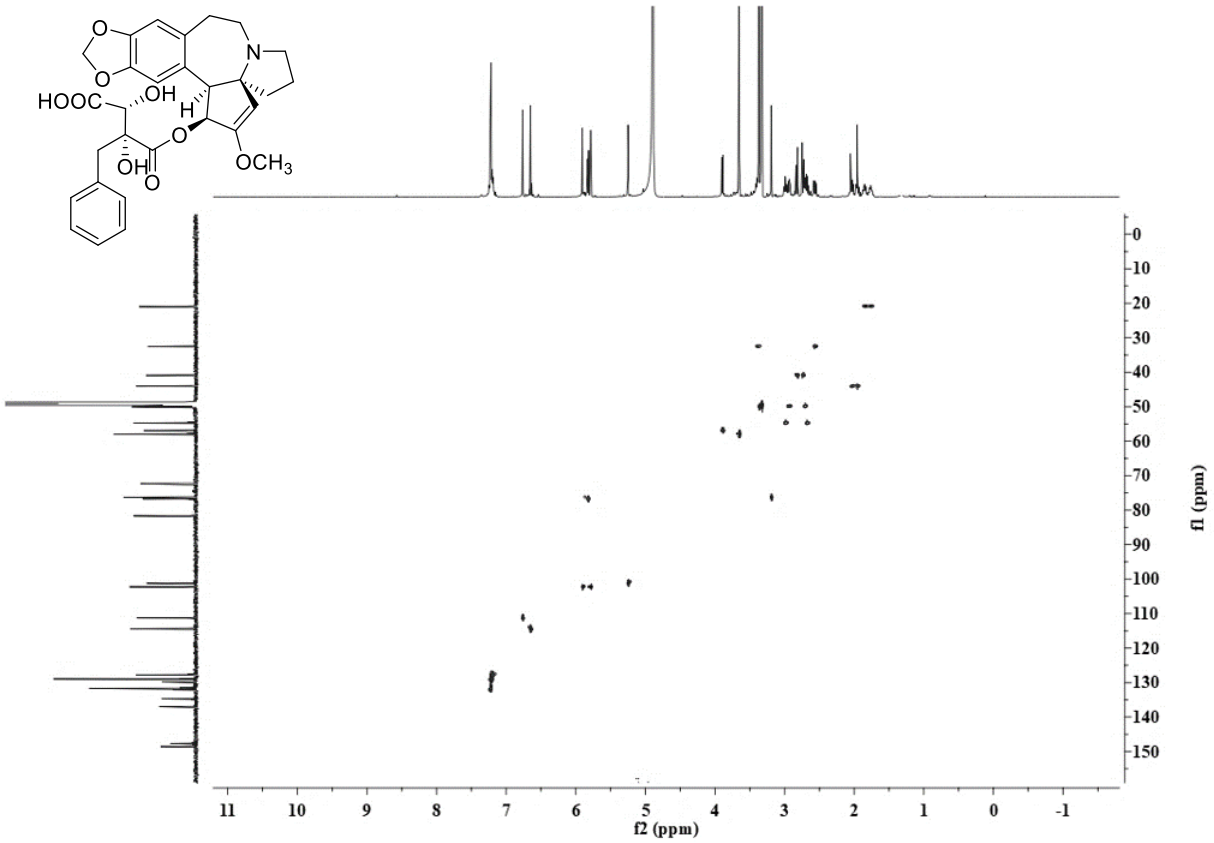

Figure S64. HSQC spectrum of **6** in CD_3OD

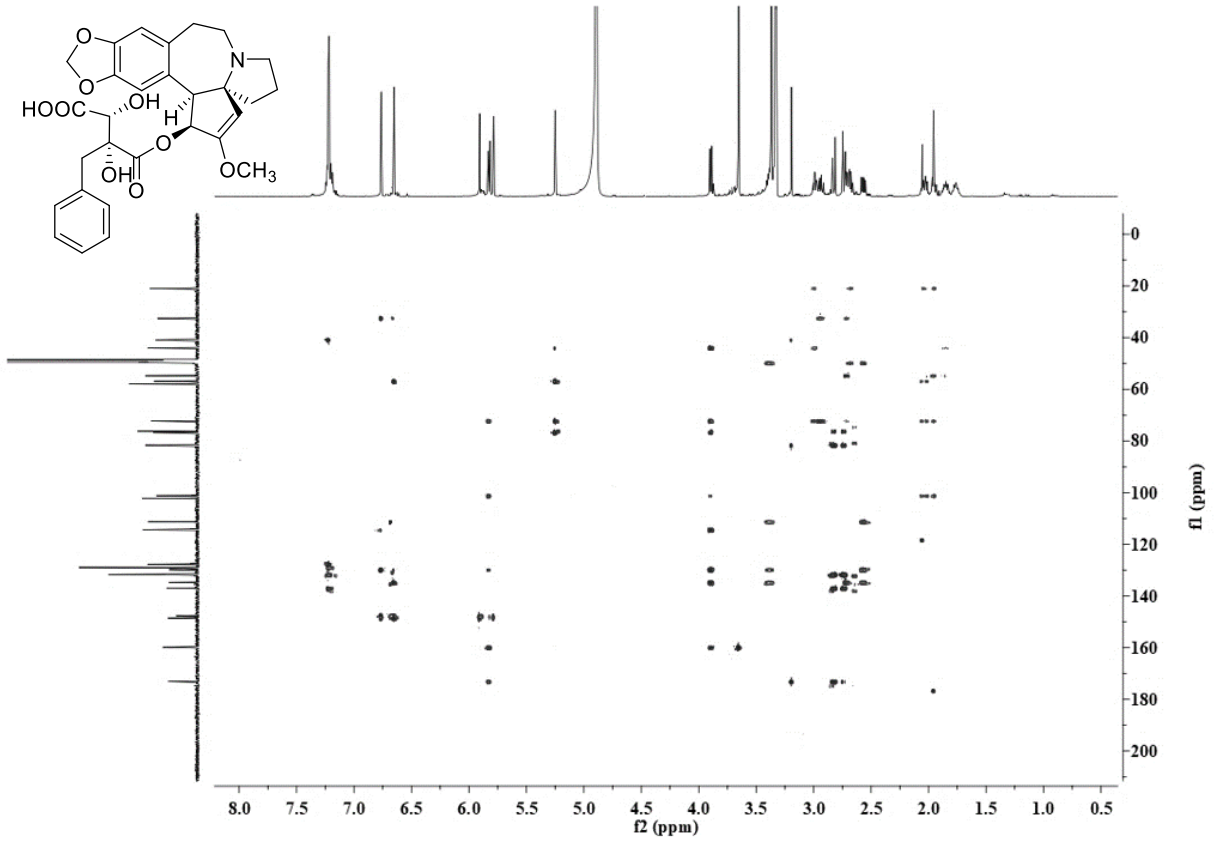

Figure S65. HMBC spectrum of **6** in CD_3OD

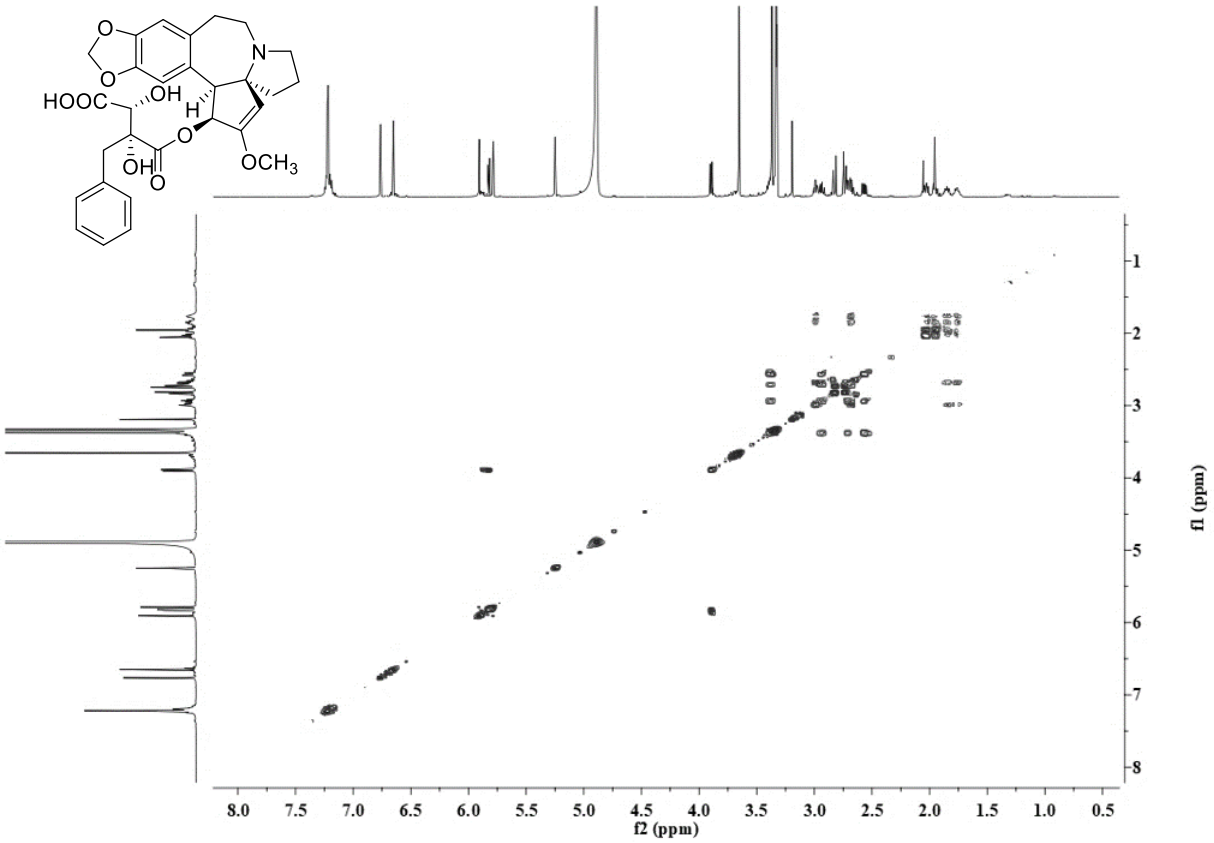

Figure S66. $^{1}H–^{1}H$ COSY spectrum of **6** in CD_3OD

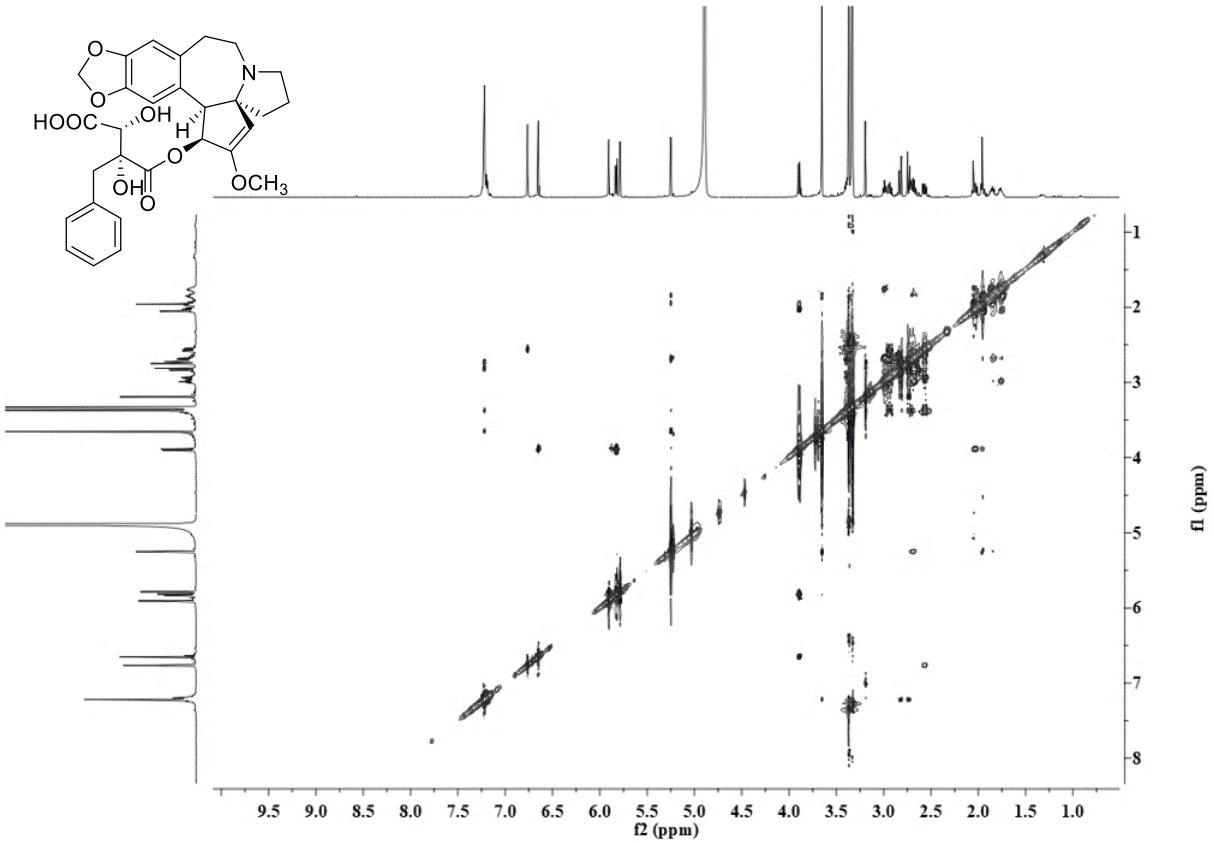

Figure S67. NOESY spectrum of **6** in CD_3OD

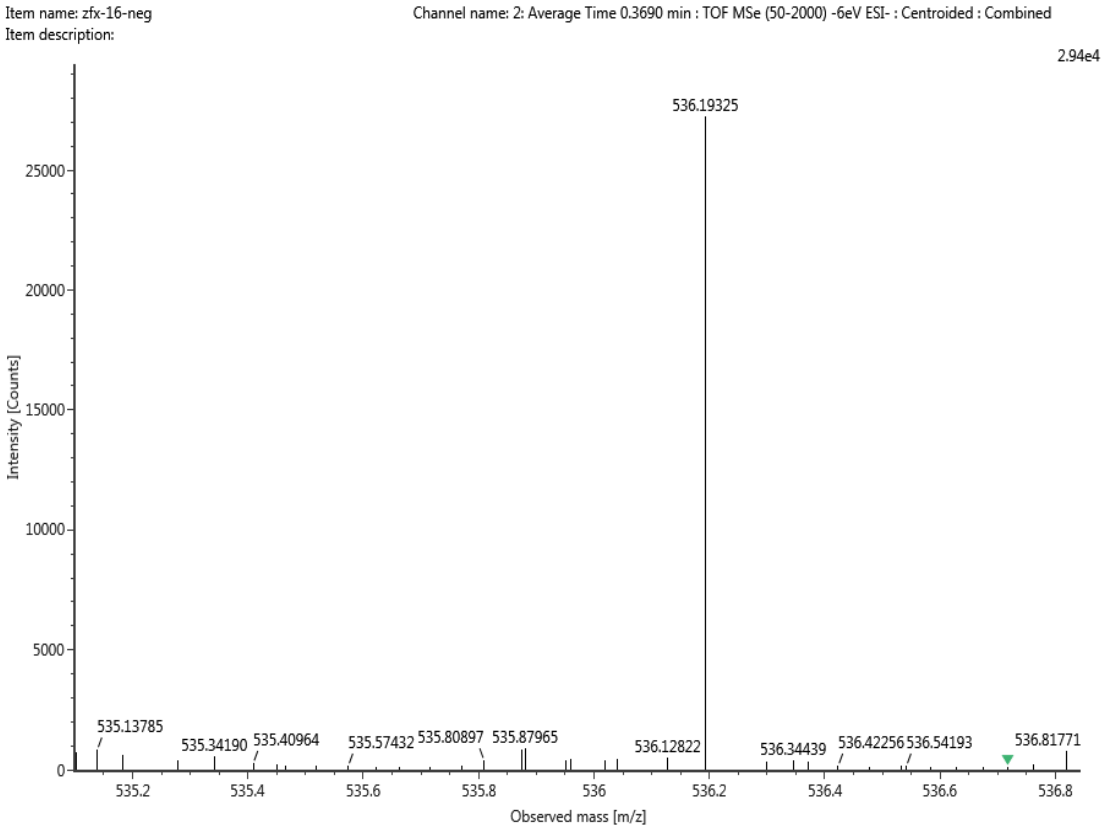

Figure S68. (+)-HR-ESI-MS spectrum of **7**

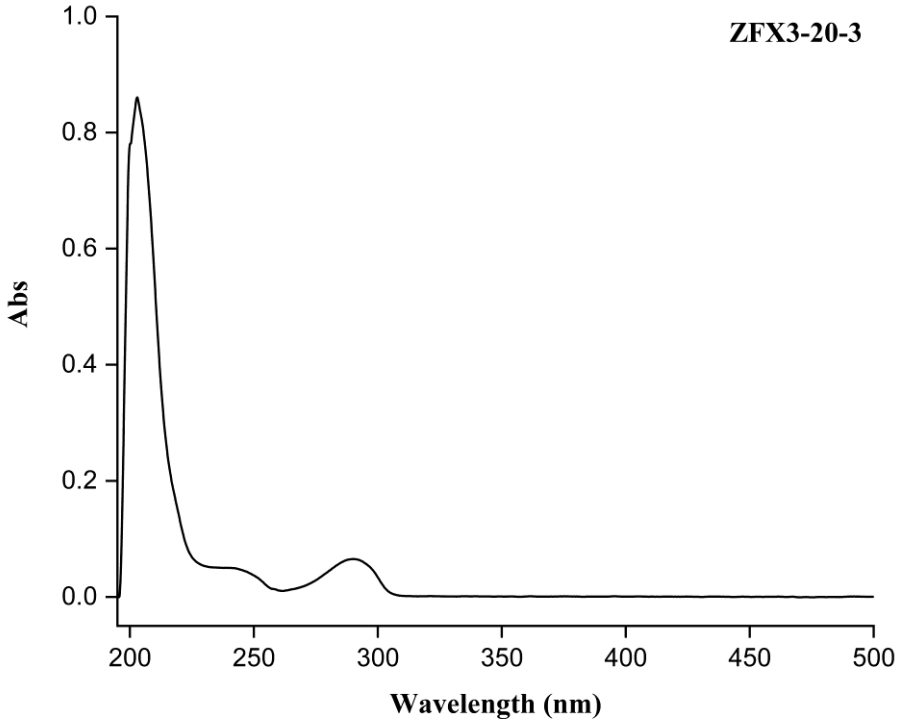

Figure S69. UV spectrum of **7** in MeOH

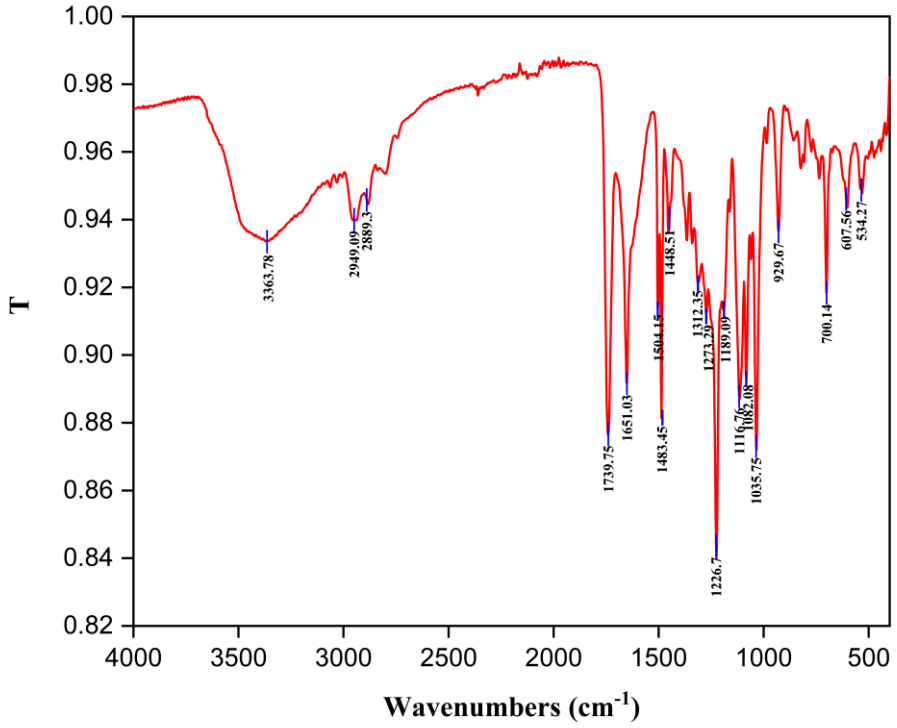

Figure S70. IR spectrum of **7**

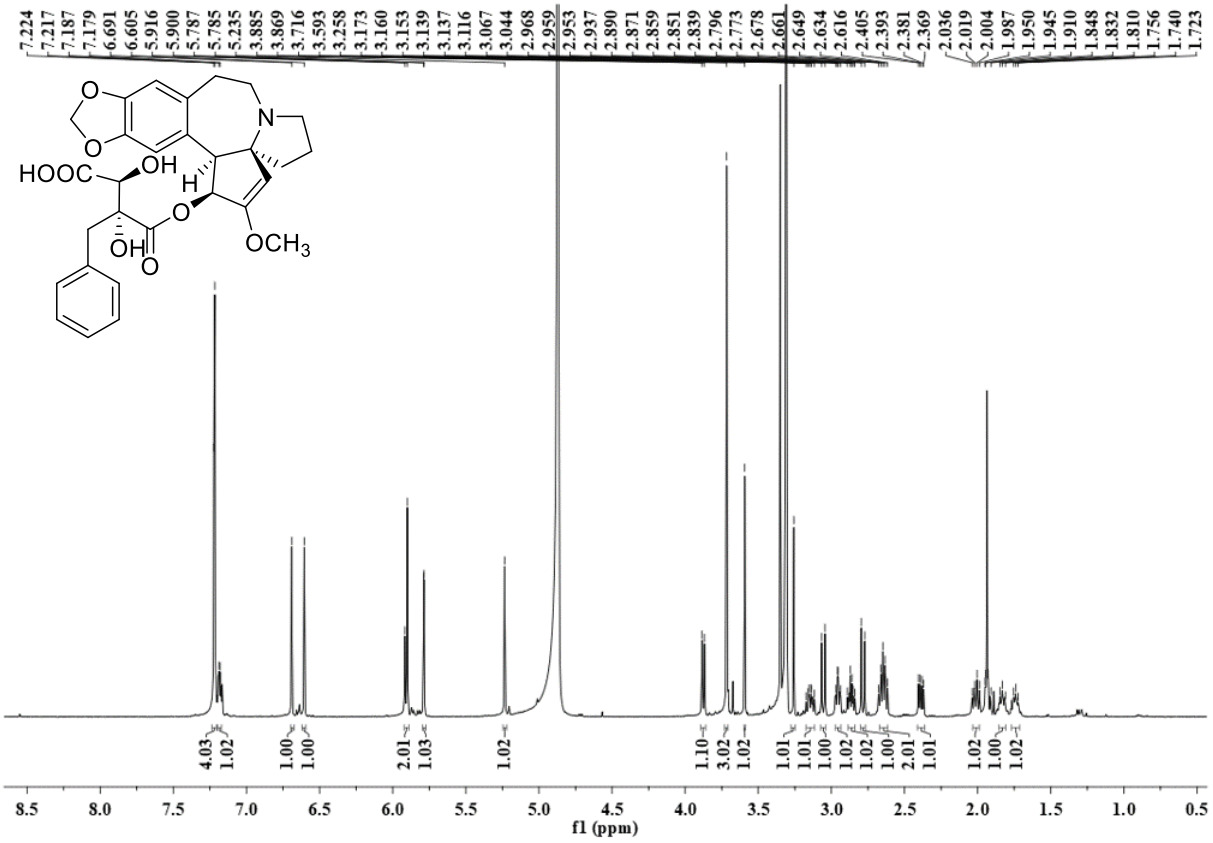

Figure S71. ^{1}H NMR (600 MHz) spectrum of **7** in CD_3OD

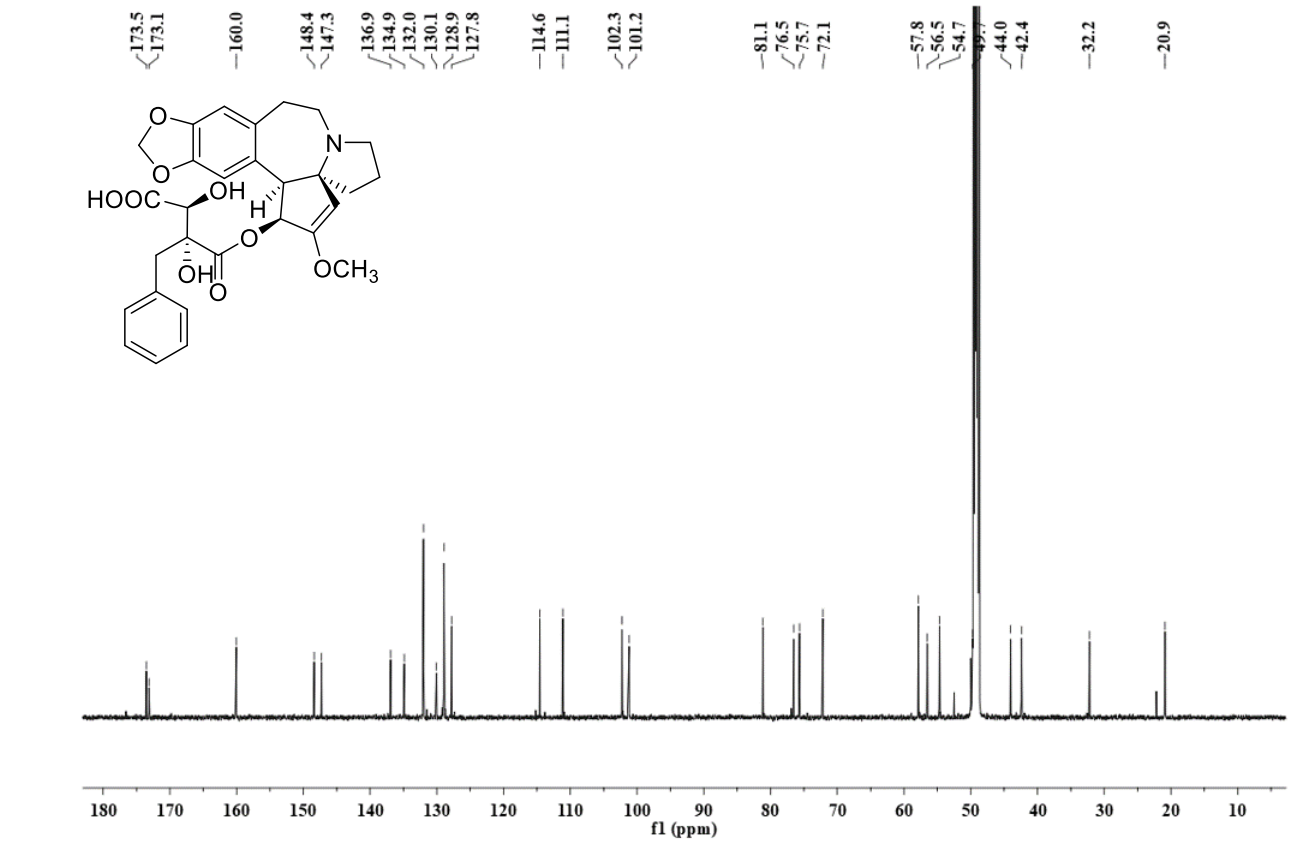

Figure S72. ^{13}C NMR (150 MHz) spectrum of **7** in CD_3OD

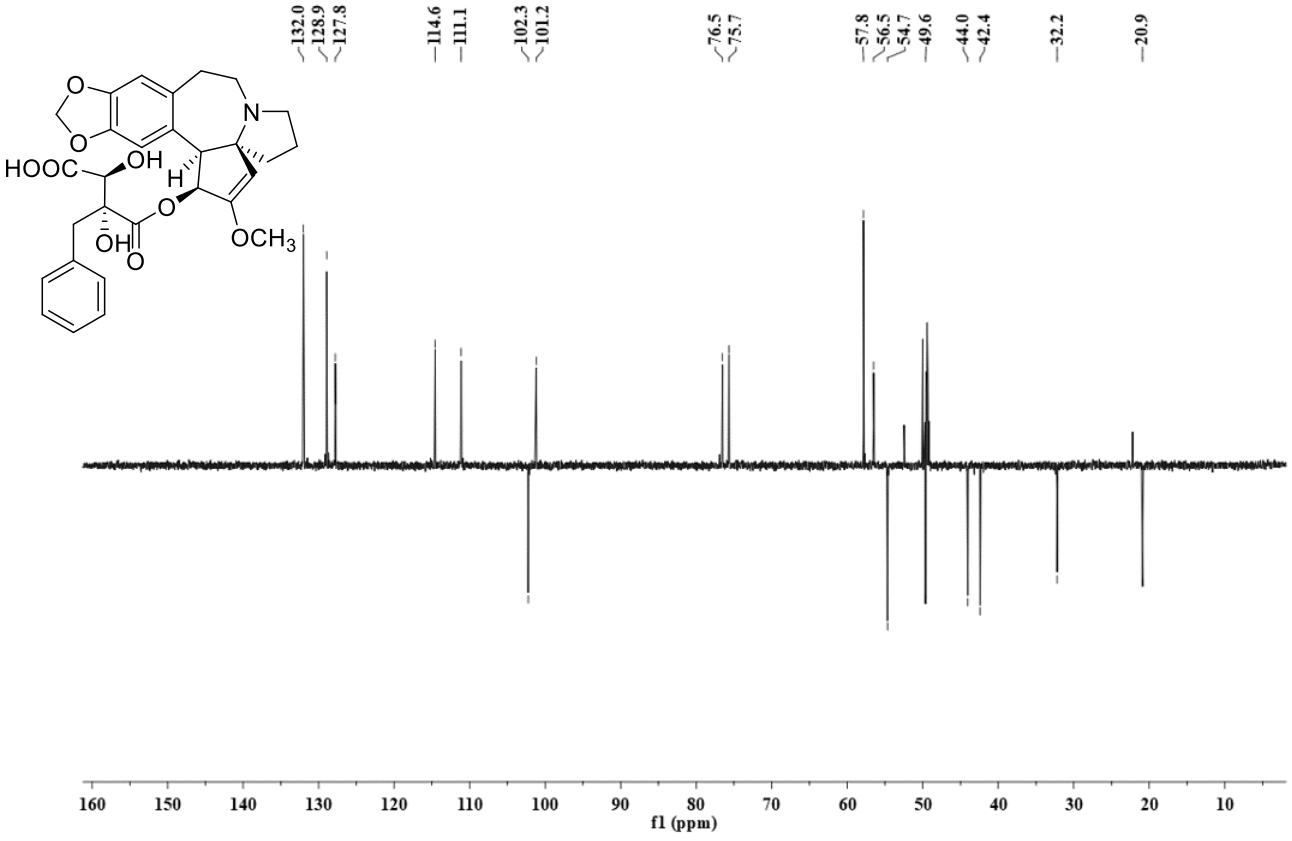

Figure S73. DEPT 135 spectrum of **7** in CD_3OD

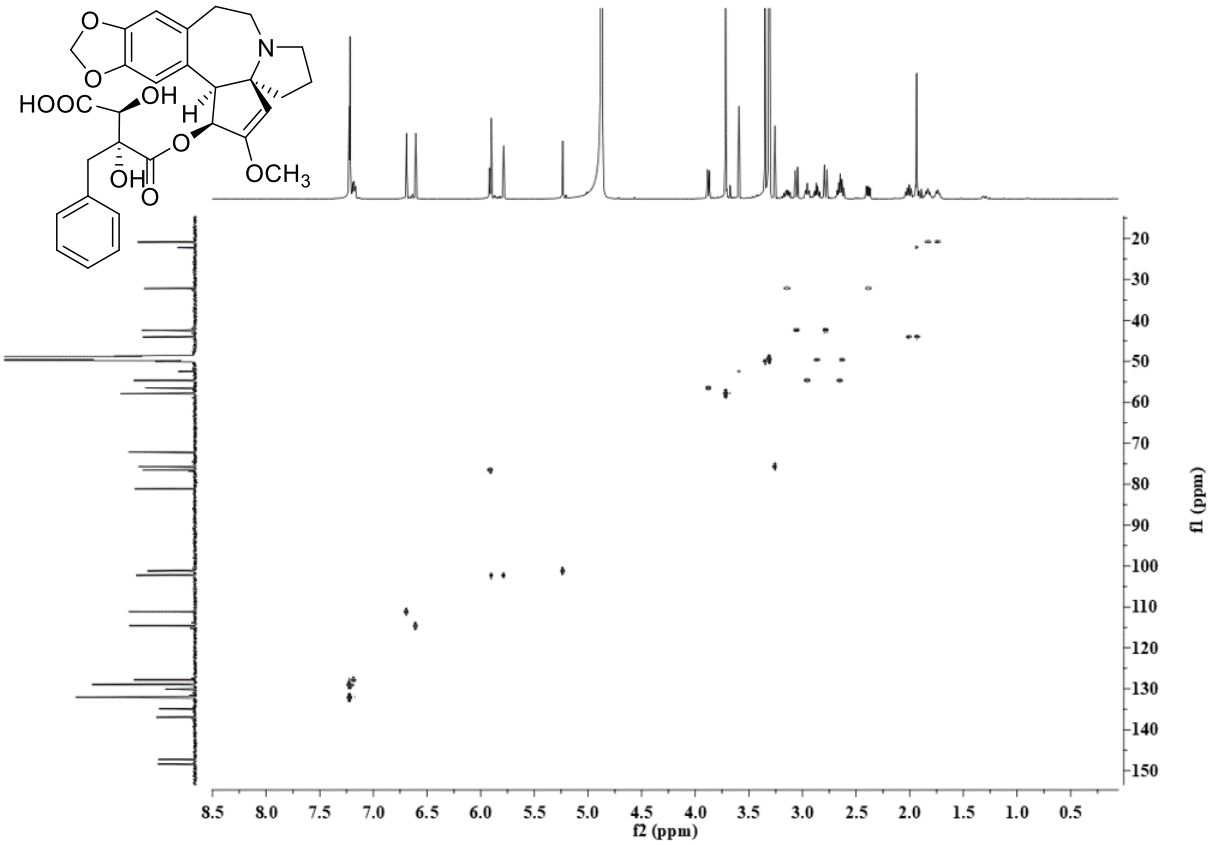

Figure S74. HSQC spectrum of **7** in CD_3OD

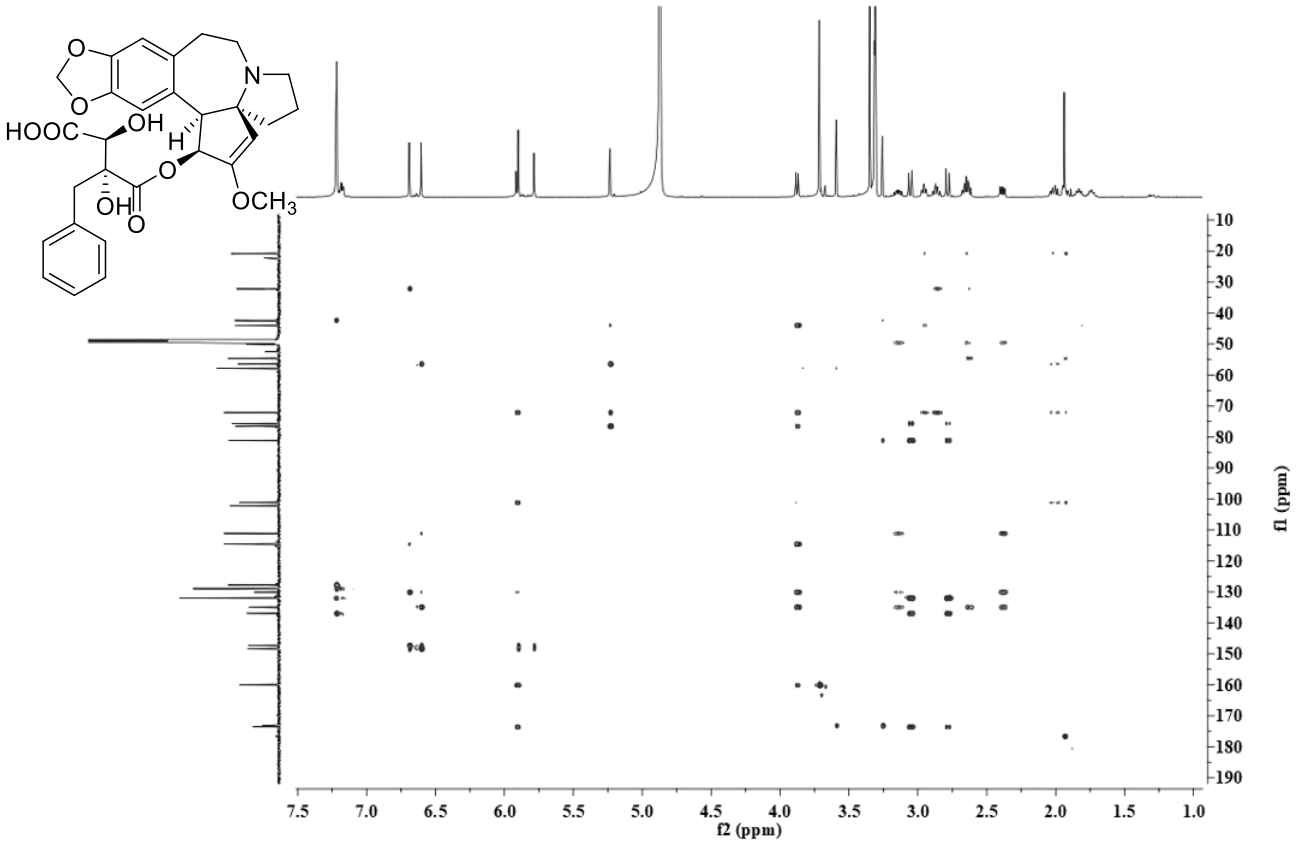

Figure S75. HMBC spectrum of **7** in CD_3OD

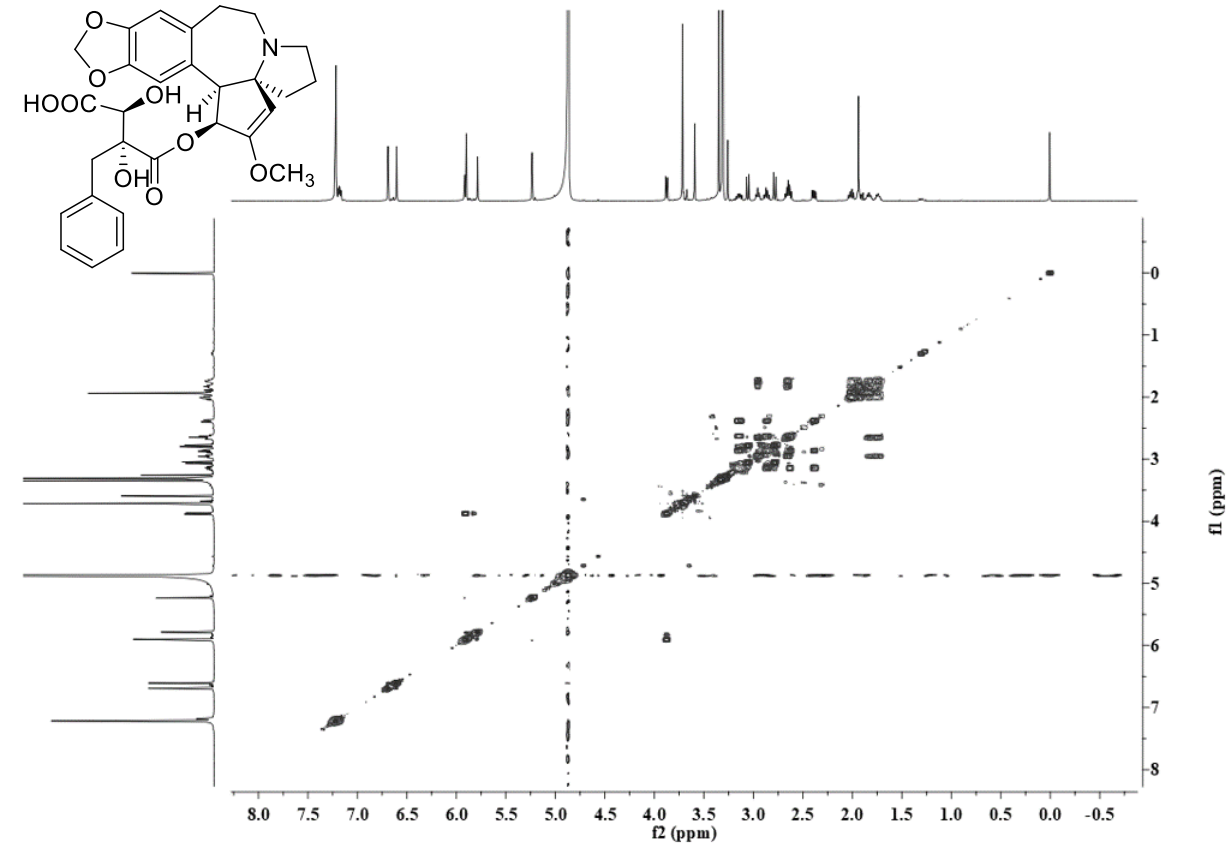

Figure S76. $^{1}H–^{1}H$ COSY spectrum of **7** in CD_3OD

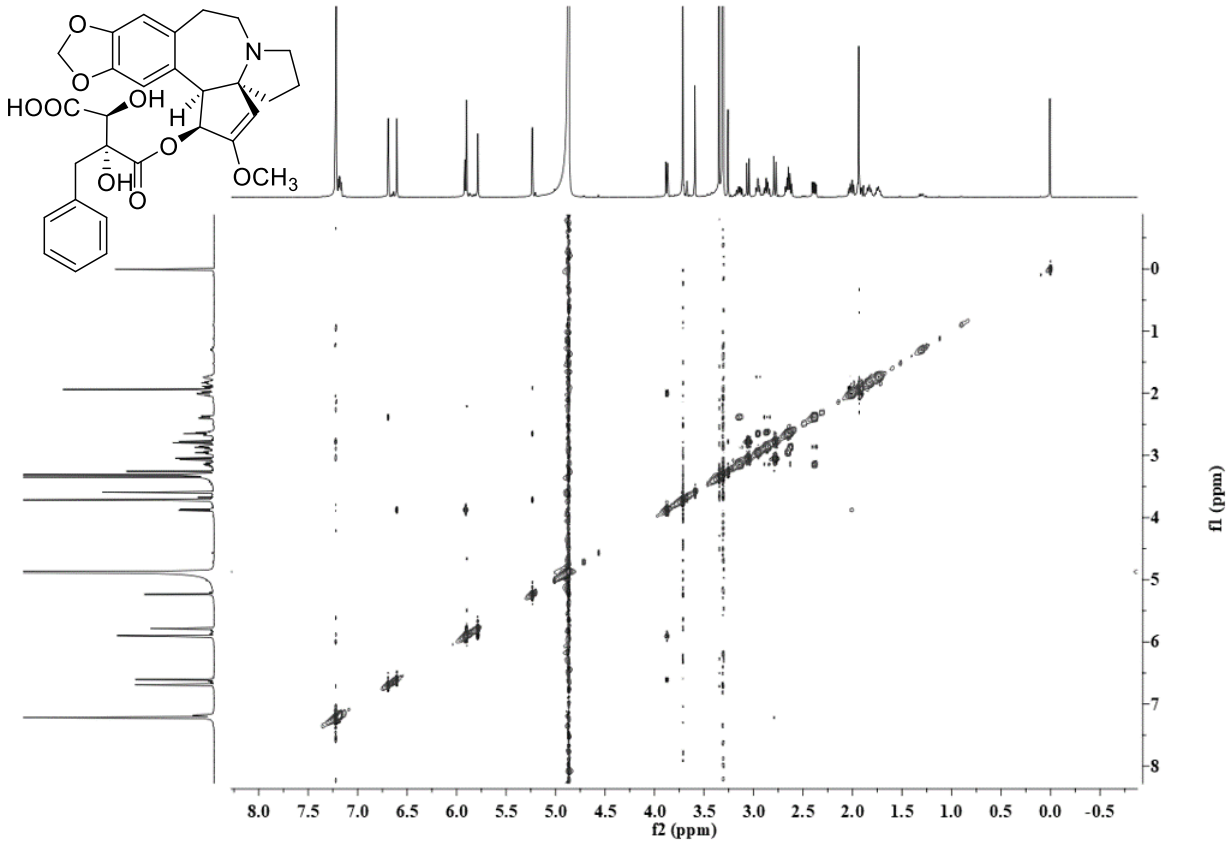

Figure S77. NOESY spectrum of **7** in CD_3OD

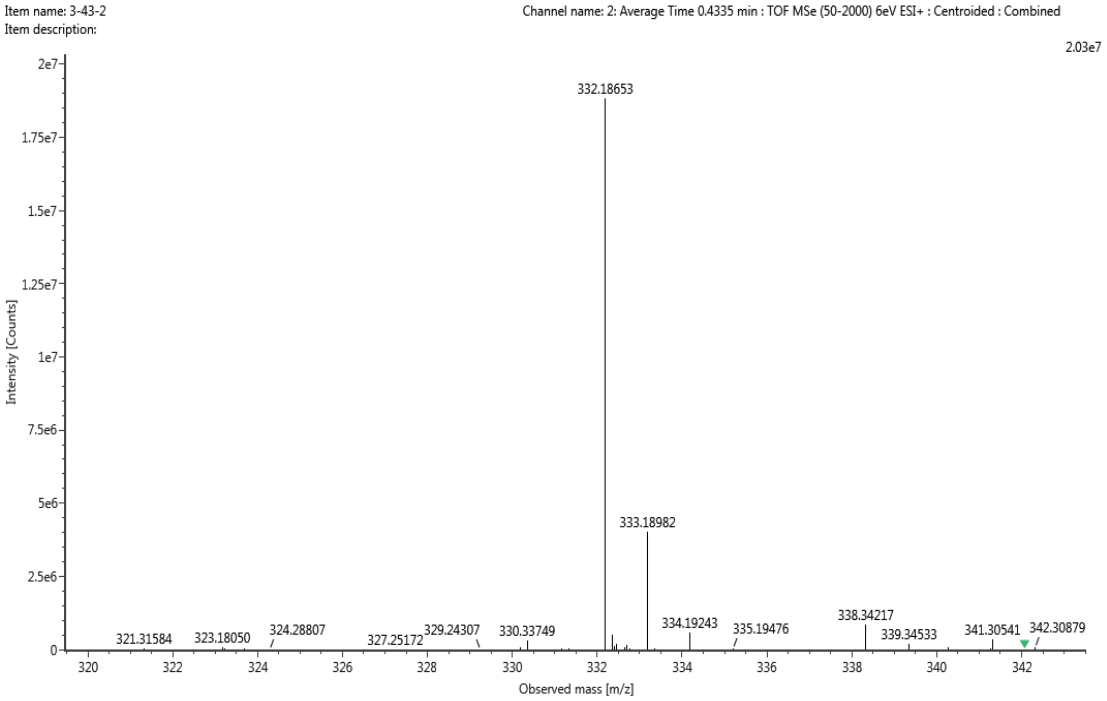

Figure S78. (+)-HR-ESI-MS spectrum of **8**

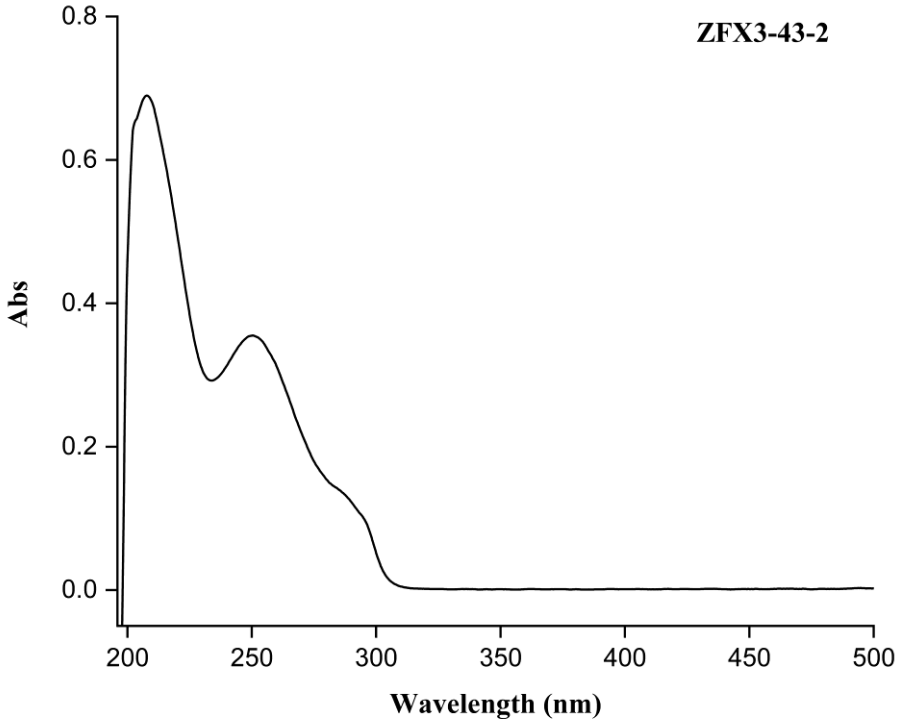

Figure S79. UV spectrum of **8** in MeOH

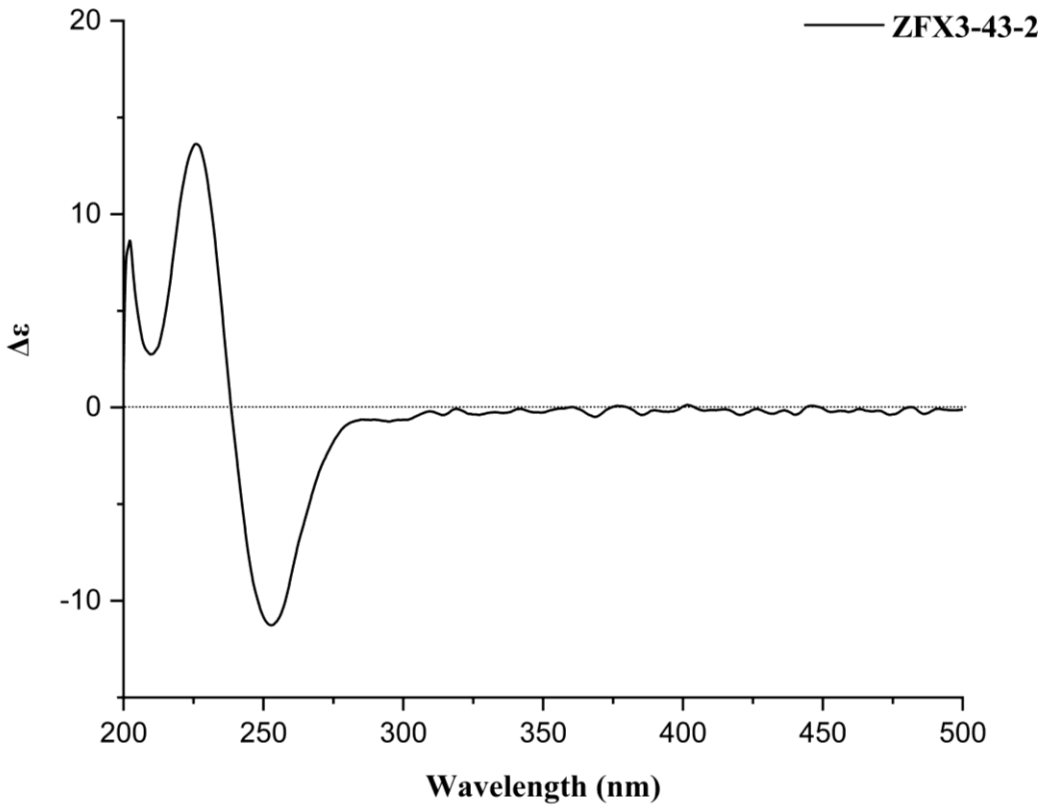

Figure S80. ECD spectrum of **8** in MeOH

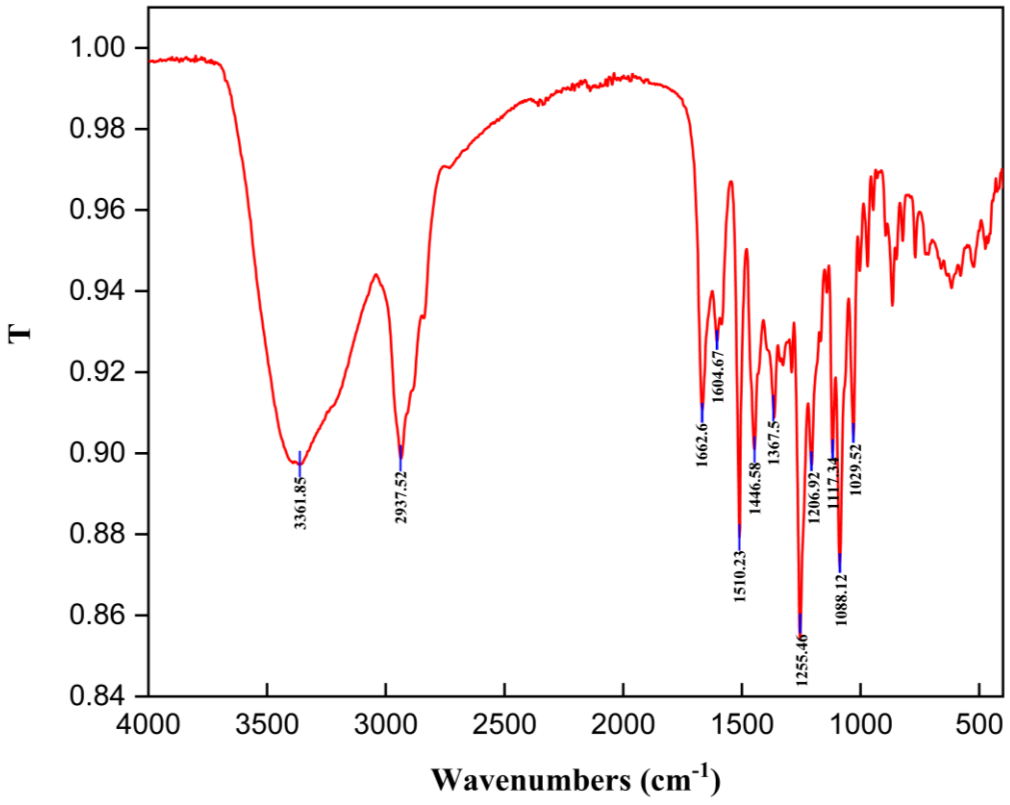

Figure S81. IR spectrum of **8**

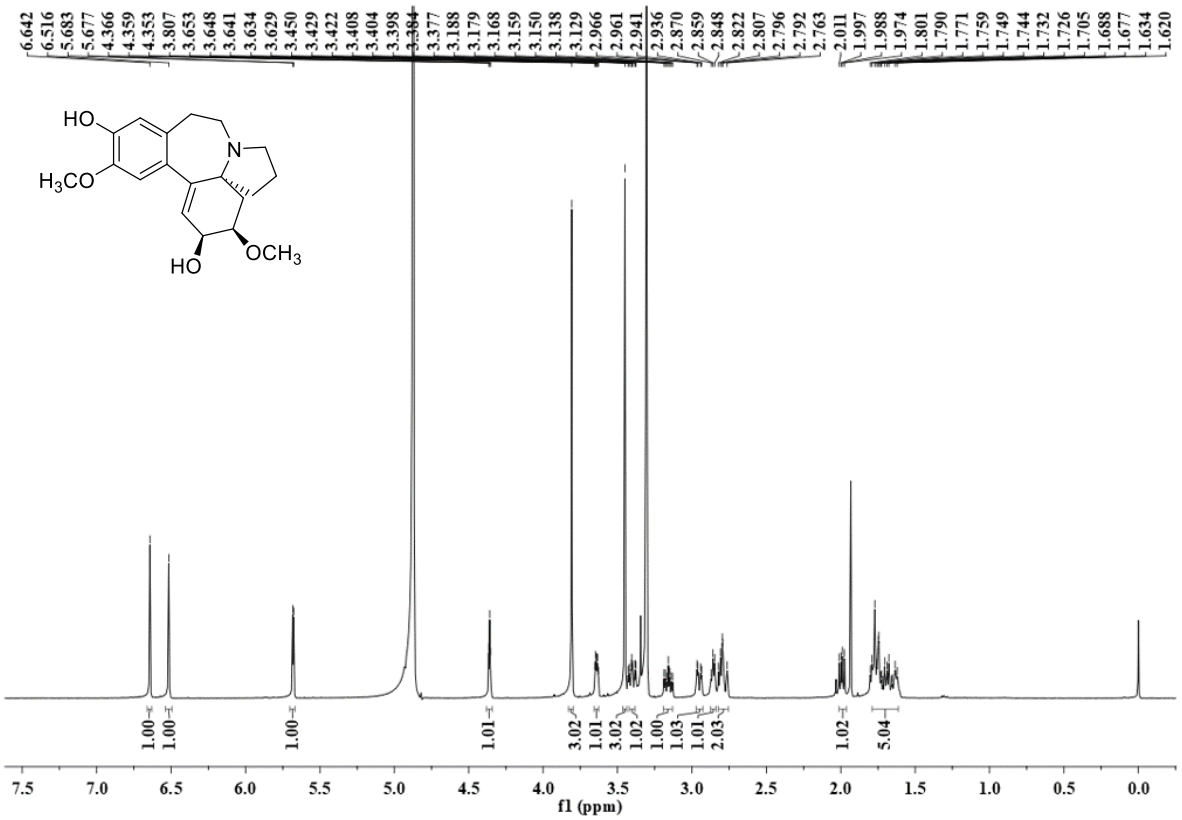

Figure S82. ^{1}H NMR (600 MHz) spectrum of **8** in CD_3OD

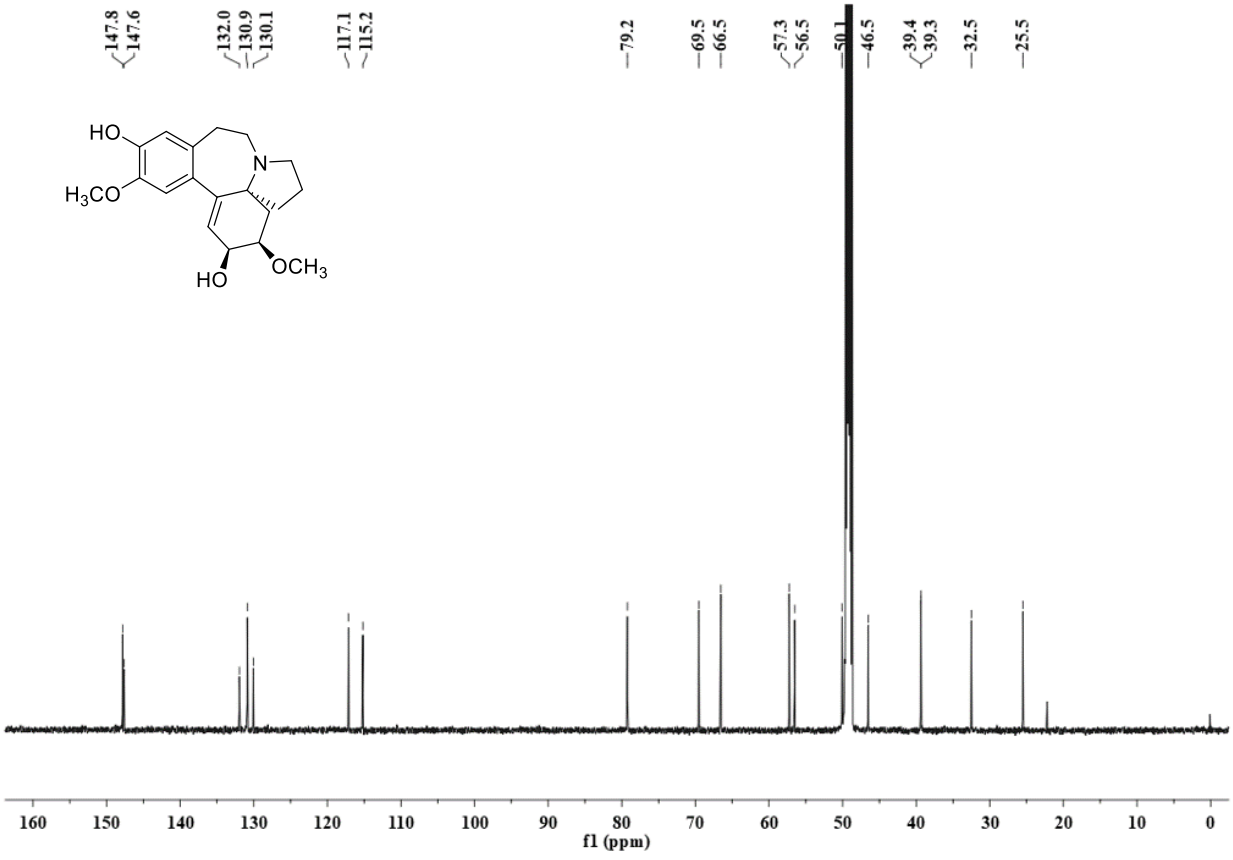

Figure S83. ^{13}C NMR (150 MHz) spectrum of **8** in CD_3OD

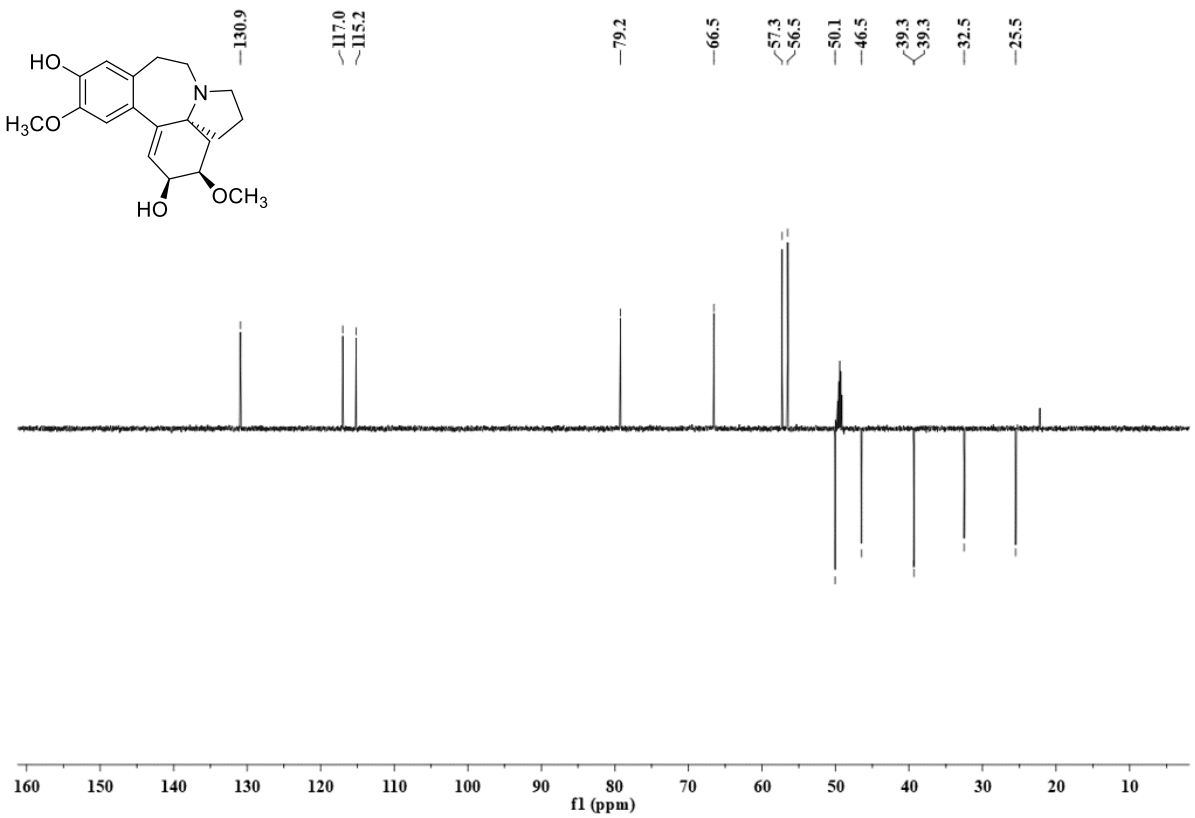

Figure S84. DEPT 135 spectrum of **8** in CD_3OD

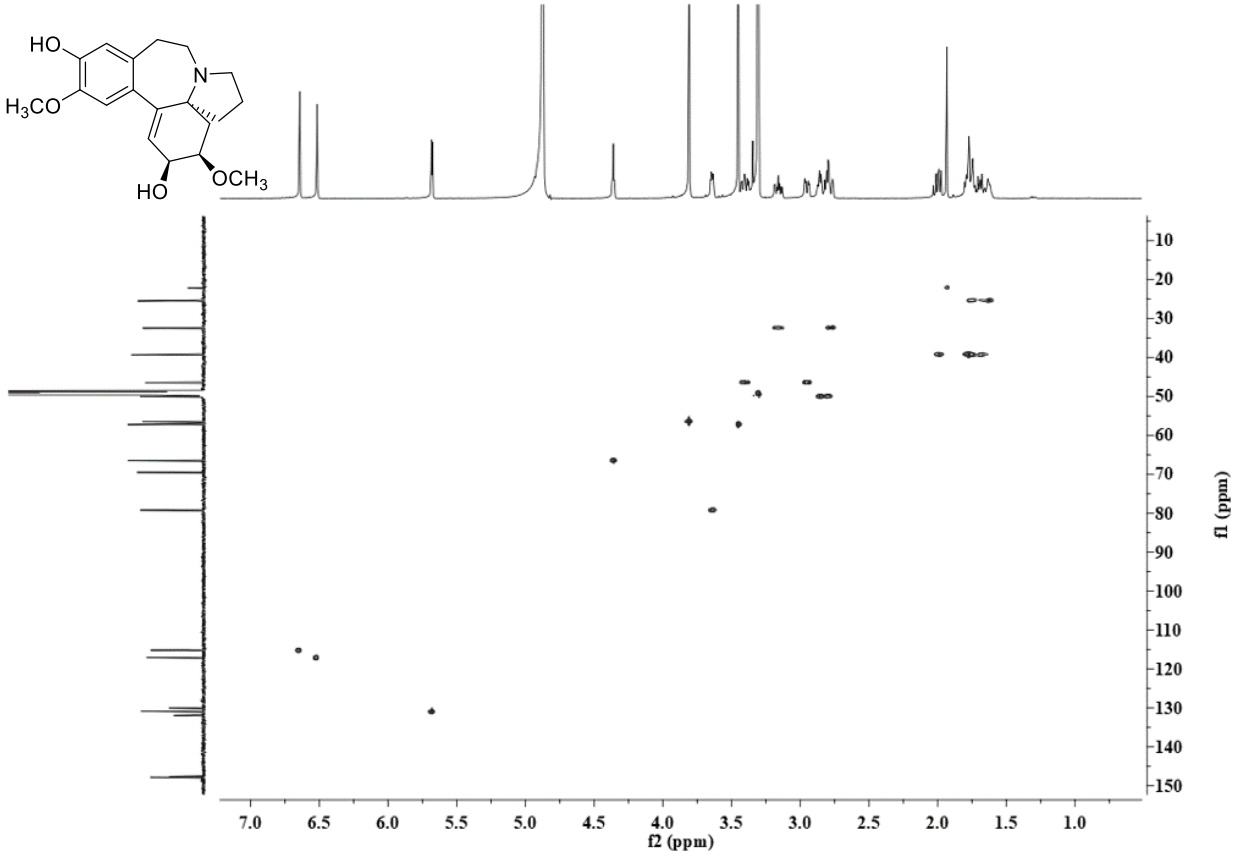

Figure S85. HSQC spectrum of **8** in CD_3OD

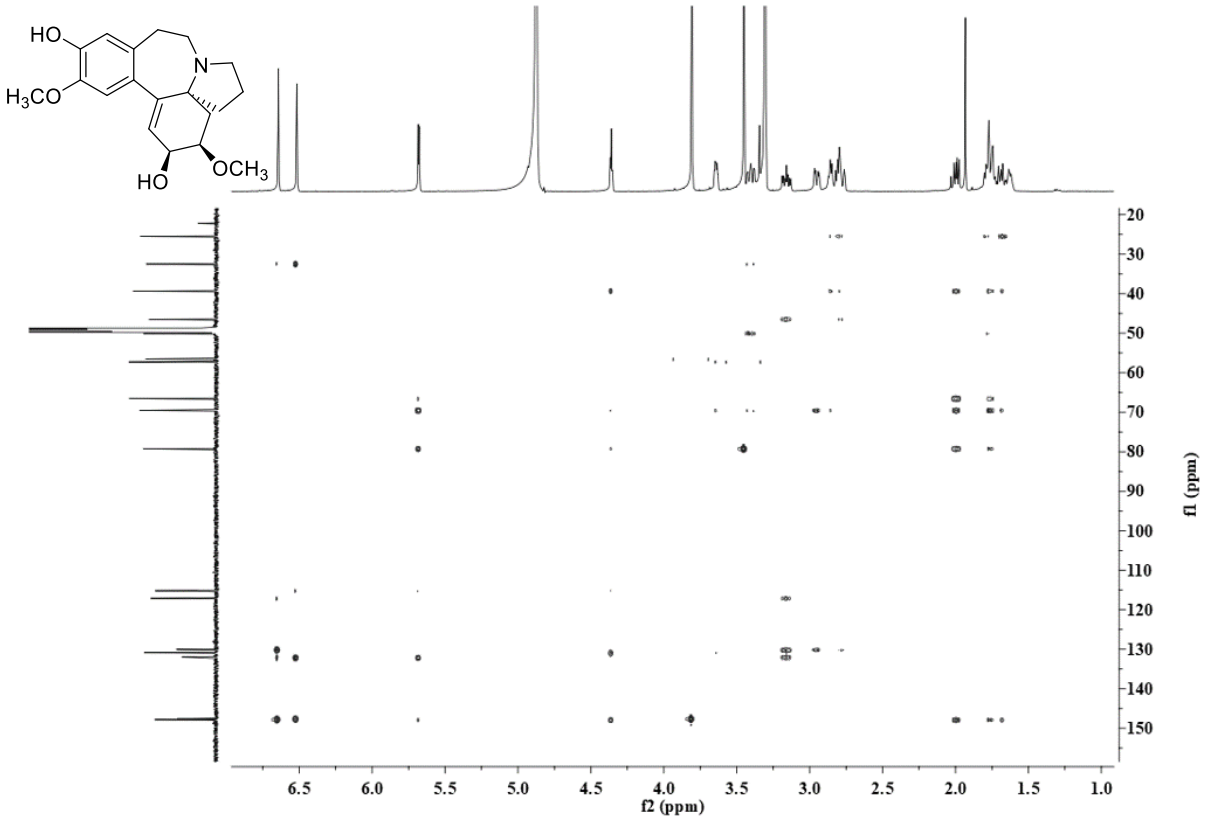

Figure S86. HMBC spectrum of **8** in CD_3OD

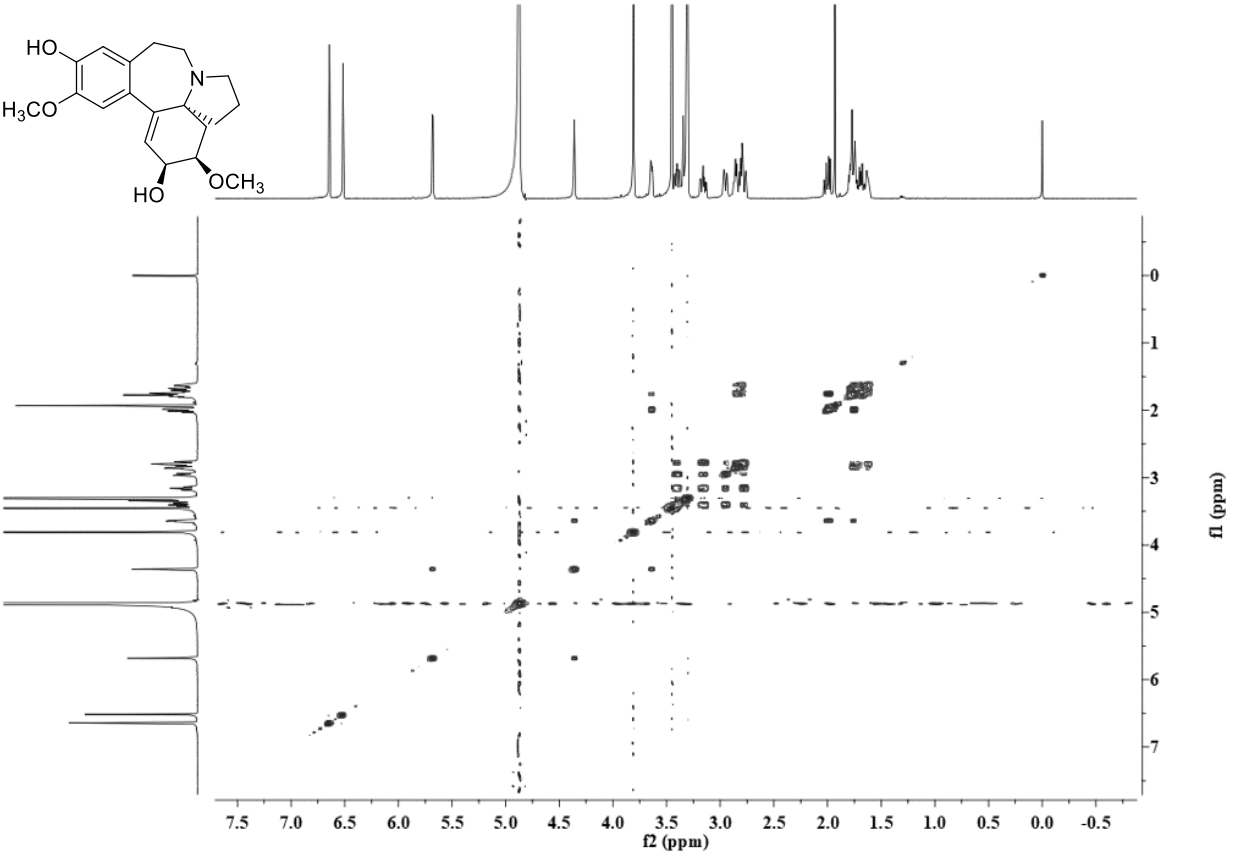

Figure S87. $^{1}H–^{1}H$ COSY spectrum of **8** in CD_3OD

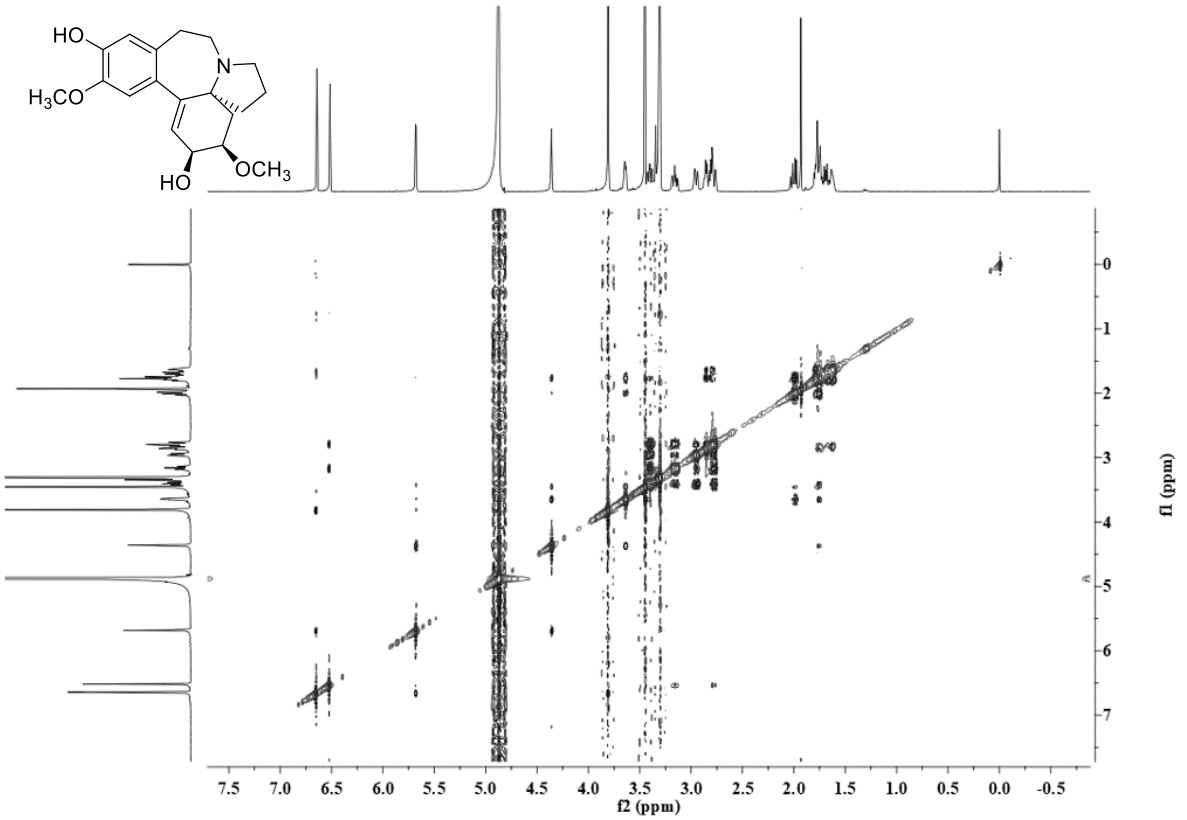

Figure S88. NOESY spectrum of **8** in CD_3OD

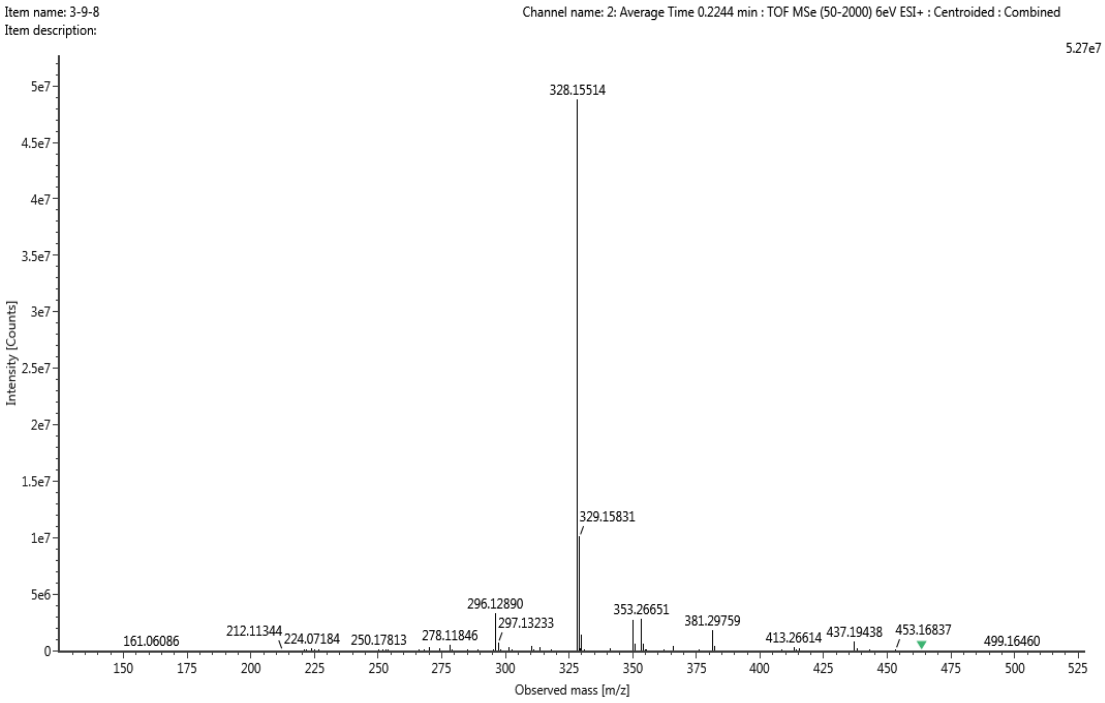

Figure S89. (+)-HR-ESI-MS spectrum of **9**

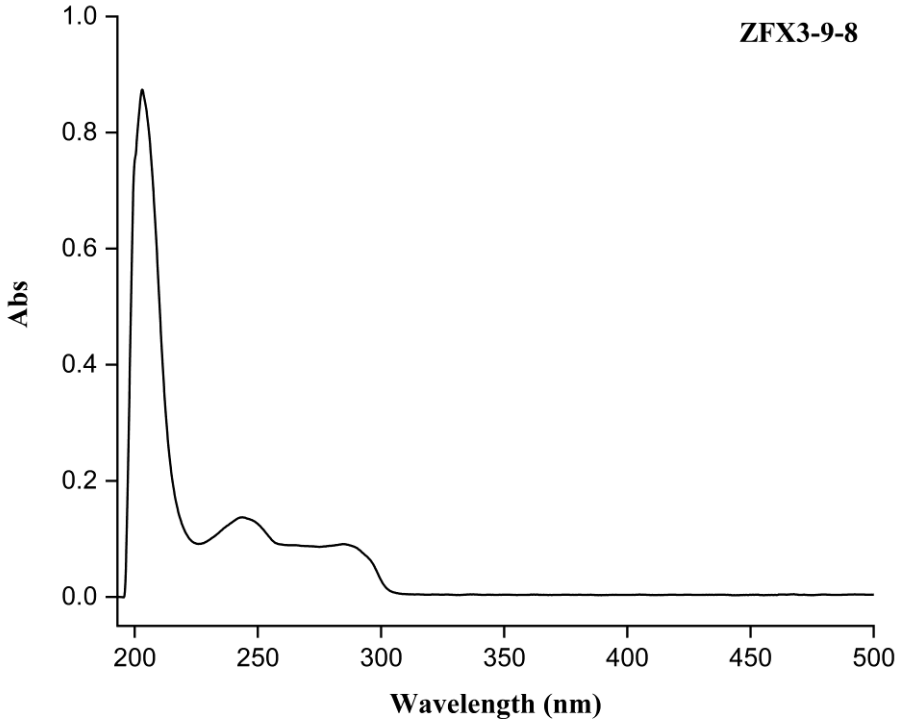

Figure S90. UV spectrum of **9** in MeOH

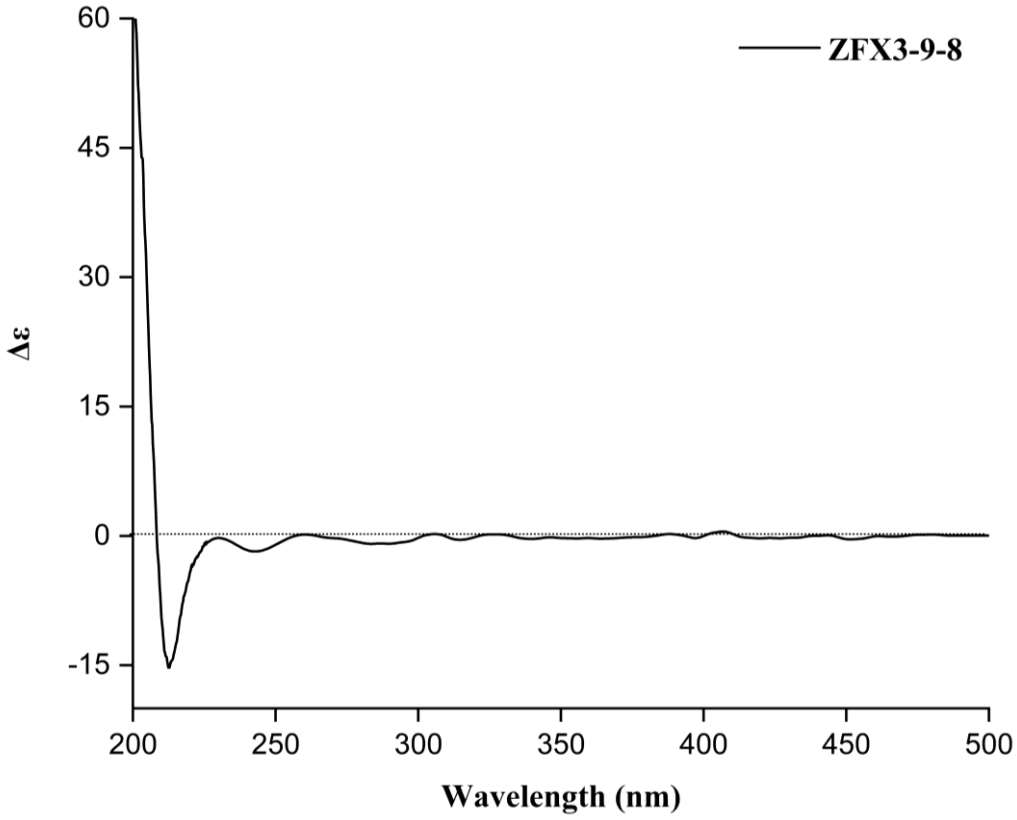

Figure S91. ECD spectrum of **9** in MeOH

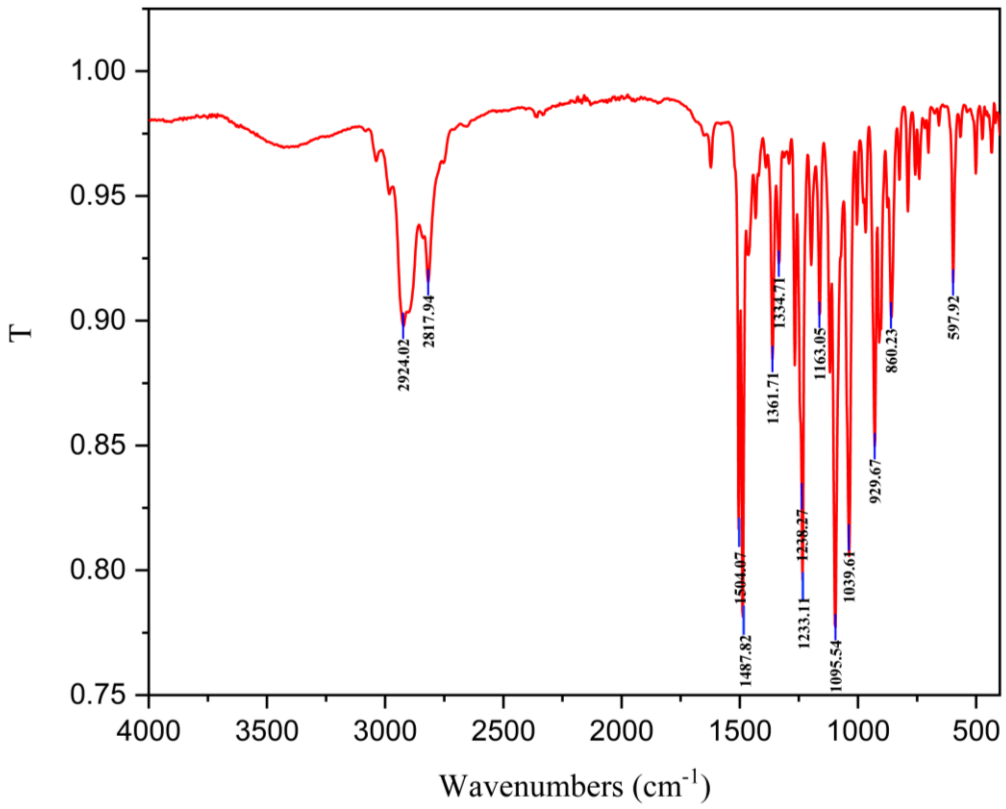

Figure S92. IR spectrum of **9**

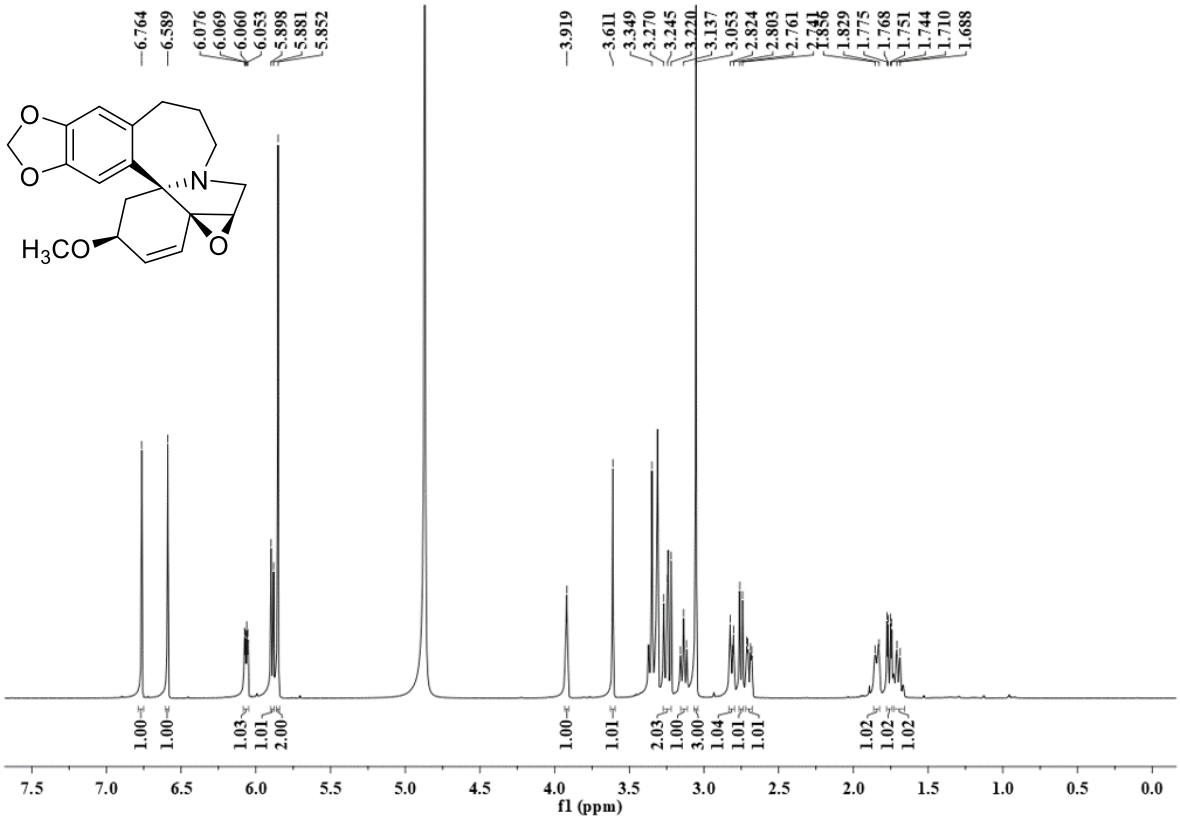

Figure S93. ^{1}H NMR (600 MHz) spectrum of **9** in CD_3OD

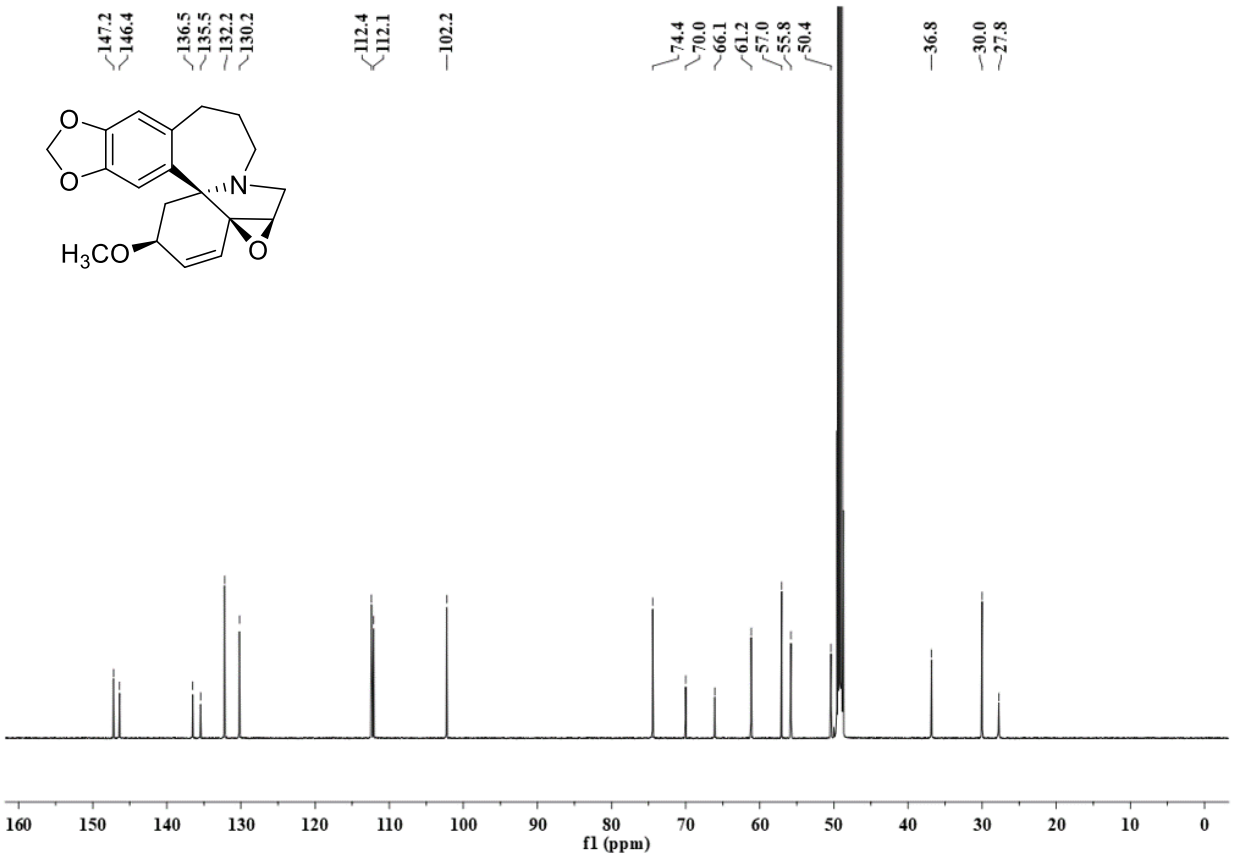

Figure S94. ^{13}C NMR (150 MHz) spectrum of 9 in CD_3OD

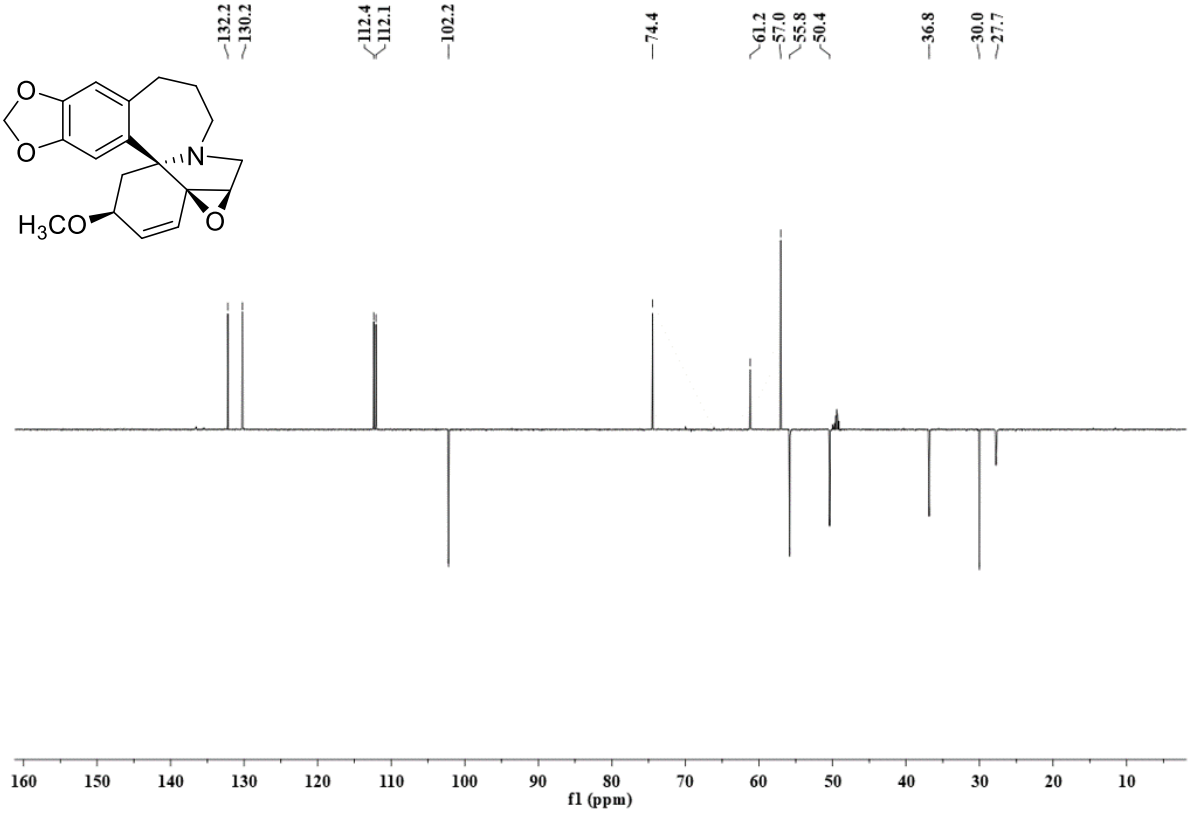

Figure S95. DEPT 135 spectrum of **9** in CD_3OD

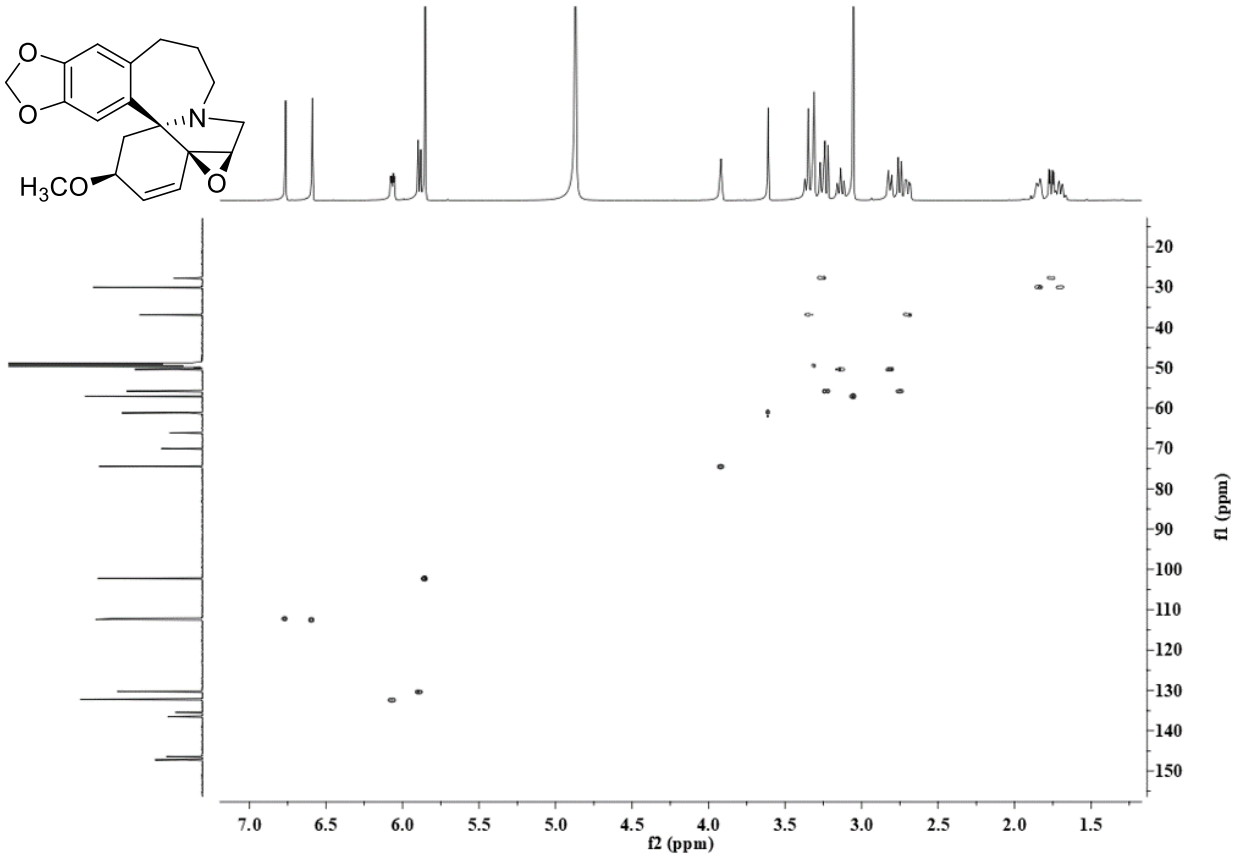

Figure S96. HSQC spectrum of **9** in CD_3OD

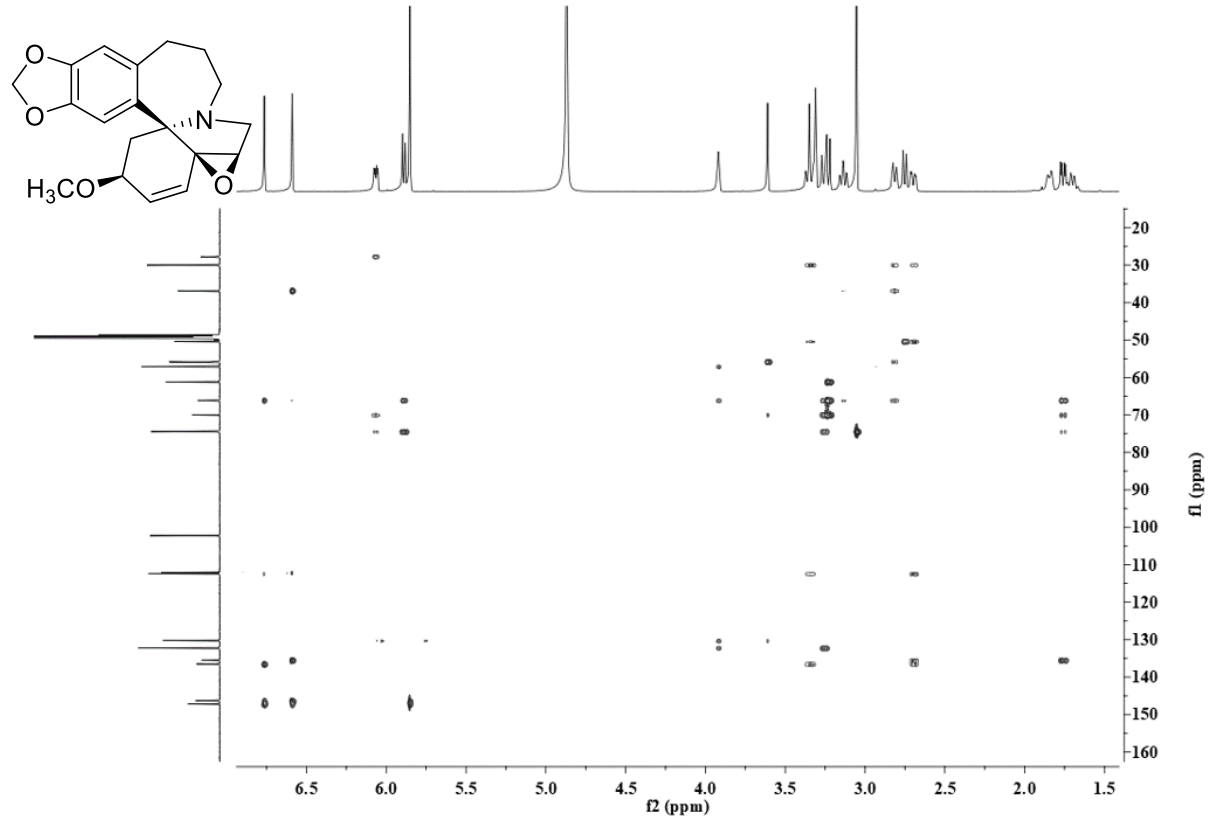

Figure S97. HMBC spectrum of **9** in CD_3OD

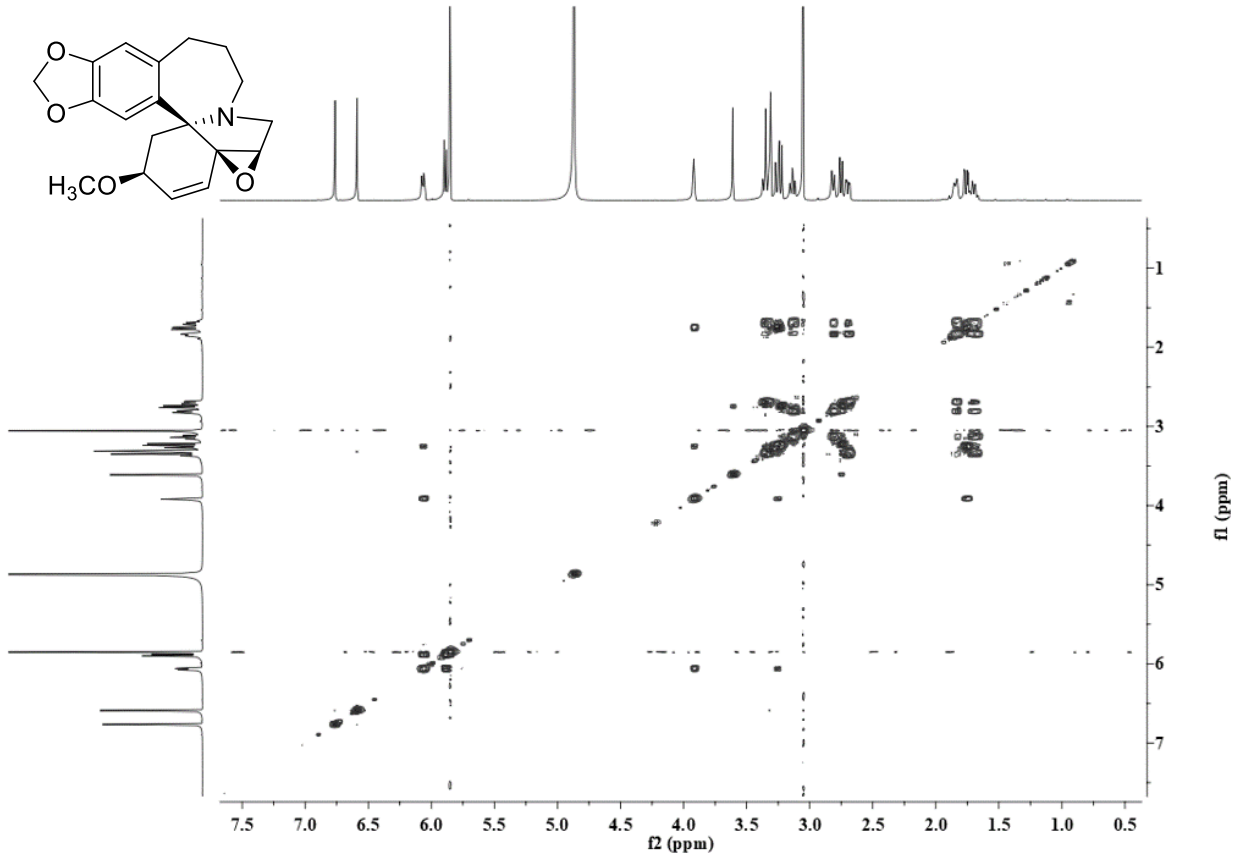

Figure S98. $^{1}H–^{1}H$ COSY spectrum of **9** in CD_3OD

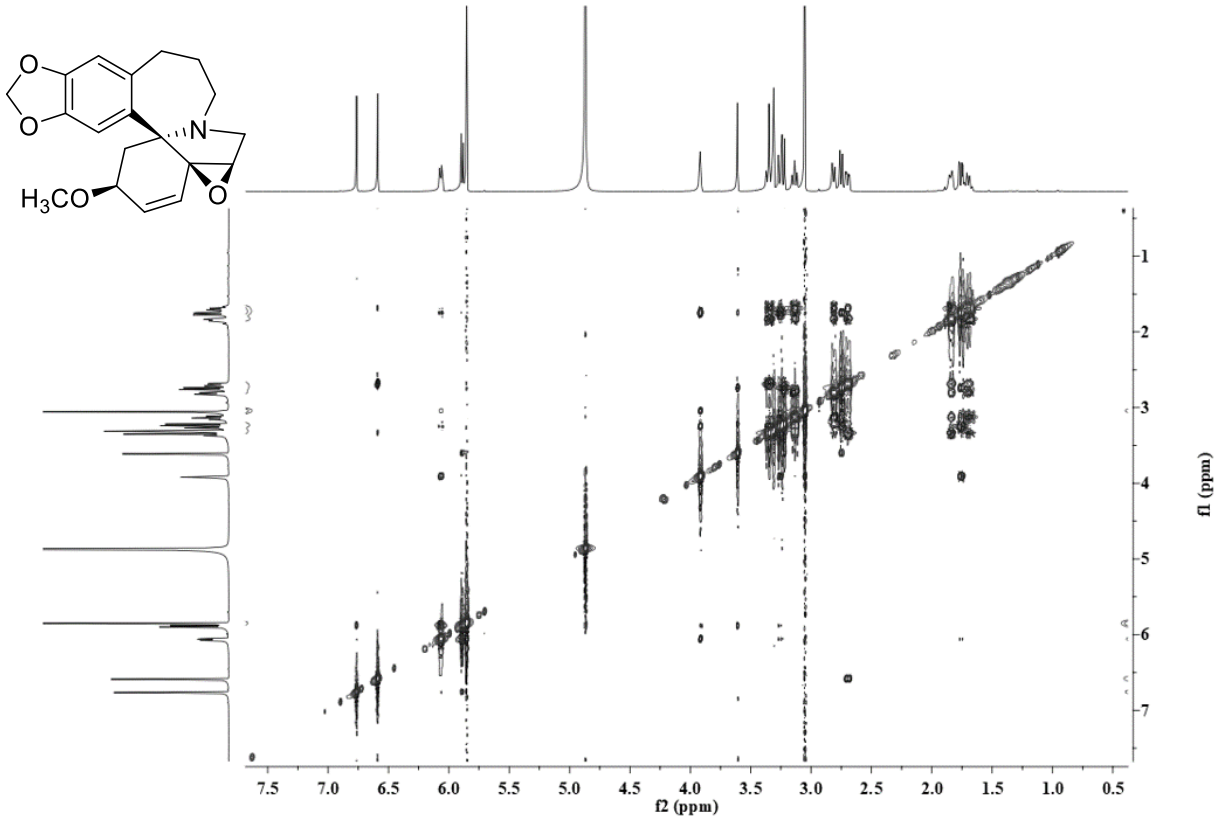

Figure S99. NOESY spectrum of **9** in CD_3OD

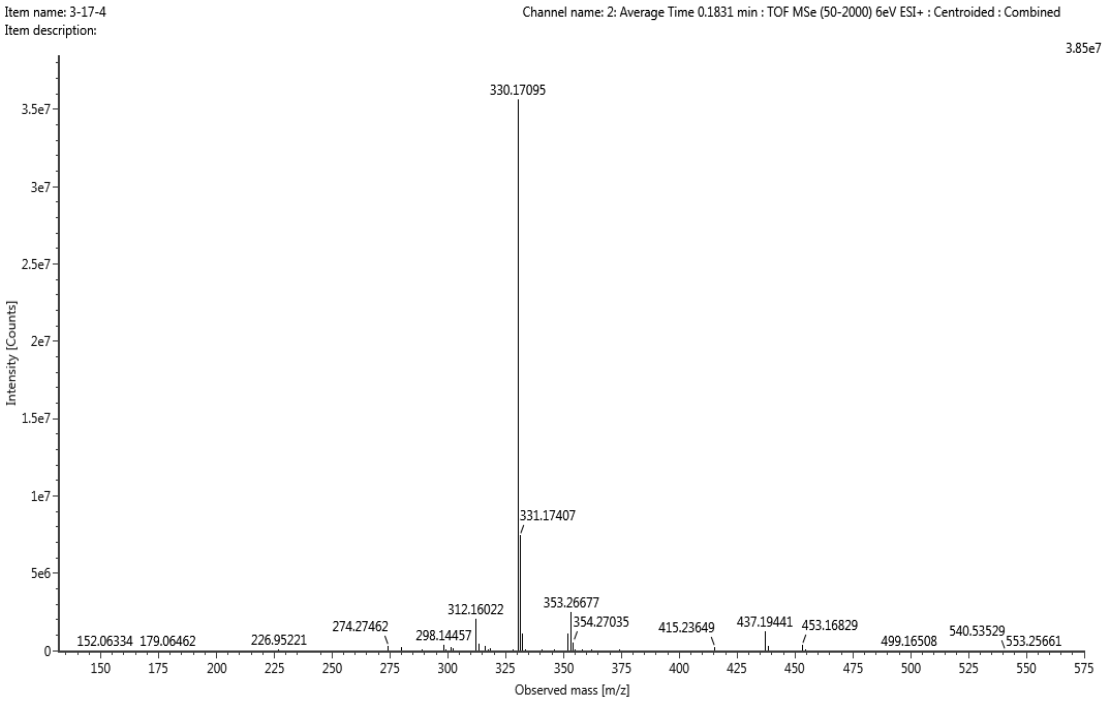

Figure S100. (+)-HR-ESI-MS spectrum of **10**

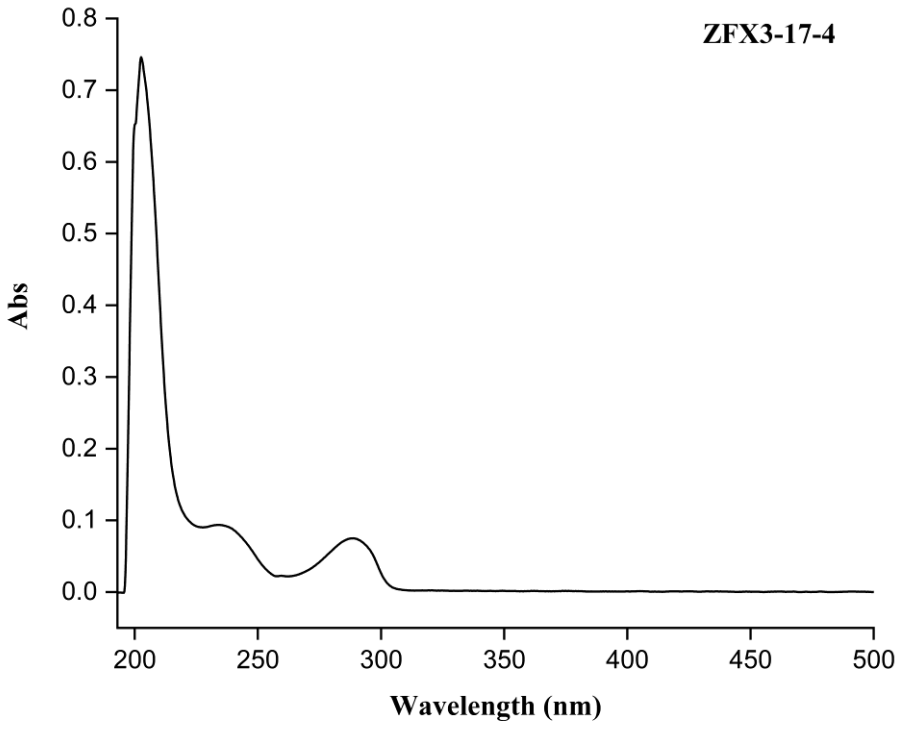

Figure S101. UV spectrum of **10** in MeOH

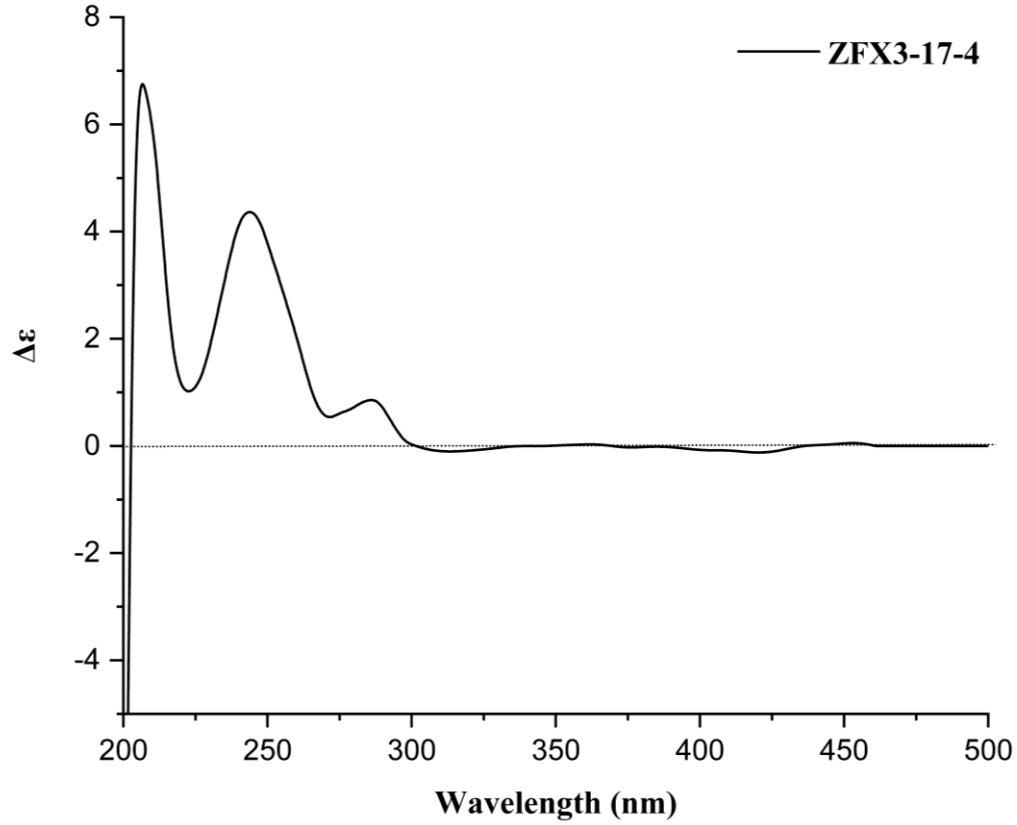

Figure S102. ECD spectrum of **10** in MeOH

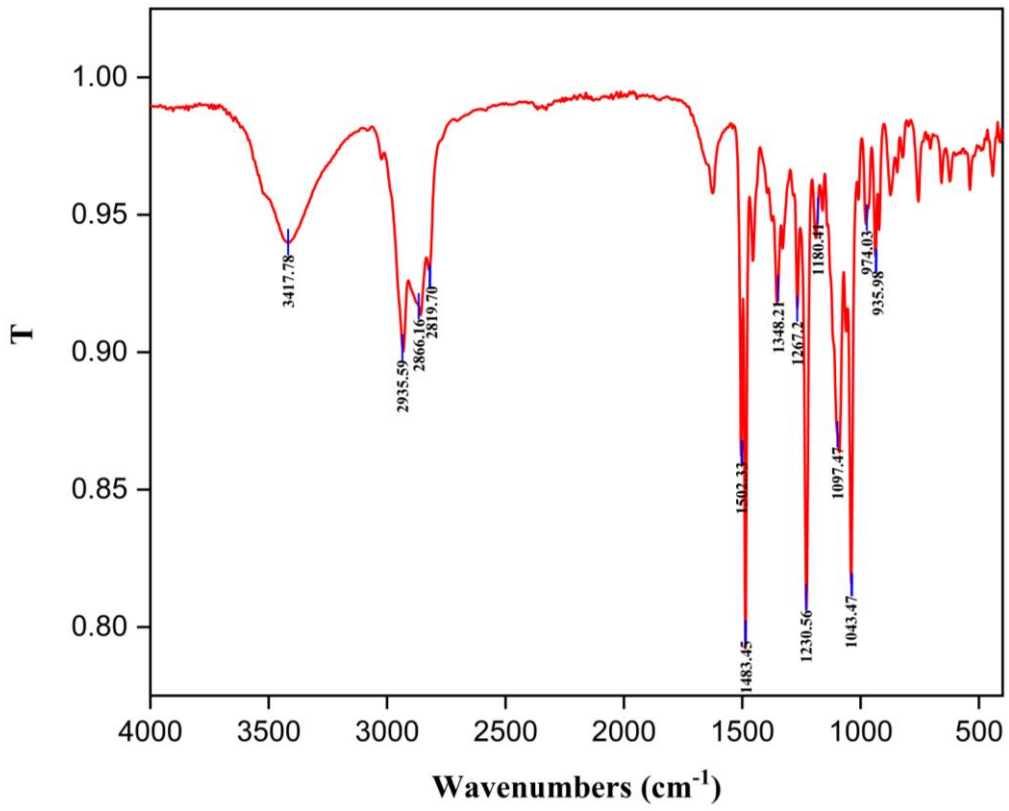

Figure S103. IR spectrum of **10**

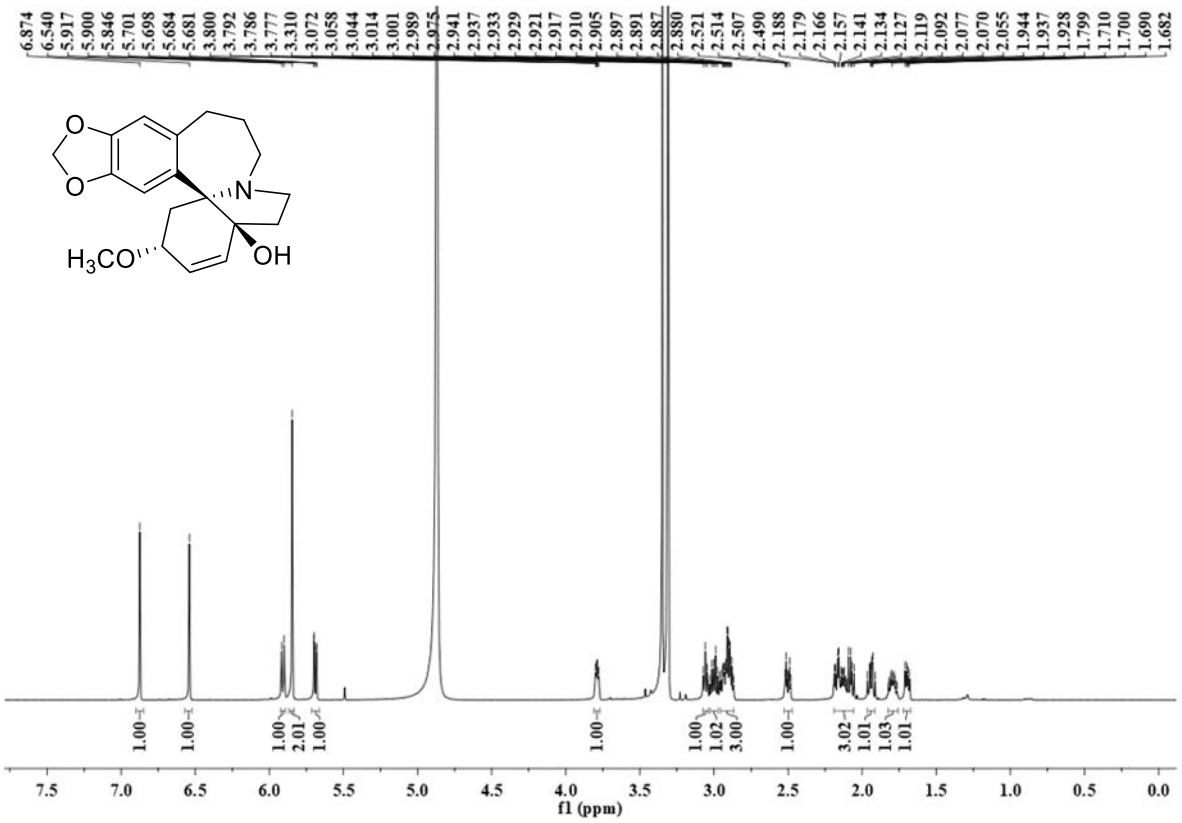

Figure S104. ^{1}H NMR (600 MHz) spectrum of **10** in CD_3OD

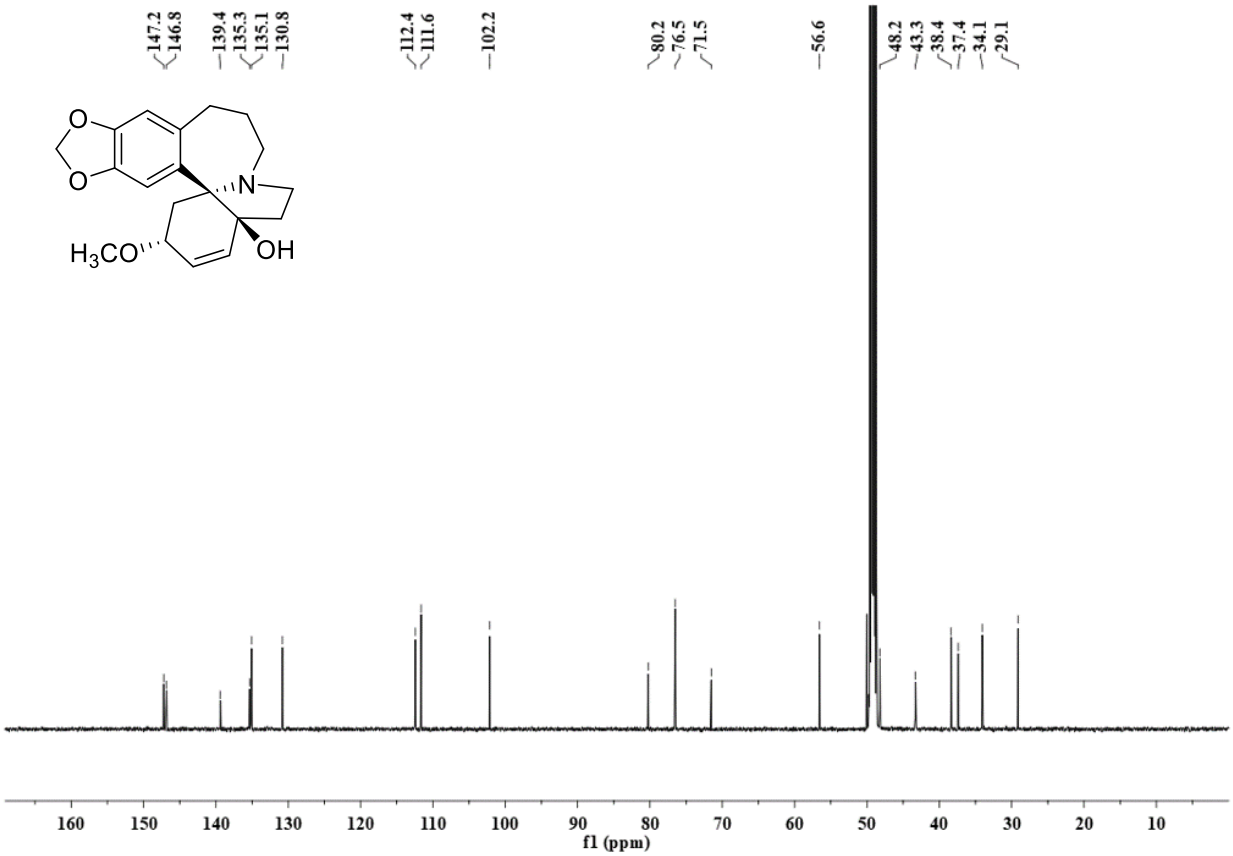

Figure S105. ^{13}C NMR (150 MHz) spectrum of **10** in CD_3OD

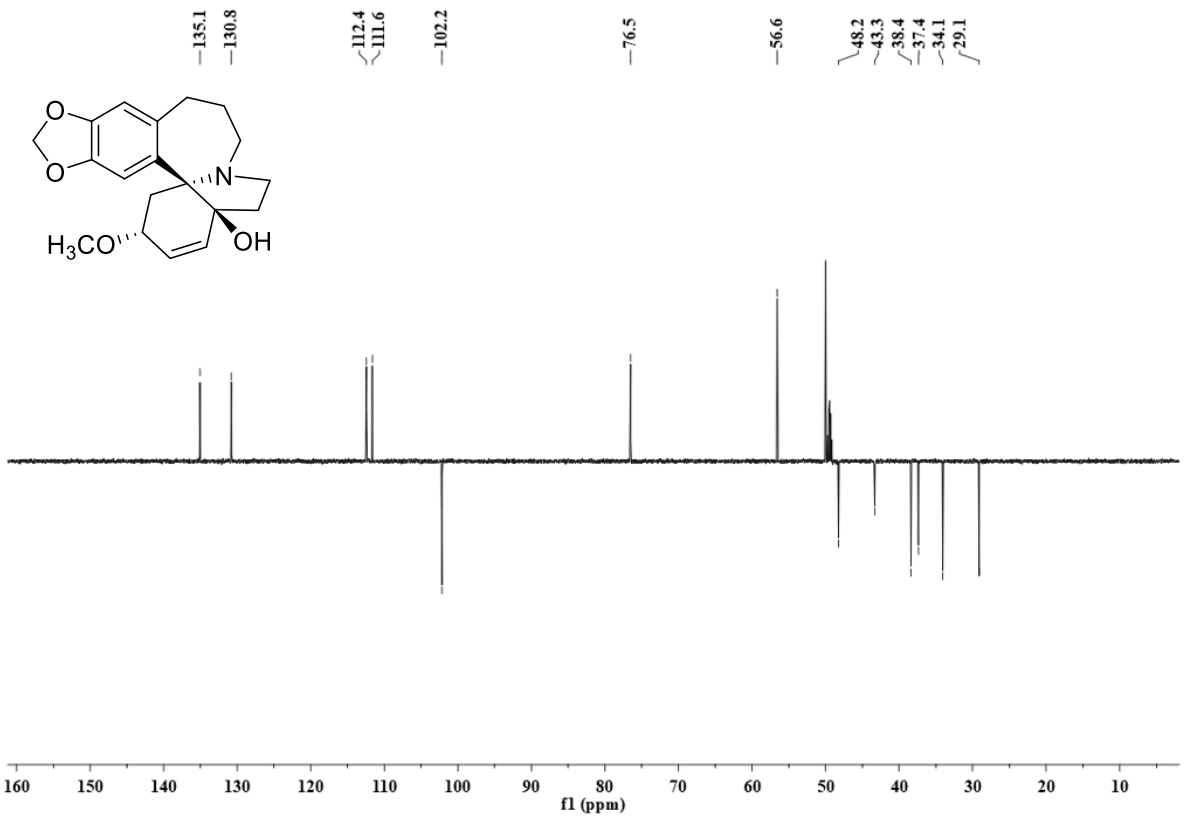

Figure S106. DEPT 135 spectrum of **10** in CD_3OD

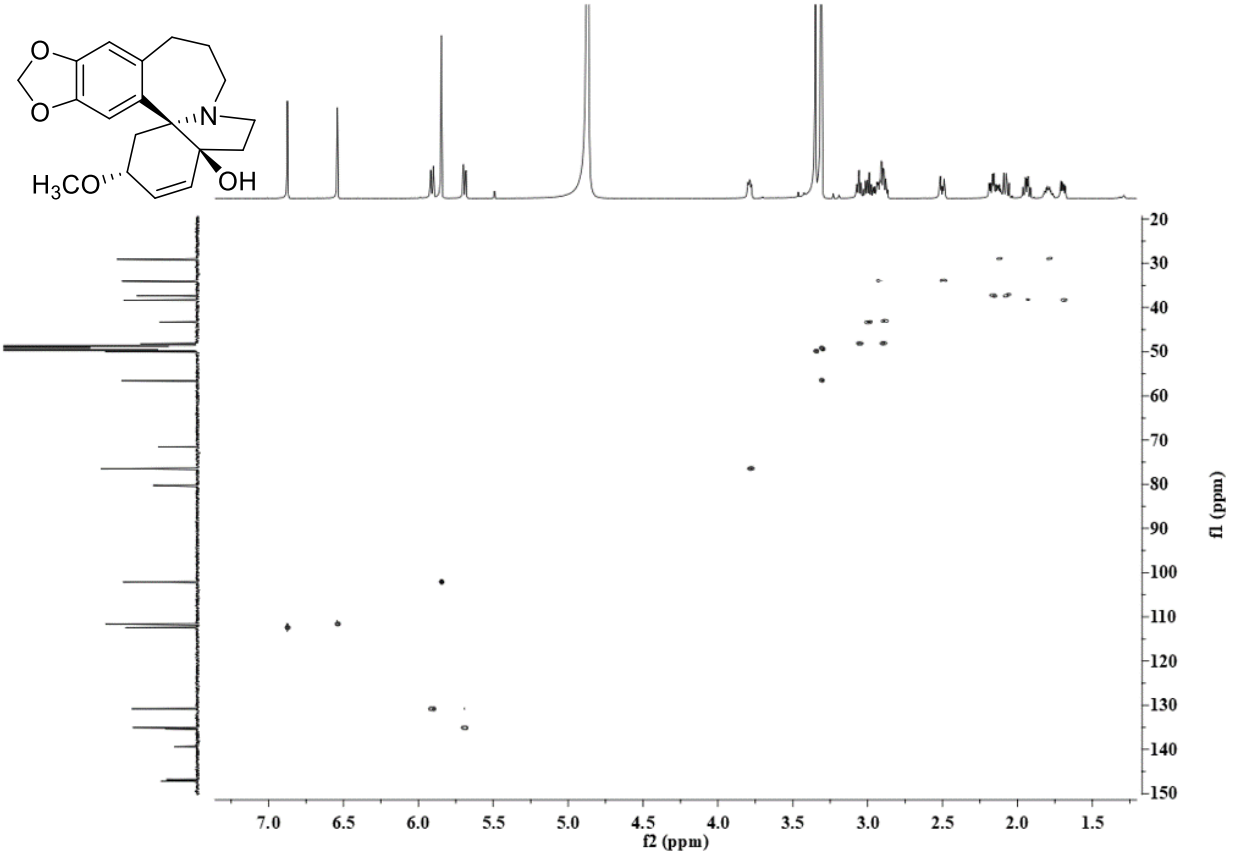

Figure S107. HSQC spectrum of **10** in CD_3OD

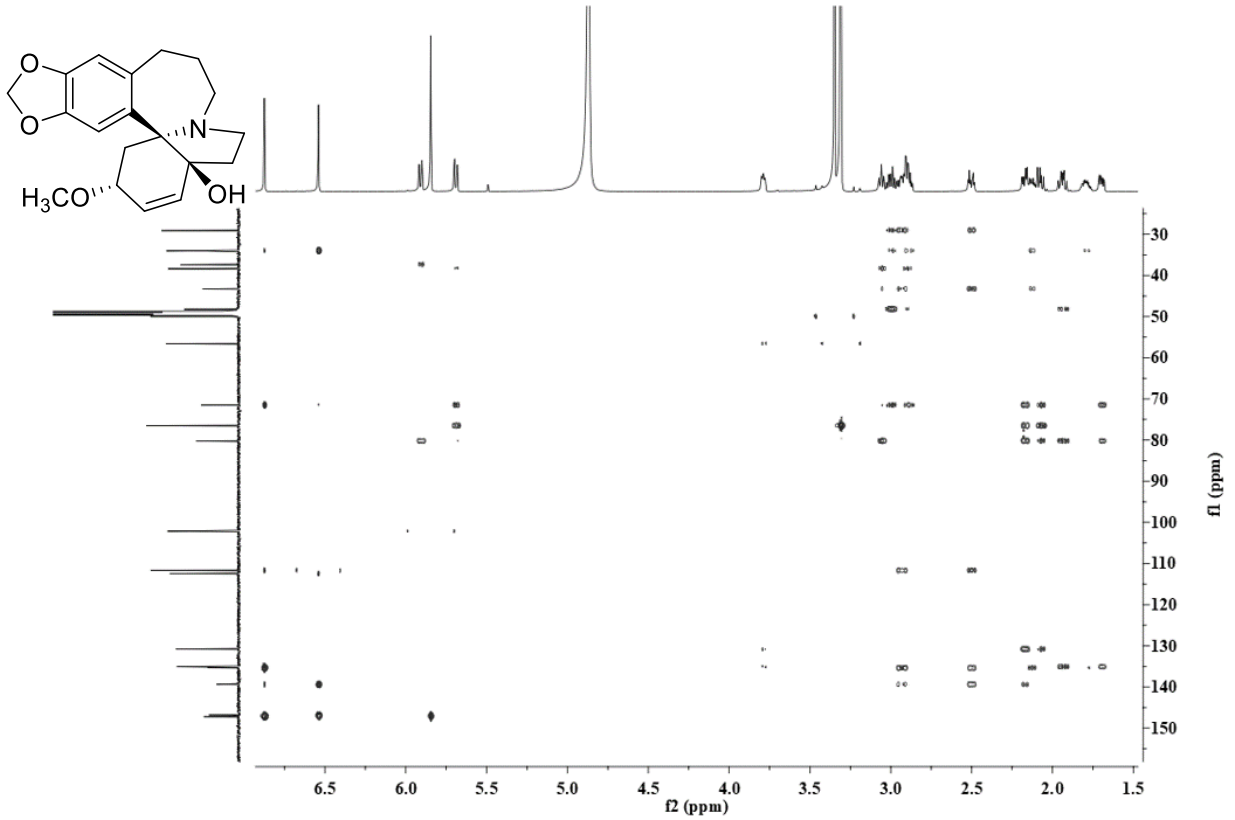

Figure S108. HMBC spectrum of **10** in CD_3OD

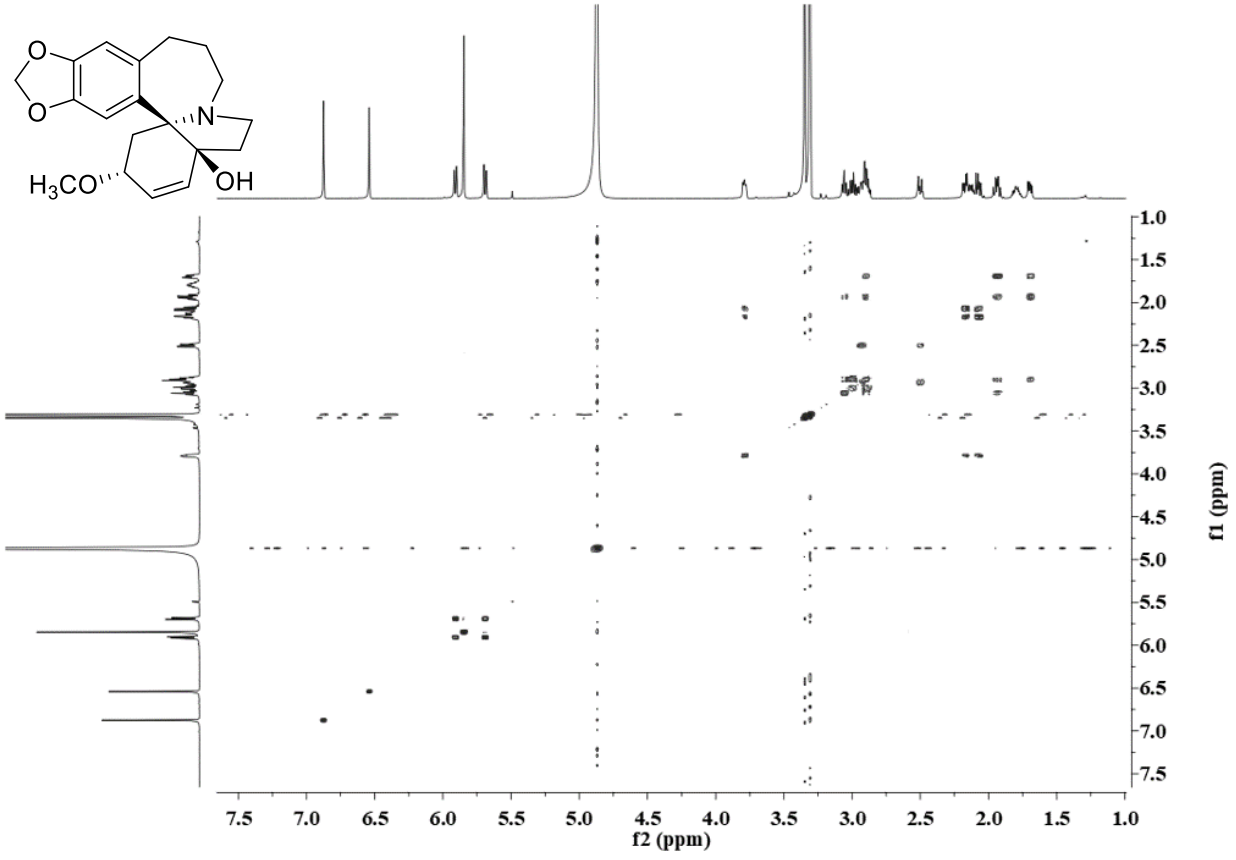

Figure S109. $^{1}H–^{1}H$ COSY spectrum of **10** in CD_3OD

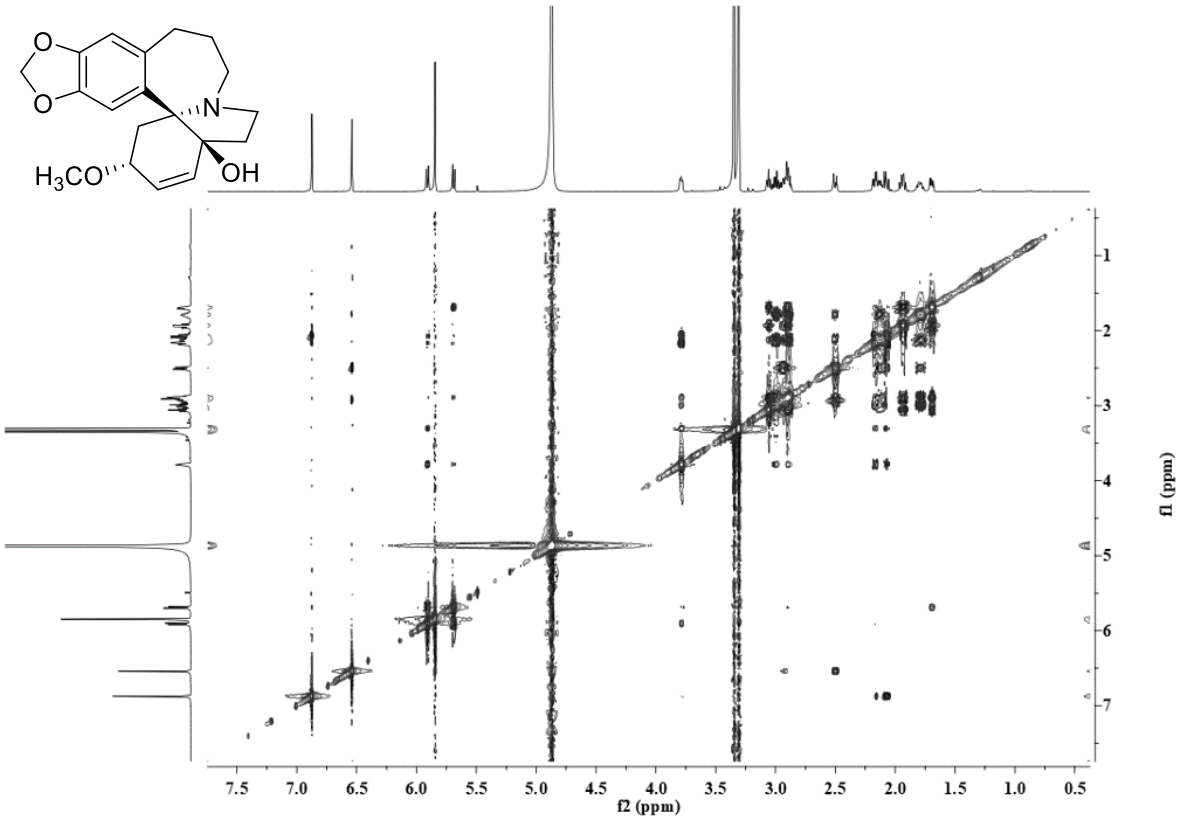

Figure S110. NOESY spectrum of **10** in CD_3OD

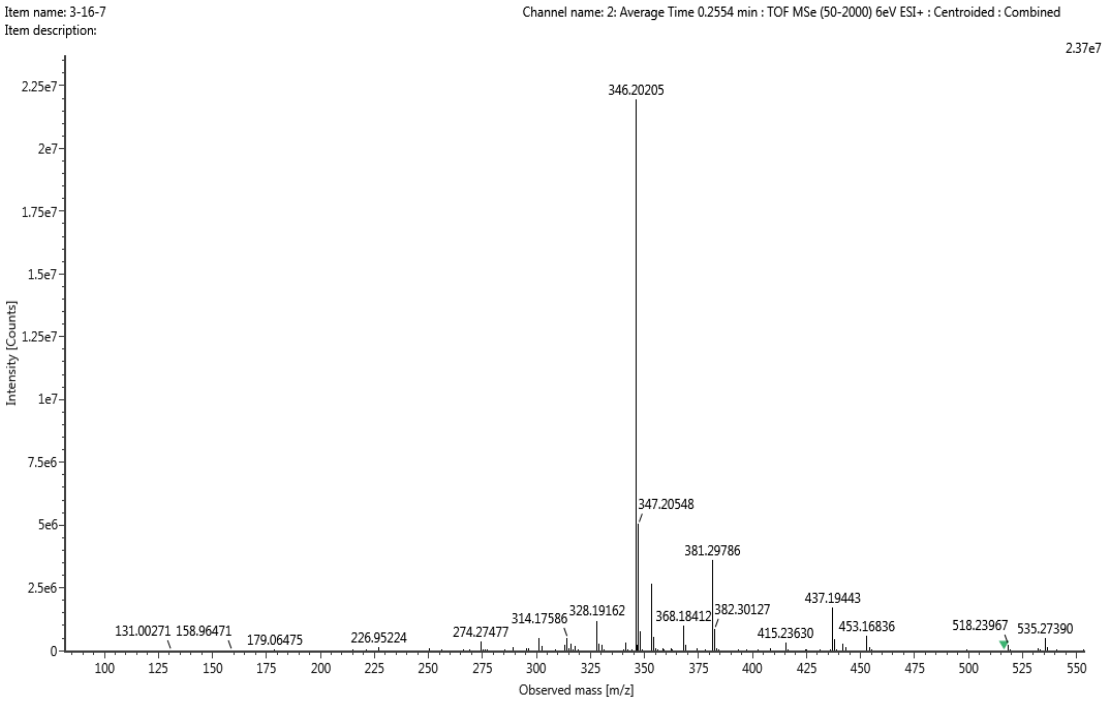

Figure S111. (+)-HR-ESI-MS spectrum of **11**

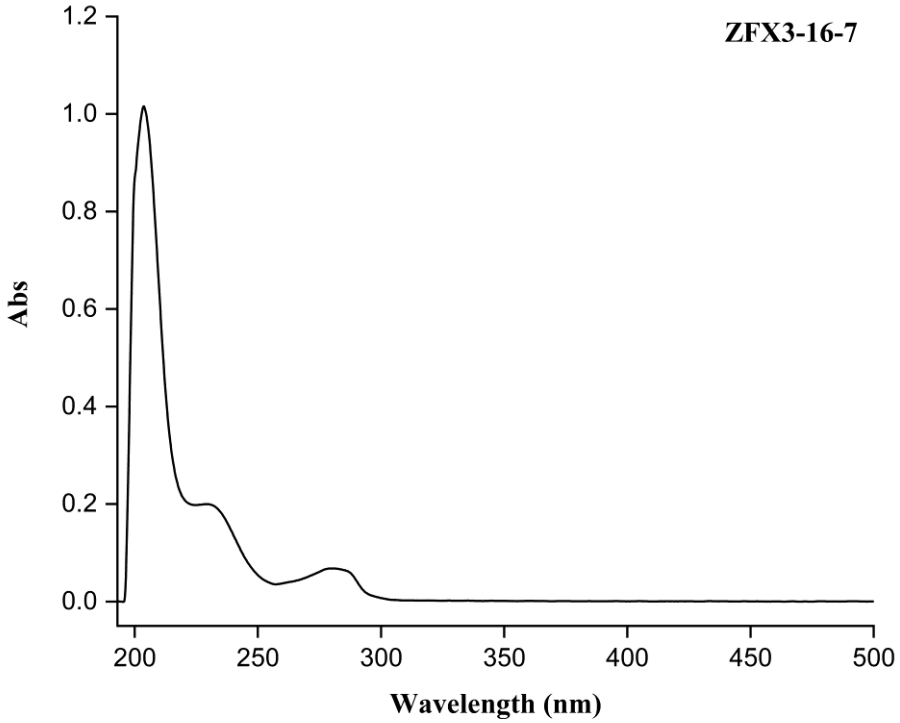

Figure S112. UV spectrum of **11** in MeOH

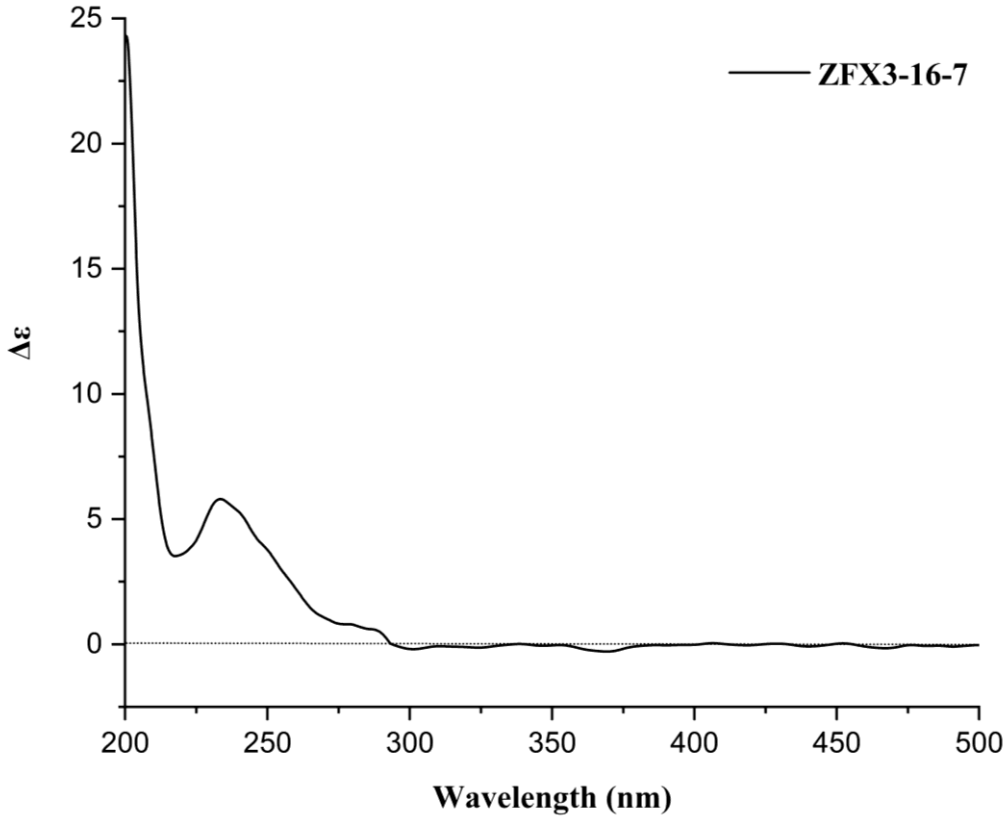

Figure S113. ECD spectrum of **11** in MeOH

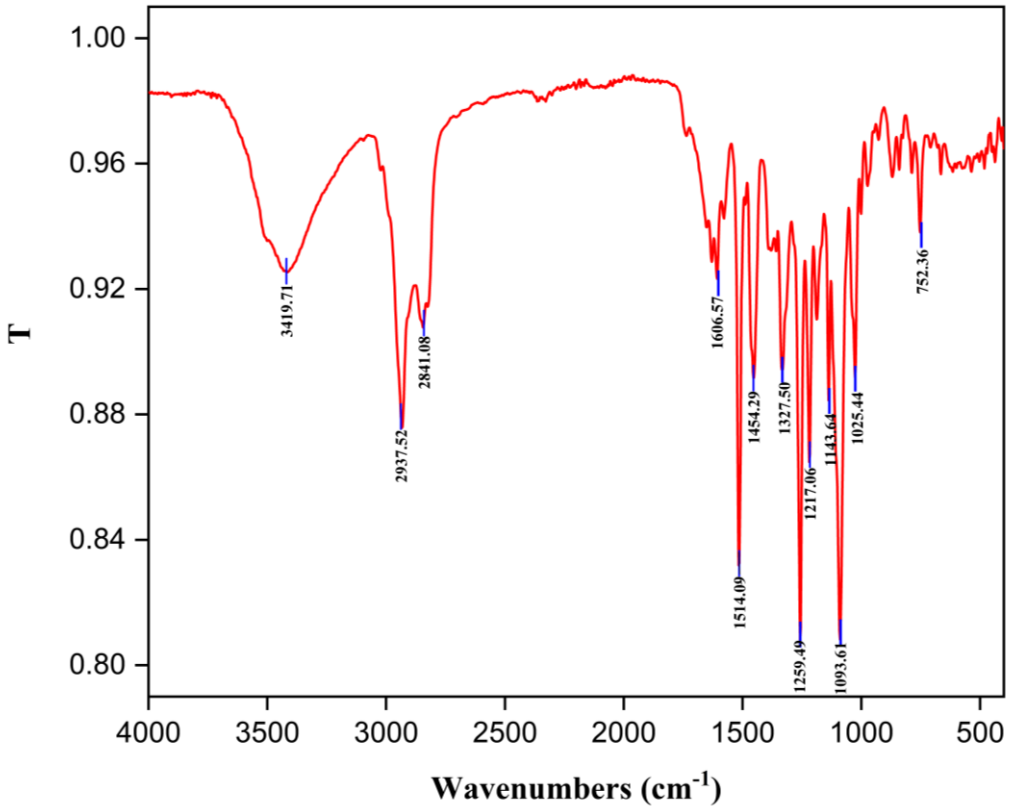

Figure S114. IR spectrum of **11**

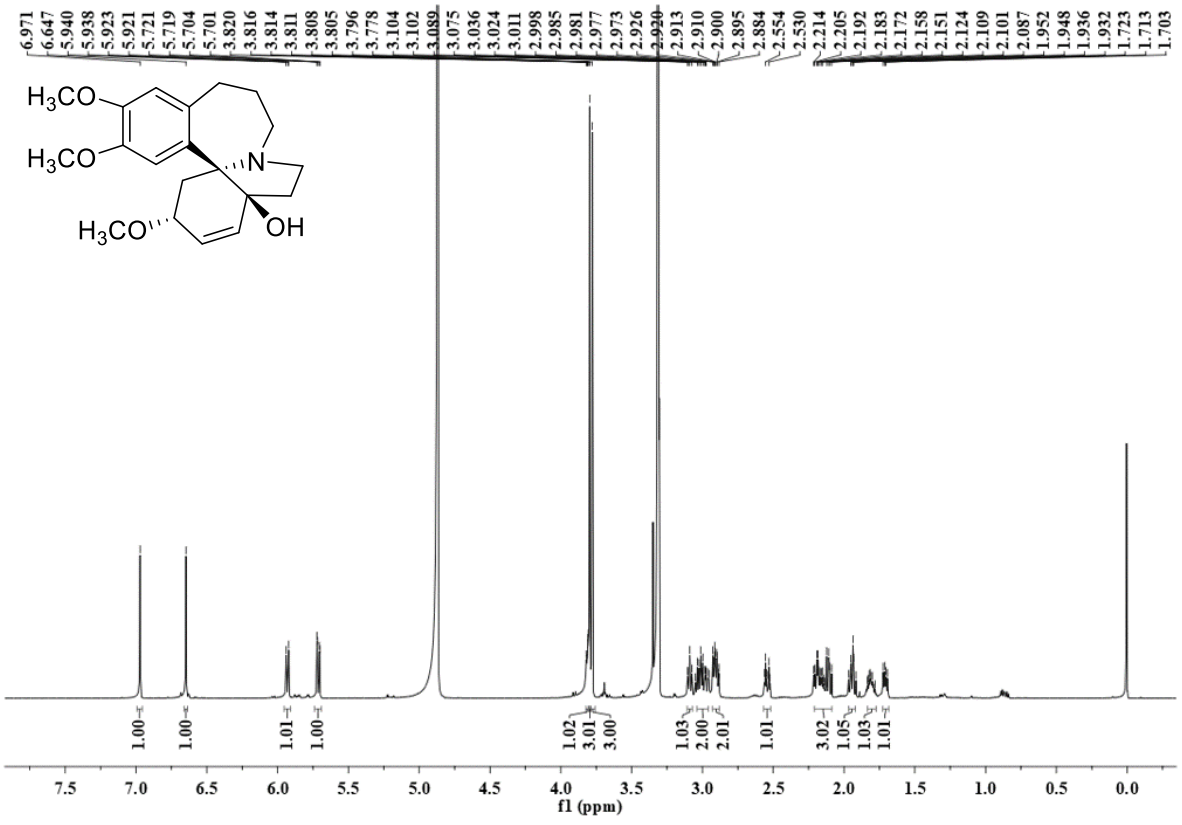

Figure S115. ^{1}H NMR (600 MHz) spectrum of **11** in CD_3OD

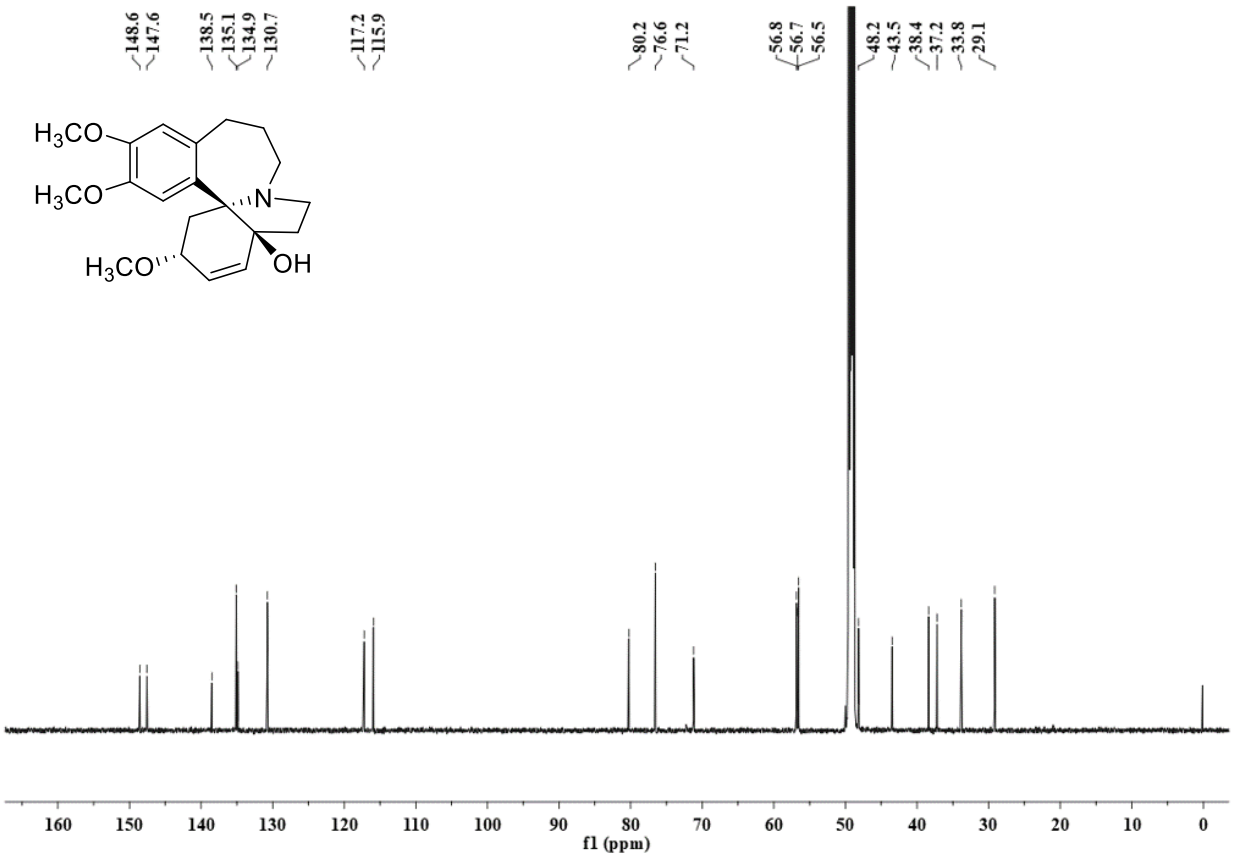

Figure S116. ^{13}C NMR (150 MHz) spectrum of **11** in CD_3OD

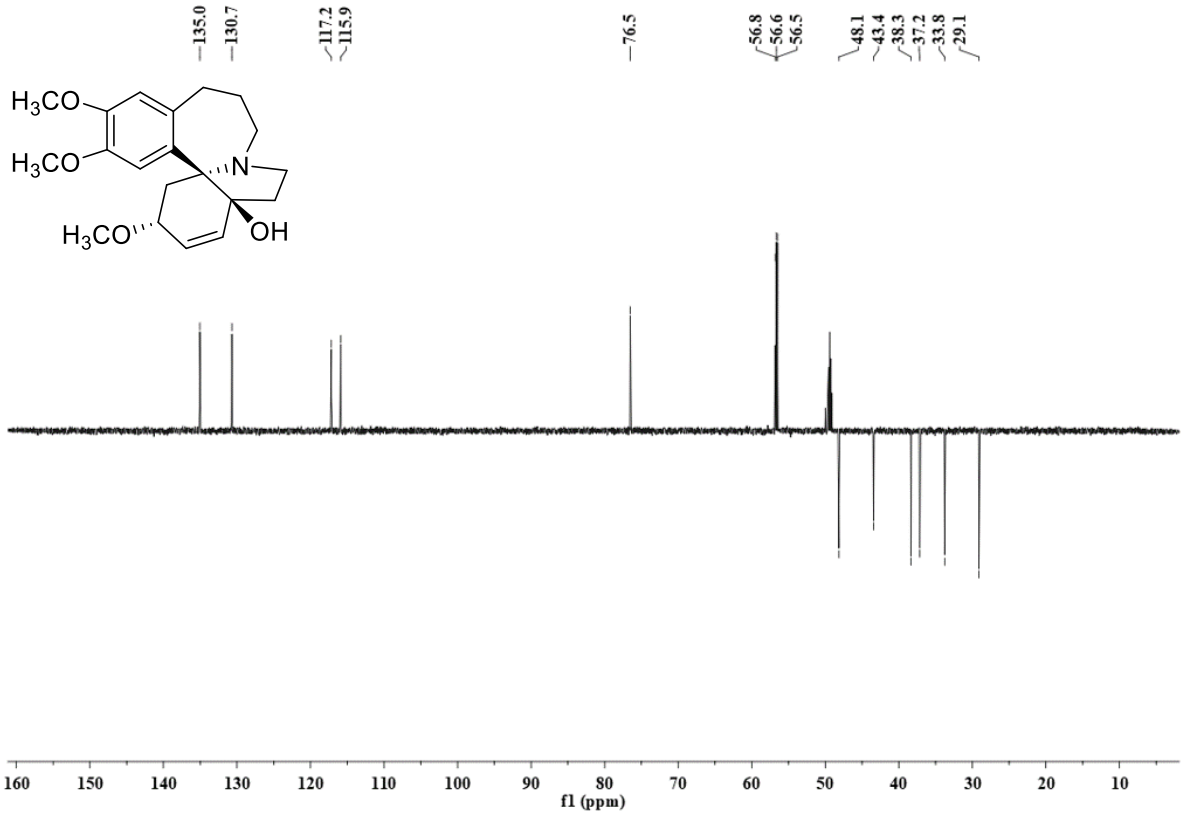

Figure S117. DEPT 135 spectrum of **11** in CD_3OD

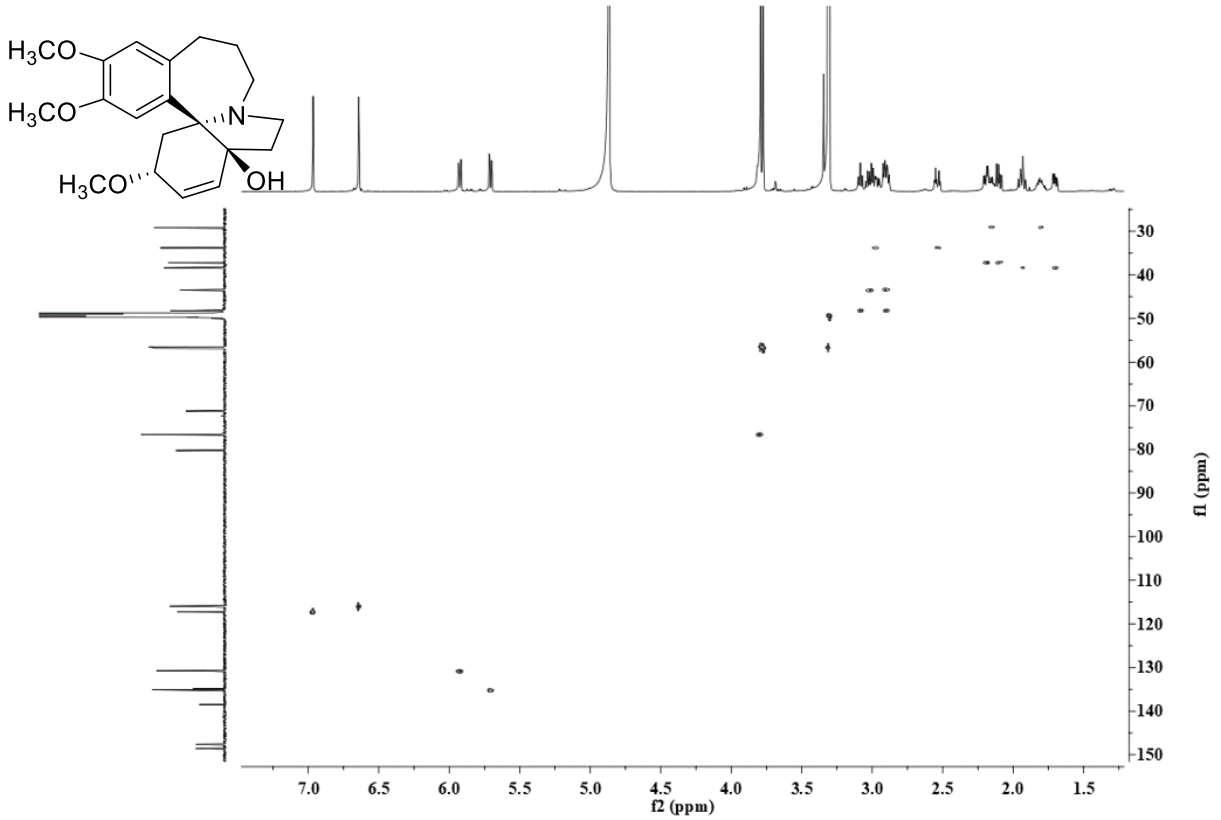

Figure S118. HSQC spectrum of **11** in CD_3OD

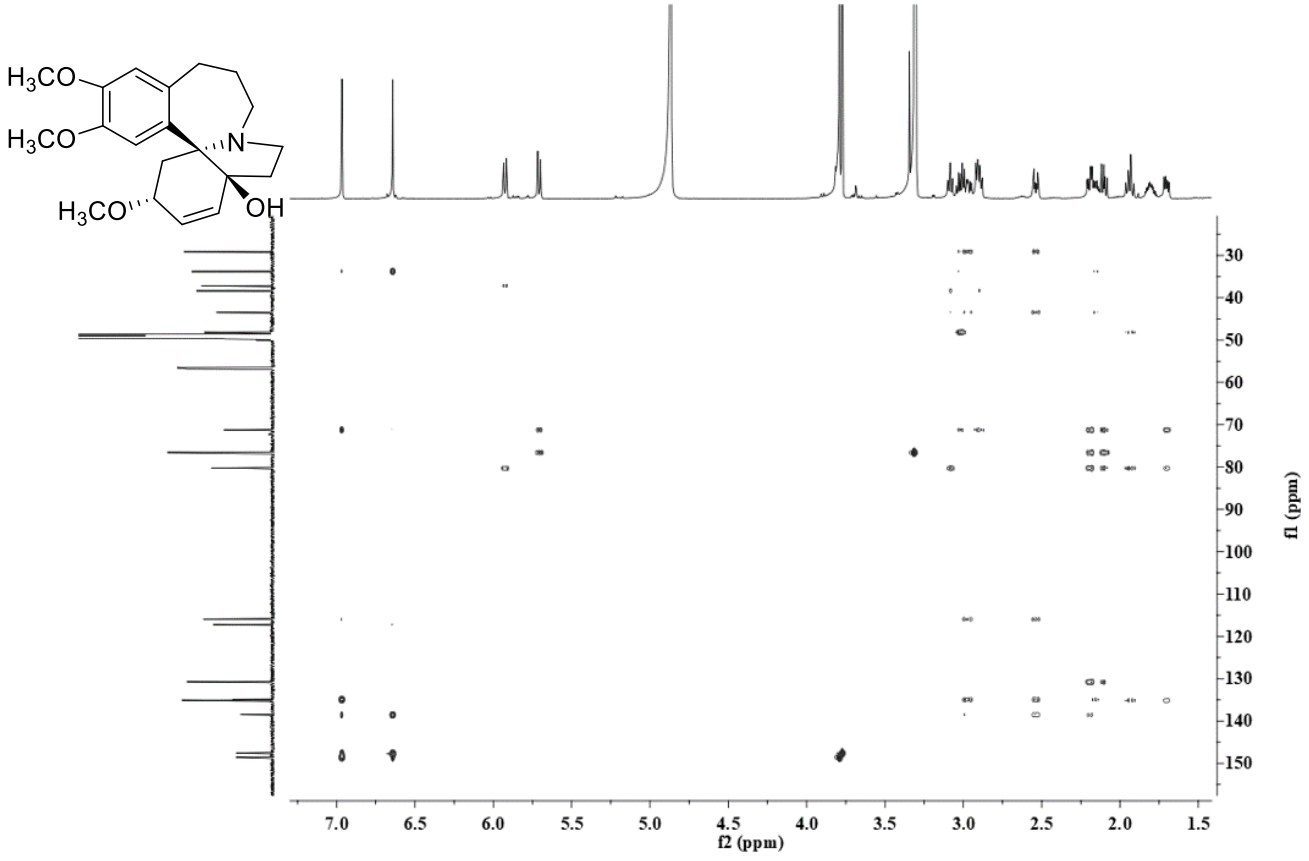

Figure S119. HMBC spectrum of **11** in CD_3OD

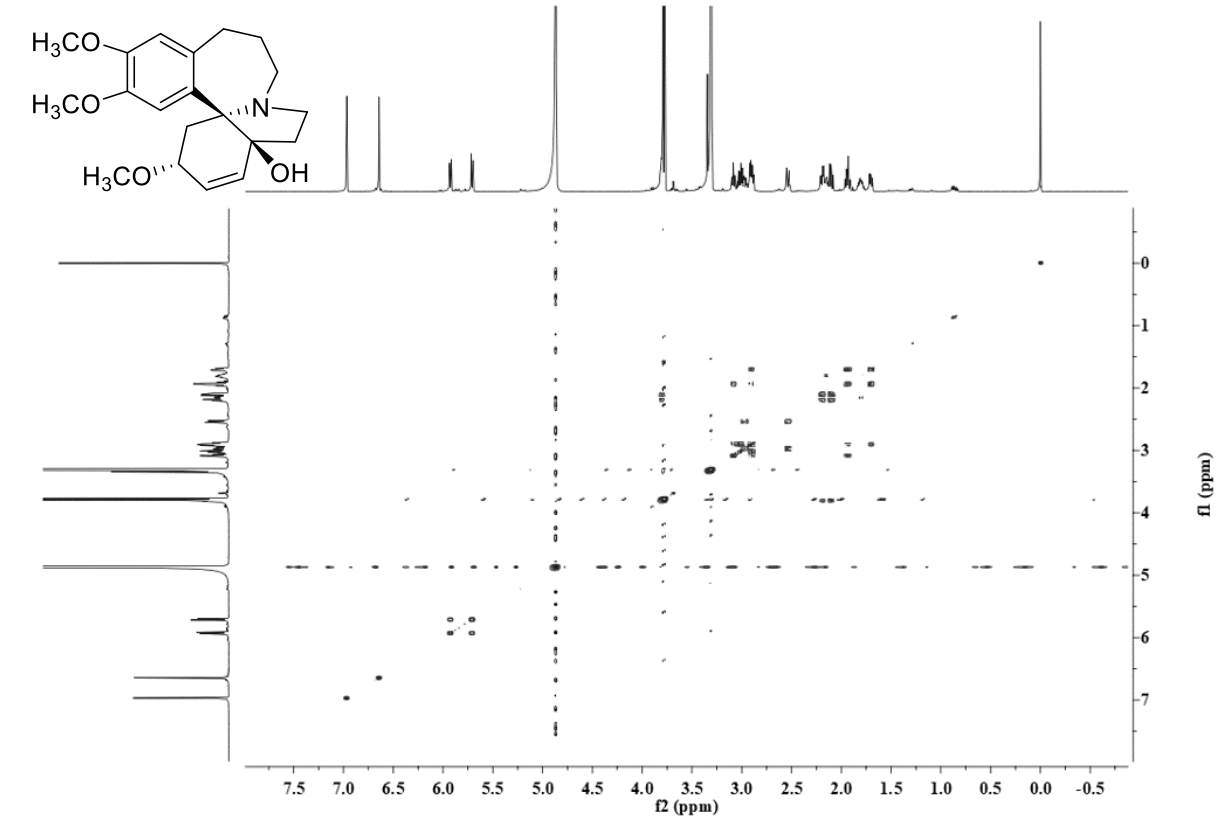

Figure S120. $^{1}H–^{1}H$ COSY spectrum of **11** in CD_3OD

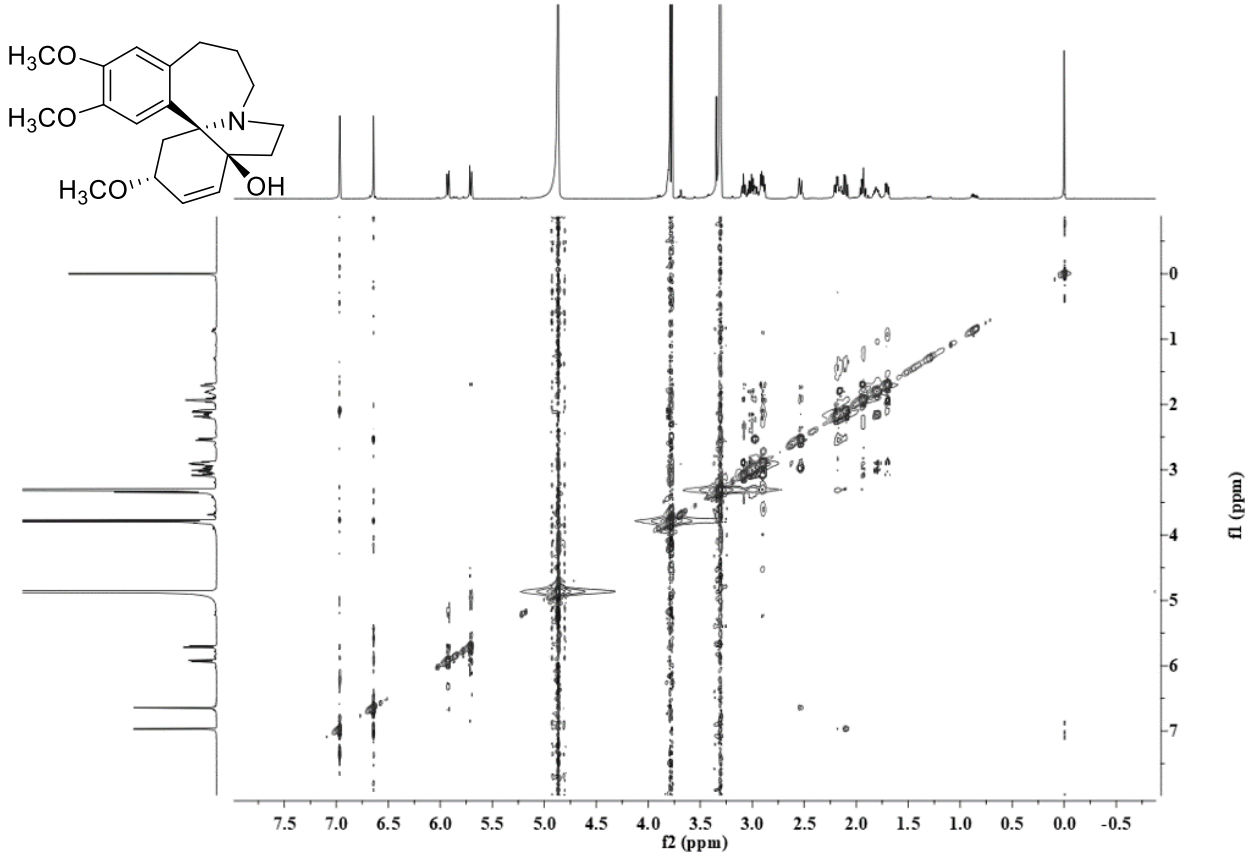

Figure S121. NOESY spectrum of **11** in CD_3OD

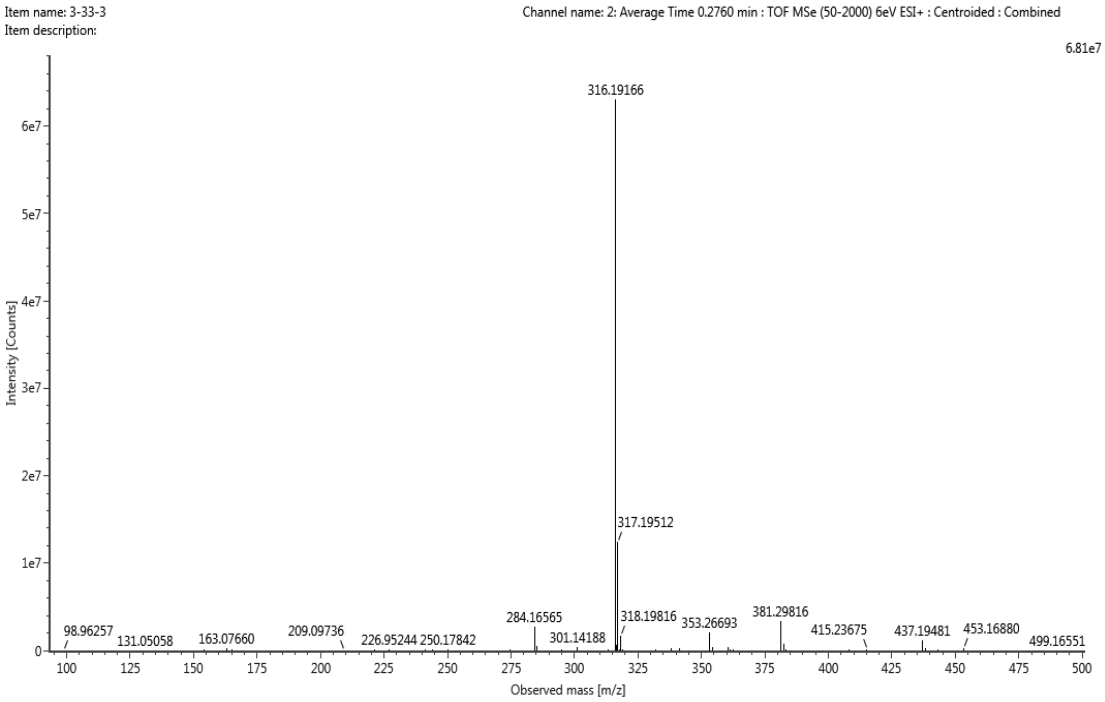

Figure S122. (+)-HR-ESI-MS spectrum of **12**

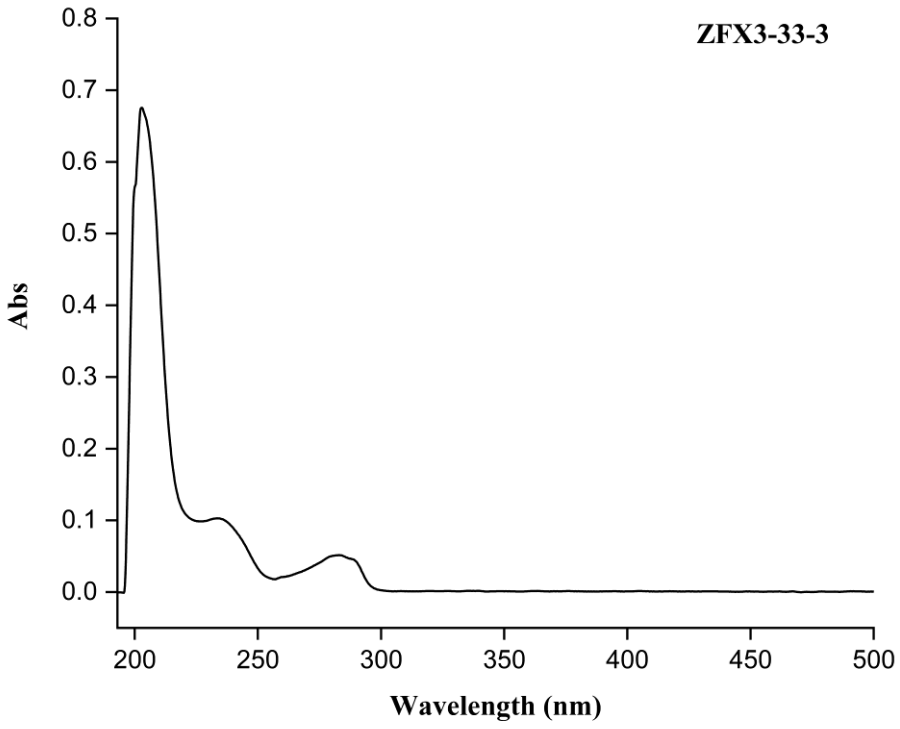

Figure S123. UV spectrum of **12** in MeOH

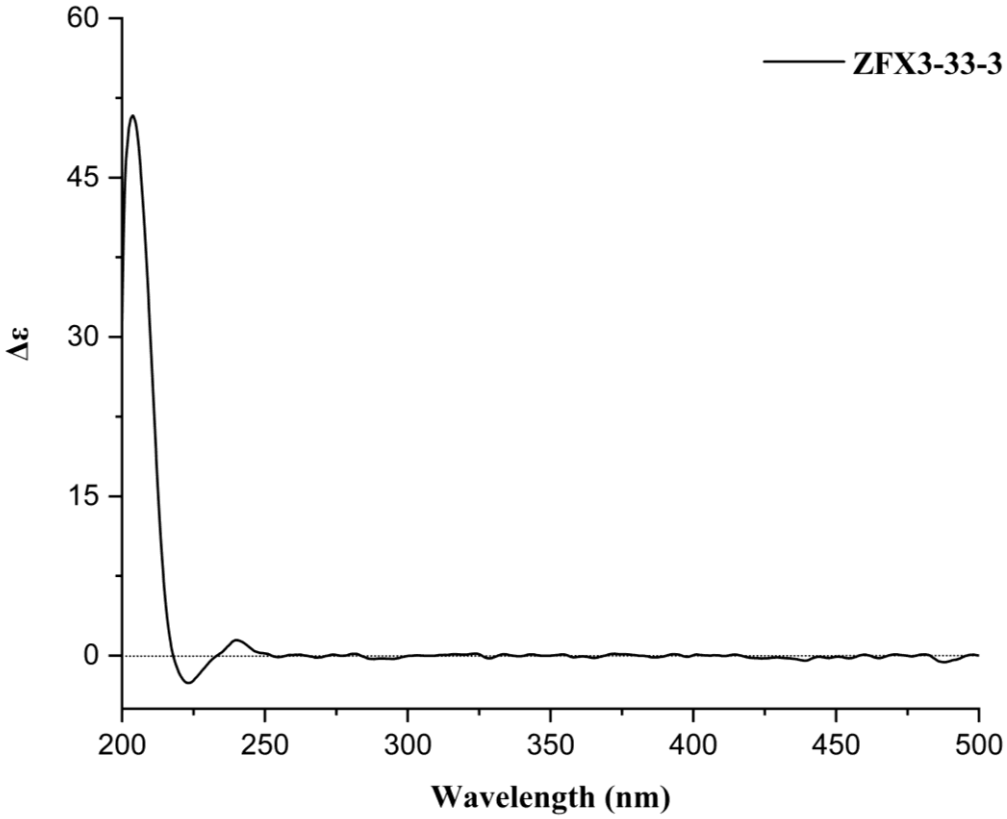

Figure S124. ECD spectrum of **12** in MeOH

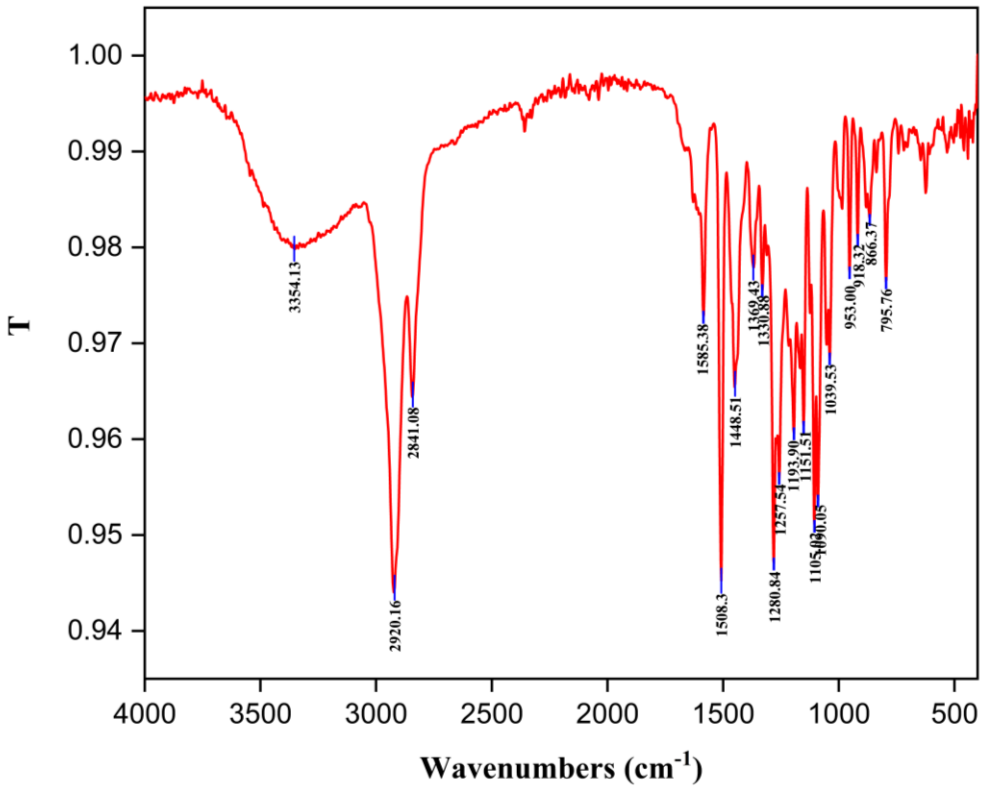

Figure S125. IR spectrum of **12**

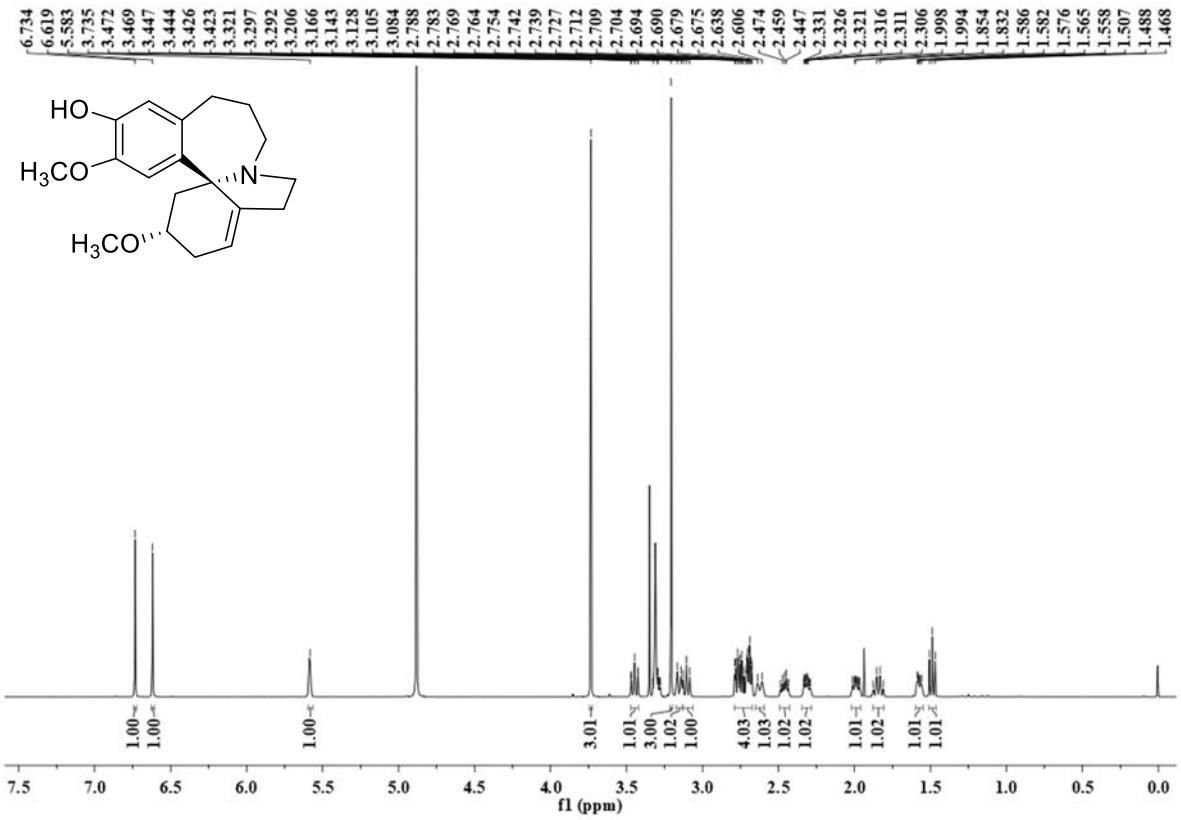

Figure S126. ^{1}H NMR (600 MHz) spectrum of **12** in CD_3OD

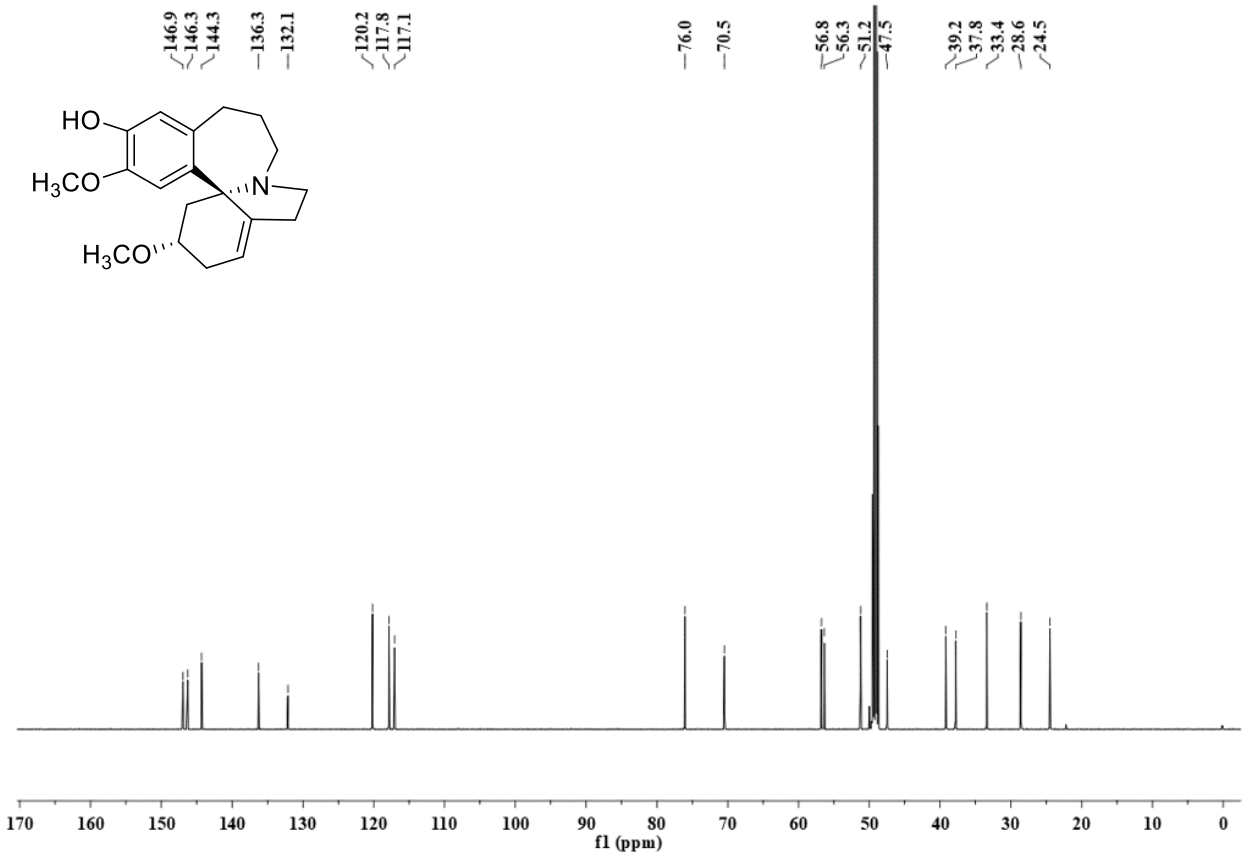

Figure S127. ^{13}C NMR (150 MHz) spectrum of **12** in CD_3OD

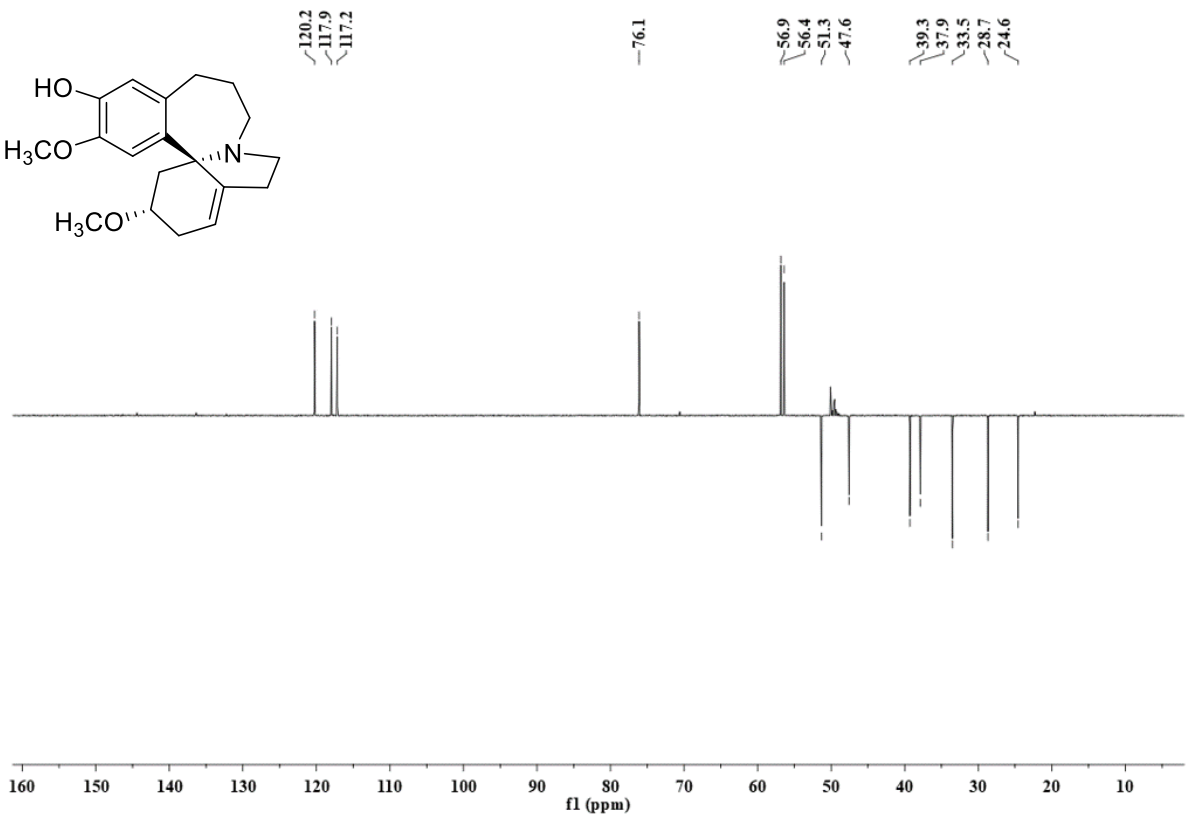

Figure S128. DEPT 135 spectrum of **12** in CD_3OD

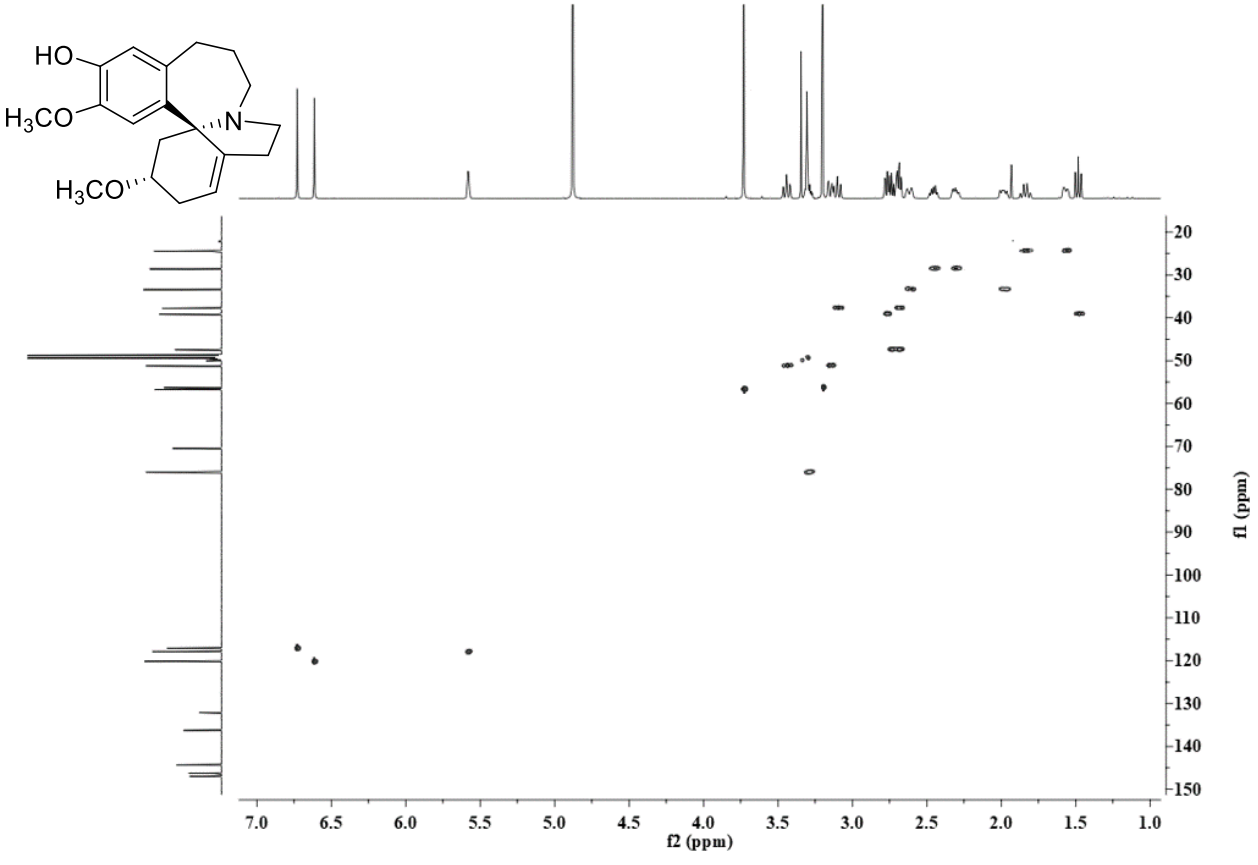

Figure S129. HSQC spectrum of **12** in CD_3OD

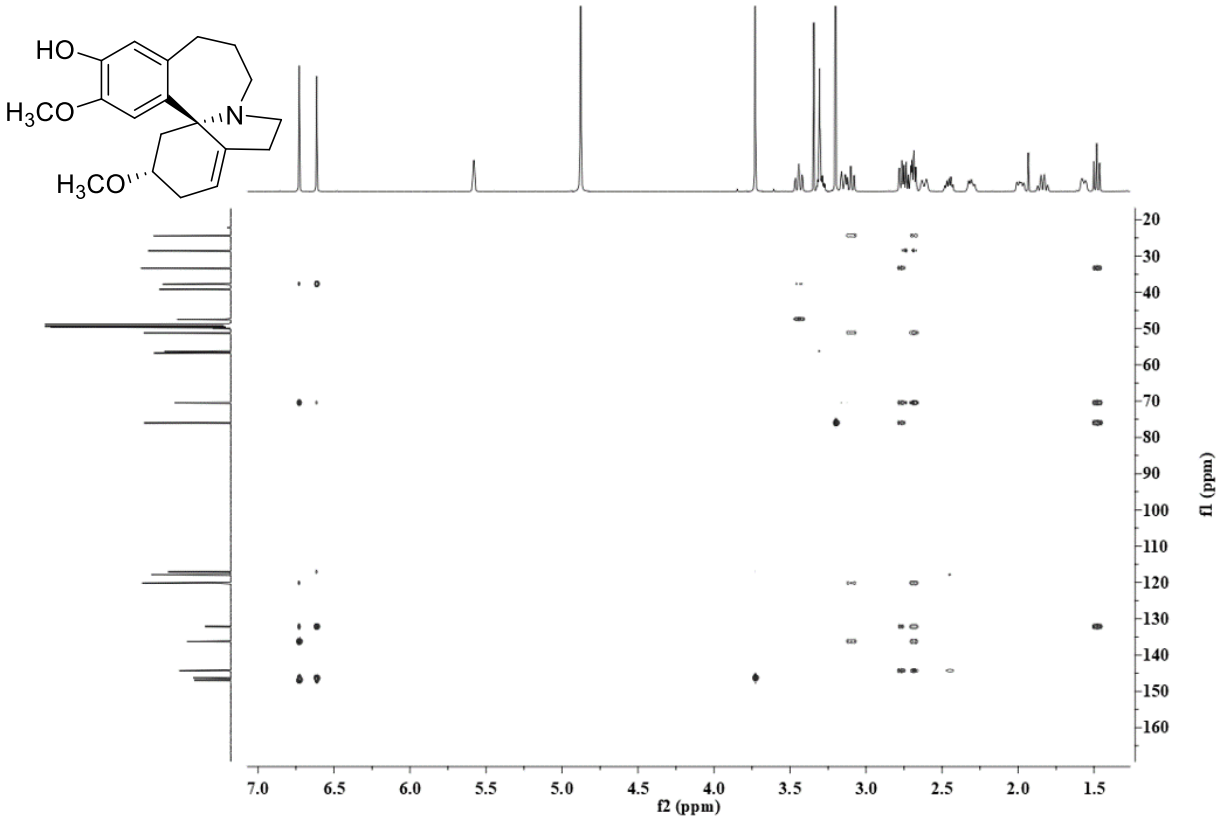

Figure S130. HMBC spectrum of **12** in CD_3OD

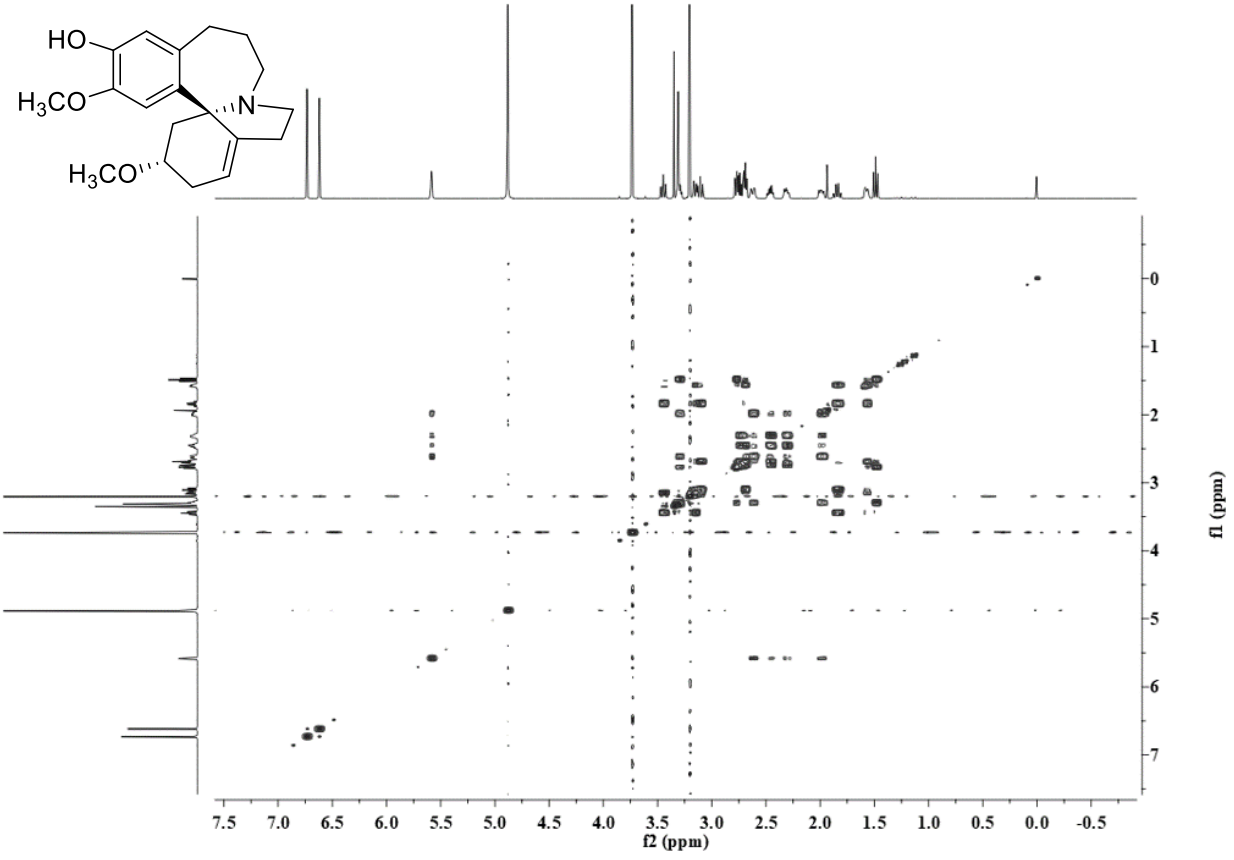

Figure S131. $^{1}H–^{1}H$ COSY spectrum of **12** in CD_3OD

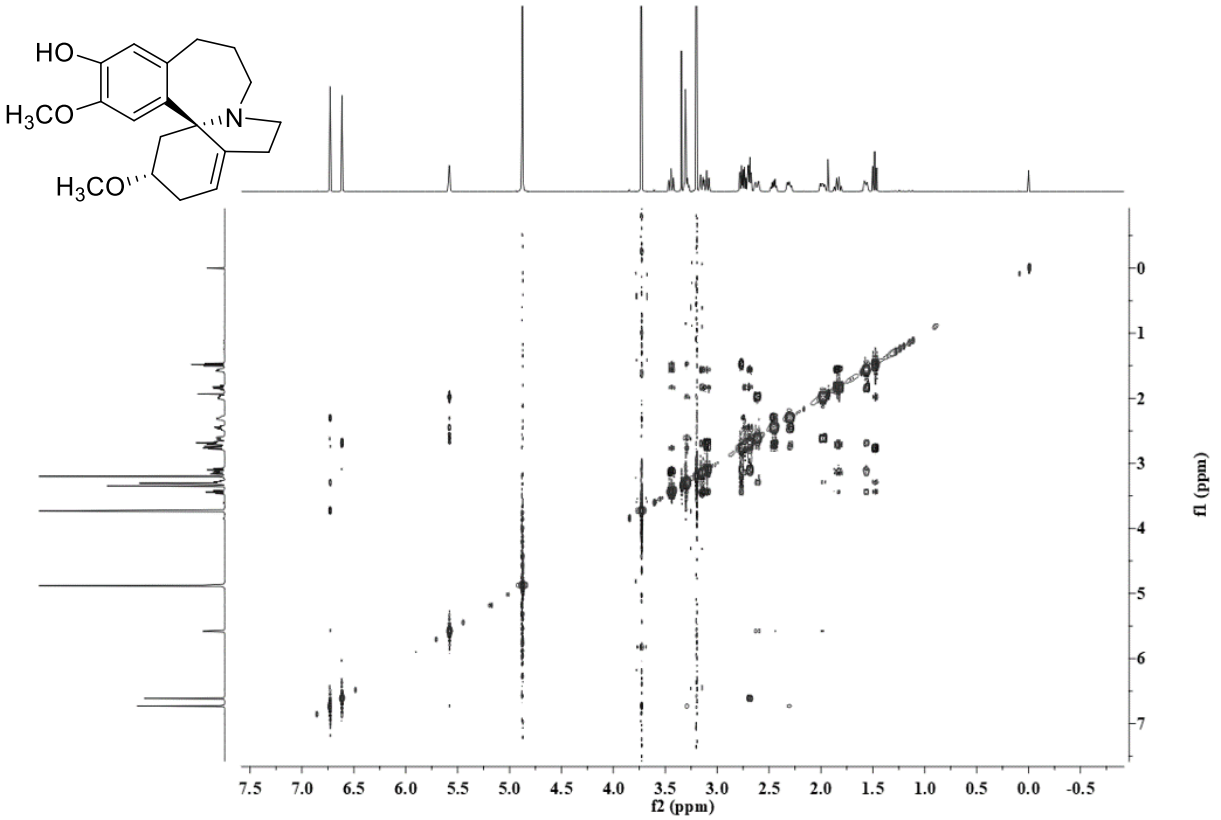

Figure S132. NOESY spectrum of **12** in CD_3OD